Photonic crystal light-emitting sources

Henri Benisty, Claude Weisbuch, Aurélien David

Photonic crystal light-emitting sources

Aurélien David[1], **Henri Benisty**[2] **and Claude Weisbuch**[3,4]

[1] Soraa Inc., Fremont, CA, USA
[2] Laboratoire Charles Fabry, Institut d'Optique, CNRS, Université Paris Sud, Palaiseau, France
[3] Materials Department, University of California, Santa Barbara, CA, USA
[4] Laboratoire de Physique de la Matière Condensée, CNRS, Ecole Polytechnique, Palaiseau, France

E-mail: aurelien.david@polytechnique.org

Abstract
Photonic crystals (PhCs) are periodically structured optical media offering the opportunity for spontaneous emission (SpE) to be strongly controlled in spatial terms (directions) or in absolute terms (rates). We discuss the application of this concept for practical light-emitting sources, summarizing the principles and actual merits of various approaches based on two- and three-dimensional PhCs. We take into consideration the numerous constraints on real-world light-emitting structures and materials. The various mechanisms through which modified photonic bands and band gaps can be used are first revisited in view of their use in light sources. We then present an in-depth discussion of planar emitters and enhanced extraction of light thanks to grating diffraction. Applications to conventional III–V semiconductors and to III-nitrides are reviewed. Comparison with random surface roughening reveals some common physical limitations. Some advanced approaches with complex structures or etched active structures are also discussed. Finally, the most promising mechanism to enhance the SpE rate, the Purcell effect, is considered. Its implementation, including through plasmonic effects, is shown to be effective only for very specific sources. We conclude by outlining the mix of physics and material parameters needed to grasp the relevant issues.

Contents

1. Introduction

This review discusses the use of photonic crystals (PhCs) to improve the properties of semiconductor light-emitting sources. It is limited to the regime of spontaneous emission (SpE), i.e. we will leave aside the equally important cases of PhC semiconductor lasers and superradiant emitters.

A semiconductor light-emitting device in the SpE regime is commonly referred to as a light-emitting diode (LED). One very important application of LEDs is as a source of (classical) light, for instance in lighting. In this context, one of the main figures of merit of an LED is its efficiency, i.e. its ability at converting electrical power into optical power. We are currently witnessing a market switch from usual sources such as incandescent lamps and compact fluorescent lamps to LED solid-state lighting due its superior performance [74, 100]. In addition, LEDs can also find applications in more specific domains with remarkable photon properties, such as single-photon emission (see [61]) or strong light–matter coupling. These two phenomena require figures of merit which are different from those of conventional LEDs used for lighting, and will not be discussed in this review.

No matter what the application of an LED, its performance depends strongly on the details of the electronic and optical properties of the LED structure (which includes all materials: active, passive, semiconductors, metals, insulators), and also sometimes on the interplay of the electronic and optical properties (in the case of strong light–matter coupling for instance). A powerful way to control and modify the photonic environment is provided by structuring the materials to form a PhC. A PhC can generally be described as a periodic modification of an optical medium on the scale of a wavelength—a generalization of the century-old concepts of diffraction grating and distributed Bragg reflector (DBR). PhCs can modify the optical properties of LEDs in a number of ways, from increasing their efficiency to enabling new physical properties. They offer the powerful advantage of being prone to *design* or *optical engineering*, somewhat similar to the band-gap engineering employed to design the electronic properties of semiconductor heterostructures, which was enabled by the progress of ultra-thin film epitaxy in the 1970s and 1980s [106].

Rather than going into a formal presentation of PhCs and their properties, in this report we consider them as a tool to modify an LED's emission mechanisms. Therefore, after a quick presentation of SpE in LEDs, we will look at the various aspects of an LED that can be improved through optical engineering and discuss how PhCs can be harnessed to this effect.

Unless otherwise stated, the original modeling results presented in this report were obtained using a scattering matrix (or S-matrix) approach, either in its one-dimensional (1D) form for multilayer systems, or in its three-dimensional (3D) form for scattering by periodic surfaces [6, 97, 107].

2. Basics of SpE in LEDs

The external quantum efficiency η_{EQE} of an LED (i.e. the ratio of useful external light to the electrically injected electron–hole pairs, which includes the internal conversion of the electron–hole pairs into internal photons and the extraction of these photons) can be expressed as

$$\eta_{\mathrm{EQE}} = \eta_{\mathrm{IQE}} \times C_{\mathrm{ex}}, \tag{1}$$

where η_{IQE} is the internal quantum efficiency, equal to the ratio of photons emitted inside the LED to the injected electron–hole pairs. C_{ex} is the light-extraction efficiency, or the probability for an emitted photon to escape from the LED. Note that we ignore current injection effects in this discussion because we focus on optical phenomena. Let us note here that the above definition can be complicated by second-order effects such as photon recycling (which we will discuss further in section 3.2), which intertwines η_{IQE} and C_{ex}.

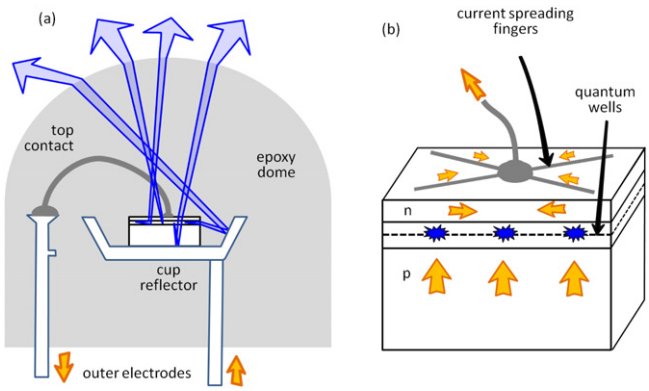

Figure 1. Cross section of an LED. (*a*) Traditional encapsulated LED. The LED chip sits on a cup reflector and is embedded in an encapsulant whose shape favors light extraction to air. (*b*) Details of the LED chip. The arrows show the current flow.

Another important metric, which will not be discussed here, is the wall-plug efficiency, i.e. the ratio of external light power to injected electrical power, which includes the electrical losses such as Ohmic losses—these are governed by the resistance of contacts and materials, which are outside the scope of this report.

A typical LED structure is sketched in figure 1. Optically speaking, it consists of a rather localized emitting region—typically a set of quantum wells whose thickness is a few nm to a few tens of nm—embedded in a host medium. The latter is usually a semiconductor stack (of higher band gap and lower refractive index) and can comprise carrier confinement layers, cladding layers, buffer layers, doped layers for electrical contacts. The value of the refractive index n depends on the semiconductor of interest. Currently, the main families of materials used in industrial applications are AlInGaAsP compounds ($n \sim 3$–3.3) for red to infra-red wavelengths and AlInGaN compounds (also designated as III-nitrides, $n \sim 2.4$–2.5) for ultra-violet to blue–green wavelengths. The epoxy or silicone in which the LED is encapsulated has a lower index $n \sim 1.5$ (the choice of the encapsulant being limited by constraints on aging and thermal behavior) so that a large fraction of the light emitted inside the semiconductor remains trapped in the LED, limiting the extraction efficiency. For instance, in the simplistic case of a planar semiconductor slab of index n_{in} capped with silicone of index n_{ext}, only light

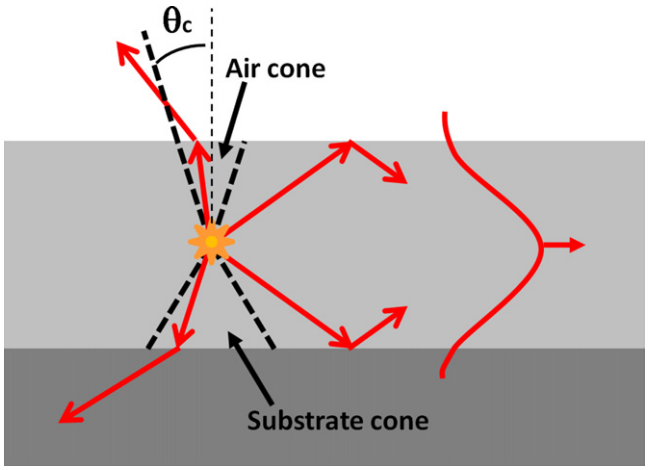

Figure 2. Light extraction from an LED. Only a fraction of the light, emitted within the air cone, escapes the LED from the top facet. Light can also propagate in the substrate—the corresponding cone is wider than the air cone due to the substrate's larger index. Finally, if the substrate's index is lower than that of the LED's epitaxial layer, guided modes are supported in these layers. Depending on the epitaxial layer's thickness, one or several modes can be supported.

propagating below the *critical angle* $\theta_c = \sin^{-1}(n_{ext}/n_{in})$ is extracted. The rest of the light is termed *guided light*. The cone of angles below the critical angle is called the *extraction cone*. The corresponding extraction by a single facet, given by the ratios of solid angles of the extraction cone and the full space, is weak: for extraction in epoxy or silicone ($n = 1.5$), it is about 10% for AlInGaP and 17% for InGaN. Figure 2 presents the basic quantities pertaining to light extraction from an LED.

The fate of the light not directly extracted depends on the details of the LED structure, i.e. its geometry and materials. In high-extraction chips, care is taken to alter the geometry of the LED in order to randomize the trajectory of trapped light. After some random propagation within the LED, a light beam therefore impinges at an interface within the extraction cone—this would ensure perfect extraction in the absence of dissipative mechanisms. Mastering this 'multiple attempt' extraction has been the focus of major efforts in the recent years, with three preferred techniques allowing for a good part of the progress in light extraction in LEDs: geometric (or macroscopic) shaping, surface roughening and growth on patterned substrates. Roughening will be discussed in section 5 in comparison with PhC extraction.

The PhC approach reviewed in the next sections relies on wave optics, and therefore has different physical properties compared with the geometrical optics approaches. It also has technological advantages: being a full planar process, it is scalable in size (whereas some geometrical approaches rely on sizable side extraction which can level off when propagating losses are high).

Therefore, an important task for PhCs is to improve C_{ex}, although improvements to η_{IQE} are also possible. To this effect, PhC-based light emitters generally aim at modifying SpE by altering some of the following characteristics: SpE lifetime, radiation pattern (both inside the semiconductor and in the outer medium), propagation of guided light. We first review the basic characteristics of these various phenomena.

2.1. SpE lifetime, the Purcell effect

Typical SpE lifetimes range from 100 ps in AlInGaP to a few ns in III-nitrides. Crucially, radiative recombinations have to compete against non-radiative channels. Usually, non-radiative recombinations are directly linked to the quality and properties of the material (density of point defects and dislocations, Auger recombination rate, etc) [84, 96]. This competition limits the internal quantum efficiency η_{IQE} as follows:

$$\eta_{IQE} = \frac{\tau_R^{-1}}{\tau_R^{-1} + \tau_{NR}^{-1}} \tag{2}$$

Here τ_R and τ_{NR} are the radiative and non-radiative lifetimes—or the inverse of the radiative and non-radiative emission probabilities p_R and p_{NR}.[5]

The value of η_{IQE} strongly depends on the material system. In mature materials such as AlInGaP compounds, η_{IQE} can reach 90%, while a more typical value for AlInGaN is ∼75% (actually, this value is strongly current-dependent: the peak value is usually reached at a low current density and decreases at stronger injection, a phenomenon commonly known as efficiency droop) [23, 24, 56, 93].

Therefore, η_{IQE} can be improved by lowering the non-radiative rate (for instance by improving the quality of the semiconductor crystal) but also by increasing the radiative emission rate. Alteration of the radiative rate p_R is commonly called the Purcell effect, and can be achieved by altering the photonic properties of the environment in which SpE occurs. Indeed, according to Fermi's golden rule [16, 47, 94]

$$p_R \sim 2\pi/\hbar\, |M_T(E_{21})|^2\, \rho_r(E_{21})\rho_O(\nu_{21}) \tag{3}$$

Here, the first factor $M_T(E_{21})$ is the transition matrix element of the electronic wavefunctions (for a given electromagnetic field), which is roughly constant in many III–V semiconductors; the second factor $\rho_r(E_{21})$ is the reduced electronic density of states (DOS), indicating which final states are allowed by energy and wavevector conservation rules; the third factor $\rho_O(\nu_{21})$ is the photonic DOS, i.e. the number of photonic states available for recombination. This last component can be factored in the expression above, and is the relevant quantity for our discussion. More precisely, the *local* DOS at the location of the light-emitting material (quantum well or quantum dot) $\rho_O(\nu_{21}, \boldsymbol{r})$ should be considered [59, 95, 103], a point arising when factoring out the electronic part.

The resulting relative modification of SpE lifetime with respect to the bulk reference case characterized by a photonic DOS ρ_{bulk} is called the Purcell factor F_p:

$$F_p = \frac{\rho_O(\nu_{21}, \boldsymbol{r})}{\rho_{bulk}}. \tag{4}$$

[5] Up to a normalization factor: the probabilities are normalized to one while the lifetimes are in s, but this does not alter arguments based on lifetime ratios or probability ratios.

Let us note that F_p may be smaller or larger than unity, depending on how the DOS is modified in a given structure.

The distribution of emitted light into extracted and guided light can also be cast in terms of lifetimes. If we call p_g and p_{ex} the probabilities for a photon to be be emitted in guided and extracted channels, respectively, the total radiative lifetime can be expressed as

$$\tau_R = 1/(p_g + p_{ex}) = 1/(\tau_g^{-1} + \tau_{ex}^{-1}). \quad (5)$$

Some approaches aim at decreasing p_g so that all the light that is emitted is extracted. As above, this can be achieved by lowering (or ideally suppressing) the photonic DOS for guided light.

2.2. *Radiation pattern, distribution of SpE*

The radiation pattern (i.e. the angular distribution of emitted light inside the semiconductor) is determined by the electronic properties of the active region and the optical environment inside the LED.

The properties of the active region intervene through the semiconductor's momentum matrix element factored in M_T. In general, it depends on the symmetry properties of the crystal and on the details of the band structure. Two simple cases are worth mentioning. The first corresponds to unstrained bulk zinc-blende materials, where emission is isotropic and unpolarized. From an electromagnetic point of view, such an isotropic emission can be represented as the superposition of emission from randomly oriented dipoles (or from the sum of the emission of three dipoles oriented along the three directions x, y and z). The second case corresponds to a random distribution of *in-plane* dipoles. It occurs in systems where the growth crystallographic direction is no longer equivalent to the two others—for instance in quantum wells, strained layers, or in bulk III-nitrides where the crystal symmetry is wurtzite. In practice, this second case corresponds to most situations in LEDs. Recalling that TE (transverse electric) and TM (transverse magnetic) are the adequate polarizations for a planar structuration (also called 's' and 'p', respectively), the most notable property is that in-plane emission is TE-polarized, as shown on figure 3. This means that photonic effects aimed at in-plane propagating light only have to deal with TE-polarized light. We note that the definitions of TE and TM are not unified between the fields of planar waveguides and PhCs—in this report, TE polarization corresponds to the electric field lying in the plane of the LED.

The optical environment of the LED further modulates this intrinsic emission pattern. Even in a simple slab LED, waveguiding effects are present and affect the emission pattern—typically by forming guided modes in which emission is channeled. Let us illustrate this with two simple examples: a monomode and a strongly multimode waveguide. The first case corresponds to an emitting region embedded in a thin, high-index layer, which supports only one mode. In this case, a macroscopic fraction of the light emission is channeled into this mode. Figure 4 illustrates such a situation in a GaAs structure, where the emission pattern can be divided into three angular sectors: light extracted to air, light emitted in the thick substrate and light emitted in guided modes—which shows up as a sharp peak in the emission diagram. This structure sustains one mode per polarization, and each mode appears in four equivalent directions in the vertical plane.

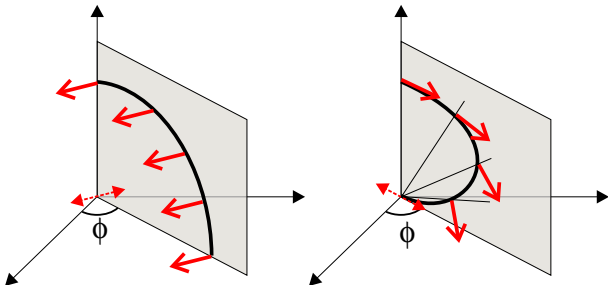

Figure 3. Emission diagrams corresponding to the semiconductor's matrix elements. Emission can be decomposed as the contribution of two oscillating dipoles. Left: the dipole perpendicular to the plane of emission produces a TE-polarized emission with constant amplitude. Right: the dipole parallel to the plane of emission produces a TM-polarized emission with an irradiance $\sim \cos^2\theta$, which vanishes in the horizontal plane.

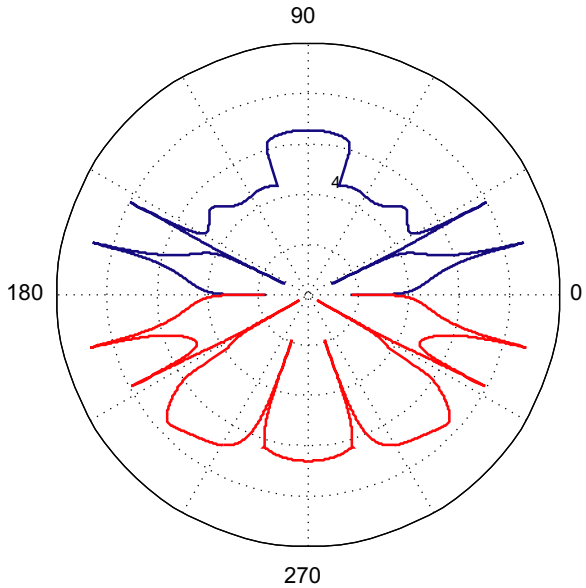

Figure 4. Emission diagram in a monomode structure. We consider a 300 nm waveguide ($n = 3.6$) sandwiched between air and a substrate ($n = 3$). The radial scale is logarithmic. Sharp peaks come in matched pairs (up–down and left–right) and correspond to guided modes. A very weak absorption term has been added to give the modes a finite width. Emission in air is the upper, weakly modulated lobe.

The second case occurs, for instance, in III-nitride structures (figure 5). Here the nitride layer is thick (about 4 μm) and supports more than a dozen guided modes. Again, three angular sectors can be distinguished in the emission diagram: light extracted to air, light propagating in the sapphire substrate and guided light, which is now distributed over the many modes of the structure.

In general PhC structures can affect this pattern in a number of ways. They can forbid the existence of guided modes (section 3), modify the dispersion relation of these modes (section 4), or favor light recycling in these structures.

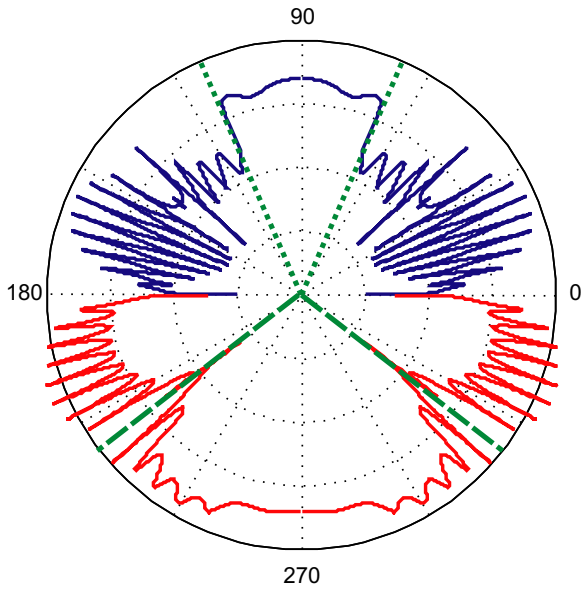

Figure 5. Emission diagram in a multimode structure (air/GaN/sapphire). Here the upper dotted lines indicate the extraction cone to air, and the lower dashed lines the extraction cone to sapphire. Light propagating beyond the latter angle is distributed among guided modes, seen as a series of sharp peaks in the emission diagram.

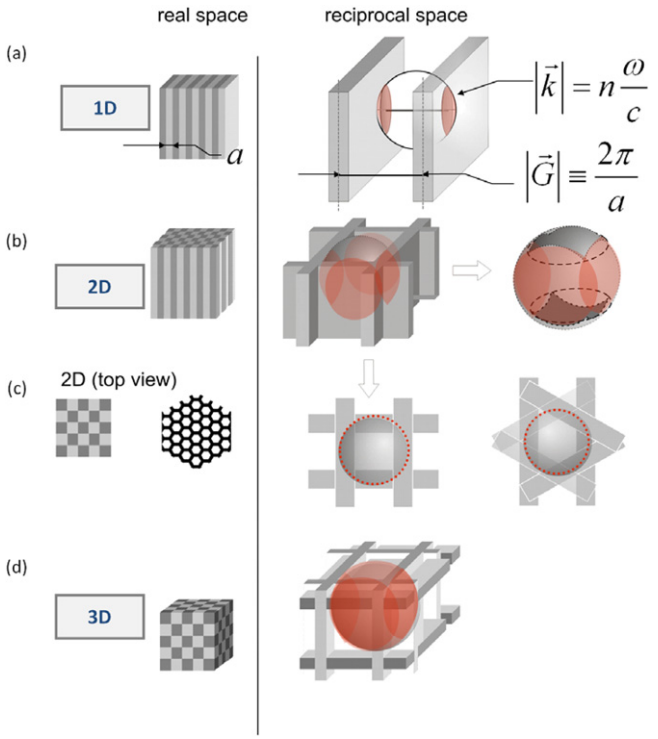

Figure 6. Band gaps of 1D, 2D and 3D PhCs. The left half shows the index distribution in real space, and the right half indicates the corresponding forbidden bands in reciprocal space. (*a*) 1D PhC (or DBR). The stop bands are angular cones normal to the DBR stack. (*b*) and (*c*) 2D PhC made of a series of infinite vertical rods. Stop bands can now be supported in more in-plane directions. (*d*) 3D PhC enabling a band gap in all directions. Reproduced with permission from [7]. Copyright 2006 Elsevier.

Also, the pattern depends on the vertical position of the emitting layer in the structure. For a given position some guided modes are more fed by the source than others, depending on their field profile overlap with the quantum wells. This is expressed through the local DOS, over which we have to integrate.

Due to the complexity of these various effects, each of these PhC-based approaches has specific properties. We are thus going to detail the various mechanisms likely to assist extraction and raise extraction efficiency, and evaluate their merits and implementation constraints.

3. Band gaps and inhibition of SpE

The first suggested application of PhCs to LEDs was based on the band-gap approach. It followed naturally from Yablonovitch's famous proposal of SpE inhibition [14, 101, 114]. In the following, we discuss the concept of photonic band gap (PBG) and its application to light extraction and its limitations for real-world devices—which in our view means operation of LEDs at a realistic temperature, with output power in the range needed for general illumination.

3.1. Photonic band gaps

In general, the periodicity of the dielectric function in an optical medium can modify the dispersion relation of photons, just like the periodicity of the electronic potential in a crystal modifies the dispersion of electrons and yields energy bands. Notably, properly designed PhCs can open PBGs (or stop bands), i.e. energy regions for which photon propagation is forbidden. Depending on the design of the PhC, the band gap can be directional (in which case photon propagation is only forbidden in a given set of directions) or omnidirectional, and is in general polarization-dependent [7, 68].

The simplest occurrence of a PhC is better known as a 1D DBR, which typically reflects photons impinging in an angular cone around normal incidence on the multilayer stack (figure 6(*a*)). Two-dimensional (2D) PhCs widen the angular range of the band gap, forming an 'equatorial belt' in k-space. In some cases, the band gap extends to all in-plane directions. Finally, some 3D PhCs are able to open an omnidirectional band gap, but they are very difficult to implement in practice [11]. This topic has been studied since the beginning of the PhC field. A first difficulty lies in the requirements for a full 3D PBG. A large index contrast is needed, which depends on the crystal structure. For the PhC structure easiest to fabricate 'naturally', the fcc inverse opal, the band gap only occurs between the eighth and ninth bands, which makes the existence of a well-defined PBG very sensitive to fluctuations: [66] shows that 2% fluctuations of the lattice constant are sufficient to suppress the band gap. The diamond structure has a much larger gap (20% of frequency) but is much more difficult to achieve [46]. Over the years, a number of man-made structures mimicking the diamond structure have been developed, such as a modified fcc structure sometimes called Yablonovite [116] or the woodpile structure (figure 7) achieved by piling up sequentially displaced 2D pierced layers [94, 115]. Such

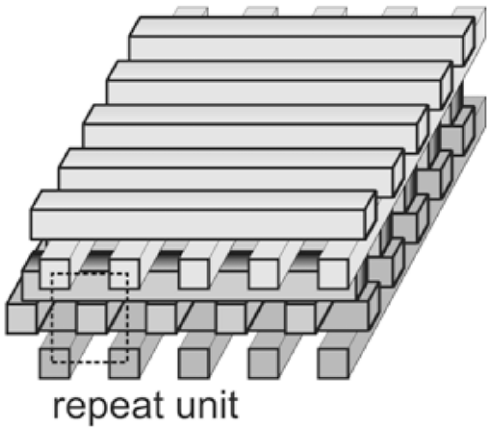

Figure 7. Woodpile structure. Reproduced with permission from [7]. Copyright 2006 Elsevier.

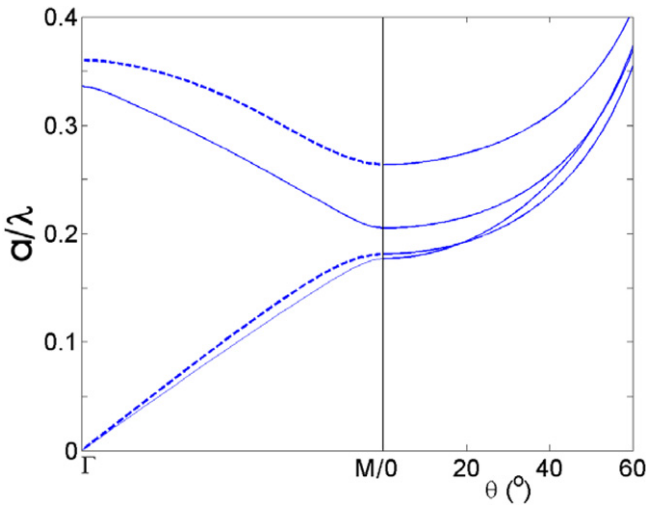

Figure 8. Band structure of a 2D PhC (triangular lattice of infinite cylinders in the z direction, $\epsilon_{\text{core}} = 12$, $\epsilon_{\text{rods}} = 1$, $f = 0.3$). Dashed $= H$ polarization, full $= E$ polarization. Left: in-plane dispersion in the ΓM direction for $k_z = 0$. Right: band structure at the M point (i.e. $k_\parallel = G_0/2 = \pi/a$, see figure 6) as a function of the off-plane angle $\theta = \tan(k_z/k_\parallel)$. The gap narrows for off-plane propagation, and drifts to higher frequencies. Reproduced with permission from [17]. Copyright 2006 EDP Sciences.

woodpile structures have full 3D PBGs with better tolerance to fluctuations than inverse opals and can accommodate up to 20% layer-to-layer displacement [48]. Reference [113] reaches the same conclusions about the robustness of the band gap, but also points to the importance of achieving taperless holes.

Besides difficulties in fabricating 3D PBG structures, one encounters the issue of placement of active species within the PhC structure to obtain SpE and avoid exciting species in the regions where the optical field is suppressed. Due to the balance between enhancements and suppression and large averaging over many PhC sites, the overall PBG effects are difficult to assess quantitatively. Electrical injection being so far elusive, most experimental assessments of PBG enhancements are carried out in photoluminescence and require expert detailed analysis to be safely translated into efficiency improvements [67].

As an example, figure 8 displays the band structure of a 2D PhC (with an infinite extension along the vertical z direction). At normal incidence (i.e. in the x–y plane of periodicity), a band gap opens in both polarizations around a frequency $a/\lambda = 0.2$. For light propagating at an angle θ out of the periodicity plane, the band gap evolves both in position and width. Note first that both polarizations are mixed at such a conical $\theta > 0$ incidence. As for the angular behavior, note that the angle θ is defined in the high-index medium surrounding the PhC. Therefore, the gap evolution with angle is strong: it is essentially dictated by a $1/\cos\theta_{\text{PhC}}$ scaling, using Snell's relation $n \sin\theta = n_{\text{PhC}} \sin\theta_{\text{PhC}}$, with n_{PhC} an average PhC index, typically lower than n, adequate for the effective medium seen by the wave. The shrinkage of the gap width can be related to the lower reflectivity around the Brewster angle ($\sim$45° here), although polarization mixing blurs the picture.

In practice, only 2D PhC structures have been incorporated in full LEDs so far. This is mostly because 3D PhCs are not straightforwardly compatible with planar fabrication technologies, as discussed above. Moreover, in an LED, as will be clear in the discussion of modal extraction below, what is needed is 3D control of light propagation, which does not necessarily imply a full 3D PBG. This is clearly illustrated by the fact that one observes 3D light confinement with ultra high-Q factors for cavities in 2D PhC cavities embedded in a membrane waveguide. In such waveguide geometries, or others supported by substrates and confining layers, the index contrast in the vertical direction forms a waveguide (figures 4 and 5). For the light which is emitted into guided modes, optical confinement is thus natural in the vertical direction, and only an additional in-plane confinement or environment modification by the PhC is necessary. In addition to the ease of fabrication of 2D periodic structures by the usual lithographic techniques, an additional advantage of 2D PhC is that PBGs occur at quite low index differences (the index difference between air and any semiconductor is sufficient). Therefore, the rest of our discussion focuses on 2D PhCs.

In the context of LEDs, one can take advantage of the PhC's stop bands either to forbid the *propagation* or to inhibit the *generation* of in-plane light, as we will discuss below.

3.2. Use of a PhC as a mirror—photon recycling

Figure 9 depicts a situation where a PhC is formed on the boundary of the light-emitting region. In this case, guided light impinging on the PhC bounces back into the light-emitting region—where it remains guided. This is only advantageous if this light is then re-absorbed in the active region and re-emitted toward the air, a phenomenon known as *photon recycling*. However, the efficiency of this process is clearly limited by the internal quantum efficiency of the LED because it relies on successive absorption–emission cycles to extract all the light. To estimate this, we denote η_{IQE} the internal quantum efficiency, C_{ex0} the initial light-extraction efficiency (without photon recycling) and A_{ar} the fraction of light that is absorbed in the active region (energy conservation then reads $C_{\text{ex0}} + A_{\text{ar}} + A_{\text{other}} = 1$, where A_{other} corresponds to the other

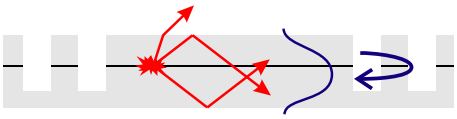

Figure 9. LED surrounded by a PhC mirror. Light emitted from the active region bounces in the LED and forms guided modes. These are reflected by the peripheral PhC and sent back into the LED, where they can undergo absorption/reemission cycles (i.e. recycling) until they are extracted.

absorption channels such as metal contacts). The enhanced light-extraction efficiency due to recycling then becomes

$$C_{\mathrm{ex}} = C_{\mathrm{ex0}} + A_{\mathrm{ar}}\eta_{\mathrm{IQE}}C_{\mathrm{ex0}} + A_{\mathrm{ar}}^2\eta_{\mathrm{IQE}}^2C_{\mathrm{ex0}}\ldots = \frac{C_{\mathrm{ex0}}}{1 - A_{\mathrm{ar}}\eta_{\mathrm{IQE}}}. \tag{6}$$

For C_{ex} to approach unity, one therefore needs to both have $\eta_{\mathrm{IQE}} \sim 1$ (nearly perfect internal quantum efficiency) and $A_{\mathrm{ar}} \sim 1 - C_{\mathrm{ex0}}$ (dissipation by reabsorption in the active region only, which requires nearly lossless metal contacts). Even if the second condition could be met, and taking $C_{\mathrm{ex0}} = 0.1$ (a typical value for a planar structure without any light-extraction feature) and a very high $\eta_{\mathrm{IQE}} = 0.9$, we would obtain $C_{\mathrm{ex}} = 0.53$ only—this is because ∼5 cycles are necessary to deplete ∼50% of the photons, but each cycle also incurs a 10% non-radiative loss. Therefore, it is very difficult to reach high-extraction efficiencies with photon recycling *alone*, because many absorption–emission cycles are necessary. Considering this limited efficiency and the fabrication complexity of PhCs, this strategy is not compelling.

On the other hand, we should note that the *contribution* of photon recycling to the efficiency of an LED can seldom be ignored, even if it is not the primary scheme to improve light extraction. To illustrate this, let us now assume that the extraction efficiency of an LED is brought to a large value of $C_{\mathrm{ex0}} = 80\%$, for instance using one of the light-extraction schemes described in the rest of this report. Figure 10 then shows the effect of η_{IQE} on C_{ex}: in a plausible situation where losses are shared equally between active region absorption and other losses, and for a reasonable $\eta_{\mathrm{IQE}} = 0.6$, we obtain $C_{\mathrm{ex}} \sim 90\%$, a clear improvement over the extraction when photon recycling is ignored.

3.3. Guided light inhibition

In contrast to figure 9, figure 11 describes a structure where the PhC is formed in the light-emitting region itself. In the ideal case of a full in-plane band gap, guided modes do not exist and all of the guided light emission is then inhibited. Light can therefore only be emitted in the out-of-plane modes, yielding the ideal result $C_{\mathrm{ex}} = 1$.

3.3.1. Experimental investigations. The concept of light inhibition by a PhC was first suggested in [33]. A first experimental demonstration was claimed in [14], at a time when inhibition and diffraction effects were not clearly distinguished. Furthermore, whatever the mechanism, normalization of extraction measurement is always a delicate

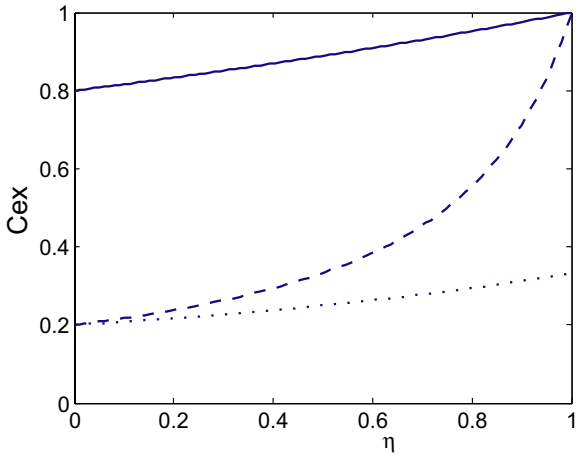

Figure 10. Photon recycling versus internal quantum efficiency η_{IQE} in various scenarios. Dotted line: LED with poor initial extraction efficiency and absorbing metal contacts ($C_{\mathrm{ex0}} = 0.2$, $A_{\mathrm{ar}} = 0.4$, $A_{\mathrm{other}} = 0.4$), C_{ex} is always low because a large fraction of the non-extracted light is lost in the metal. Dashed line: LED with poor initial extraction efficiency and reabsorption losses only in the active region ($C_{\mathrm{ex0}} = 0.2$, $A_{\mathrm{ar}} = 0.8$), C_{ex} is only acceptable for very high values of η_{IQE}. Full line: LED with high initial extraction efficiency and losses only in the active region ($C_{\mathrm{ex0}} = 0.8$, $A_{\mathrm{ar}} = 0.2$), photon recycling helps further improve C_{ex} with a trend almost proportional to η_{IQE}.

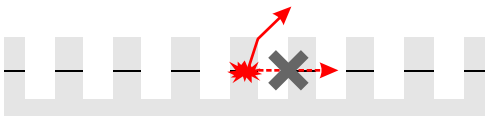

Figure 11. LED with a PhC in the light-emitting region: if a full band gap exists, emission into guided modes is inhibited and all emission is extracted.

issue, as follows from considering the various effects listed above (different top-view filling fraction of quantum well when etched, non-radiative recombination at surfaces, etc). Another caveat is that this work and several subsequent ones used photoluminescence, and it is unclear in such circumstances if the observed increase in the luminescence signal can be attributed only to enhanced extraction, or if a sizable contribution stems from increased excitation due to better coupling of excitation light into the guided modes at the excitation wavelength.

A clear experimental demonstration of the band-gap SpE effect was presented several years later in [38] (figure 12). This experiment was carried out at cryogenic temperatures, where non-radiative recombinations were quenched. This was also the first solid-state demonstration of Yablonovitch's famous inhibition idea in [114] with a strong inhibition factor, a fact that calls to our attention the profound difficulty in inhibiting nearly-all radiative channels. We note that this is in stark contrast to the opposite task of favoring a modest subset of channels at the expense of all others, which was achieved in the strings of micro-cavity emitter results, either of planar type in the 1990s or PhC-type in the early 2000s. In the case of [38], the authors fabricate several PhC membranes with various pitches, so that emission from the same InAs quantum wells is continuously swept through the band gap. The luminescence

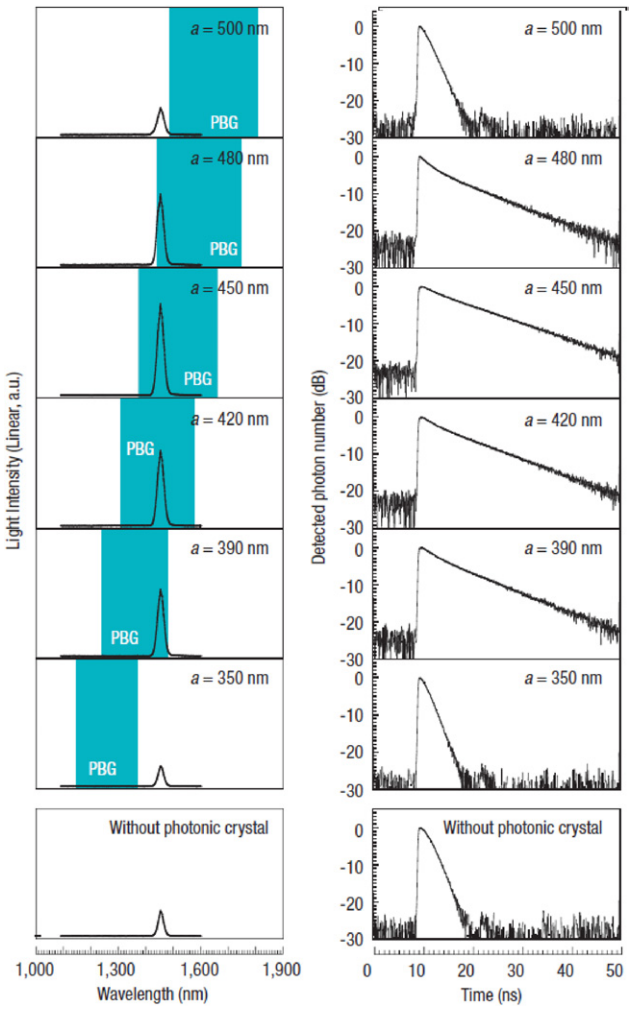

Figure 12. Evolution of the photoluminescence signal (left) and of the corresponding lifetime (right) for a series of PhC membranes of varying band-gap frequencies. When the SpE falls inside the band gap, both the intensity and lifetime increase. Reproduced with permission from [38]. Copyright 2005 American Association for the Advancement of Science.

signal and the radiative lifetime are seen to increase when the emission spectrum fully lies inside the gap. This is attributed to the inhibition of guided light emission: the total photonic DOS is dramatically diminished (see section 6) and the SpE lifetime becomes much longer. Similar inhibition effects have recently been observed for quantum dots immersed in 3D PhC structures, as will be discussed in section 7.5.

3.3.2. Limitations of the band-gap approach. The band-gap approach is seducing owing to its conceptual simplicity. However, it suffers from two—somewhat related—drawbacks: integration in a realistic device structure and impact on internal quantum efficiency.

In practice an LED structure has a finite vertical extension, unlike the ideal two-dimensional PhCs described above. The light propagating in-plane is distributed into guided modes (one or several modes, depending on the thickness of the LED film). As discussed previously, in a 2D PhC the band gap only extends up to a maximum off-plane propagation angle (figure 8). In a thin monomode LED structure this is not problematic: the single guide mode typically propagates at a large (near-glancing) angle ($\theta \sim 20^\circ$ off-plane in figure 8) and will fall within the band gap of the PhC if the structure is well designed. Therefore, in-plane light emission can be fully suppressed and the light extraction should be unity. In a thick structure, on the other hand, many guided modes are present and it is not straightforward to prevent propagation for all the modes—namely it is difficult to retain a band gap for the whole range of angles $\theta = 0$–70°. In that case, emission into guided modes still occurs and these need to be extracted by some other means before they are dissipated by absorption or scattering to the substrate.

A true monomode structure (with no substrate emission) can only be obtained by forming a membrane. In such a suspended structure, however, current injection becomes extremely difficult. It is indeed unclear how to inject current inside the membrane—especially as regards contacting the bottom layer. In principle, one may take advantage of current spreading in the material, and form electrodes in specific peripheral areas from which current would spread in the surrounding membrane. Nevertheless, the geometry remains very challenging and contacting of a full membrane of decent area has not been demonstrated so far. A rare and remarkable example of a fully injected PhC membrane with a small pedestal was demonstrated for a PhC laser in [82] (figure 13). An additional issue would be the high thermal resistance of a membrane LED, which would probably limit the use of such devices to very low power densities, incompatible with real-world requirements.

Figure 14 compares a membrane with two more realistic structures and discusses the partial application of the band-gap approach in these cases. In the case of a monomode waveguide on a substrate, use of the band-gap approach is still possible but one must deal with emission toward the substrate. Second-order effects can also be detrimental, such as the loss of up–down symmetry which mixes TE and TM modes and reduces the band-gap's robustness. Finally, in the case of a multimode waveguide, the band-gap approach is challenging: it is in general difficult to open omnidirectional gaps for all modes, so that some modes are still present in the etched structure and carry away some of the SpE.

The second, more fundamental, challenge of the band-gap approach resides in its impact on internal quantum efficiency. In a realistic LED at room temperature, the internal quantum efficiency η_{IQE} is limited by non-radiative recombinations, according to equation (2). The band-gap approach can alter η_{IQE} in two ways. First, drilling holes through the active region is likely to create surface defect states prone to non-radiative recombinations, therefore lowering τ_{nr}. This effect is material-dependent, but is known to be important in AlInGaAsP compounds [13]. Second, a PBG implies a depletion of the photonic modes to which electron–hole pairs can recombine. As a consequence of the reduced photonic DOS, the radiative recombination rate decreases as seen on figure 12—in other words, the Purcell factor (equation (4)) becomes smaller than one.

Let us quantify this second effect. As was mentioned, 5% to 10% of SpE in a semiconductor is naturally extracted

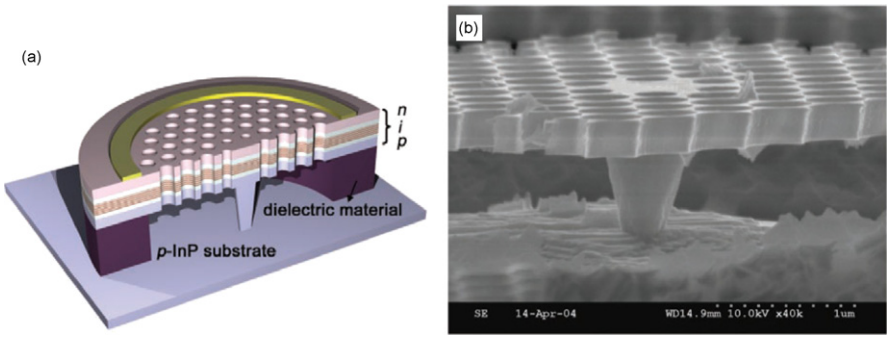

Figure 13. Single cell electrically pumped PhC laser. It is based on a PhC membrane with injection by a ring on top and by a p-doped pedestal on bottom. Reproduced with permission from [82]. Copyright 2004 American Association for the Advancement of Science.

to the air/epoxy top interface (depending on the material), the rest being guided. The radiative lifetimes corresponding to guided and extracted emission are thus on the order of $\tau_{\text{ex}} \sim 10 \times \tau_{\text{guided}}$–$20 \times \tau_{\text{guided}}$.

The internal quantum efficiency contains two radiative contributions, to guided and extracted modes. If emission in guided modes is inhibited, $\tau_{\text{guided}} \to \infty$. Therefore, the internal quantum efficiency is modified as follows:

$$\eta_{\text{IQE}} = \frac{\tau_{\text{ex}}^{-1} + \tau_{\text{guided}}^{-1}}{\tau_{\text{ex}}^{-1} + \tau_{\text{guided}}^{-1} + \tau_{\text{NR}}^{-1}} \to \frac{\tau_{\text{ex}}^{-1}}{\tau_{\text{ex}}^{-1} + \tau_{\text{NR}}^{-1}}. \tag{7}$$

Thus the competition of the sole extracted channel in the face of non-radiative channels can lead to quite a poor IQE, even if these non-radiative channels are no stronger than in usual structures. Equation (7) reveals the 'buffering' role of the guided channel rate: it maintains IQE closer to unity when it is large, but cannot prevent a plummeting IQE when it vanishes. As a consequence, η_{IQE} is significantly impacted in practical cases. More precisely, figure 15 depicts the effect for two scenarios corresponding to AlInGaP and GaN, respectively.

Solving this issue is not trivial. The authors of [38] have suggested using materials that would keep high internal quantum efficiency at high temperature (such as quantum dots, where carrier localization makes electron–hole pairs more robust against surface-state non-radiative recombinations, [39]). However, while some improvements could be observed up to temperatures of 200 K, no conclusive demonstration of the band-gap approach has been achieved so far at room temperature, either in photo- or electro-luminescence.

We conclude that despite its conceptual simplicity, the band-gap approach is actually very challenging to apply in a realistic structure. In addition to the practical difficulty to inject the device, internal quantum efficiency is degraded, both by the increase in non-radiative recombinations and by the decrease in radiative recombinations, which makes η_{IQE} far more vulnerable.

Finally, one may wonder whether the band-gap approach can be applied with a *partial* band gap (e.g. a band gap which only opens for a set of azimuthal directions), in order to mitigate the detrimental impact on the radiative rate. Unfortunately, it turns out that for any given guided mode, a full band gap is necessary to suppress the guided radiative rate into the mode. In the case of a partial band gap, the radiative rate toward the mode is (roughly) unaffected, as shown in [19], because the DOS tends to be redistributed toward the allowed emission direction. Therefore, the ratio of guided to extracted light is not affected if the band gap is not full (however, guided light is now emitted in a limited range of azimuthal angles, a potentially useful situation, which we will explore in section 6).

4. Extraction of guided light—the diffraction grating approach

As discussed above, the band-gap approach is hindered by several factors: difficulty of injecting current, potential damage to the active region, decrease in radiative rate. It can therefore be seen as 'too aggressive'. The grating approach, on the other hand, uses a PhC in the propagative mode regime, with weaker effects, which does not prevent light emission into guided modes but subsequently diffracts them out-of-plane.

Because the PhC does not have to be pierced through the active region, a PhC-LED in the grating approach can retain a classic geometry, and current injection is less problematic than with the band-gap approach. Therefore, the grating approach has been extensively explored experimentally in the literature. In the following we describe the basic theory of this approach and review published work, making the distinction between AlInGaP and III-nitrides because of their different optical environment, notably as regards vertical guiding.

4.1. Principle of operation

Figure 16 describes the basic structure used in the grating approach. In general, the modes of such a periodic structure are so-called Bloch modes, of the form

$$\boldsymbol{E} = \sum_{\boldsymbol{G}} \boldsymbol{E}_{\boldsymbol{G}}(z) \mathrm{e}^{\mathrm{i}(\boldsymbol{k}_{\parallel} + \boldsymbol{G})\boldsymbol{r}} \tag{8}$$

Here $\boldsymbol{G}$ runs over the reciprocal lattice of the PhC. Each term of the sum is a spatial harmonic of the Bloch mode. Guided modes of a uniform planar slab are a simple form of Bloch modes where only one harmonic is non-zero. A Bloch mode is called a leaky mode if at least one harmonic satisfies the condition

$$|\boldsymbol{k}_{\parallel} + \boldsymbol{G}| < n_{\text{ext}} k_0, \tag{9}$$

where n_{ext} is the index of the extraction medium (air or epoxy). This condition is similar to the usual expression for

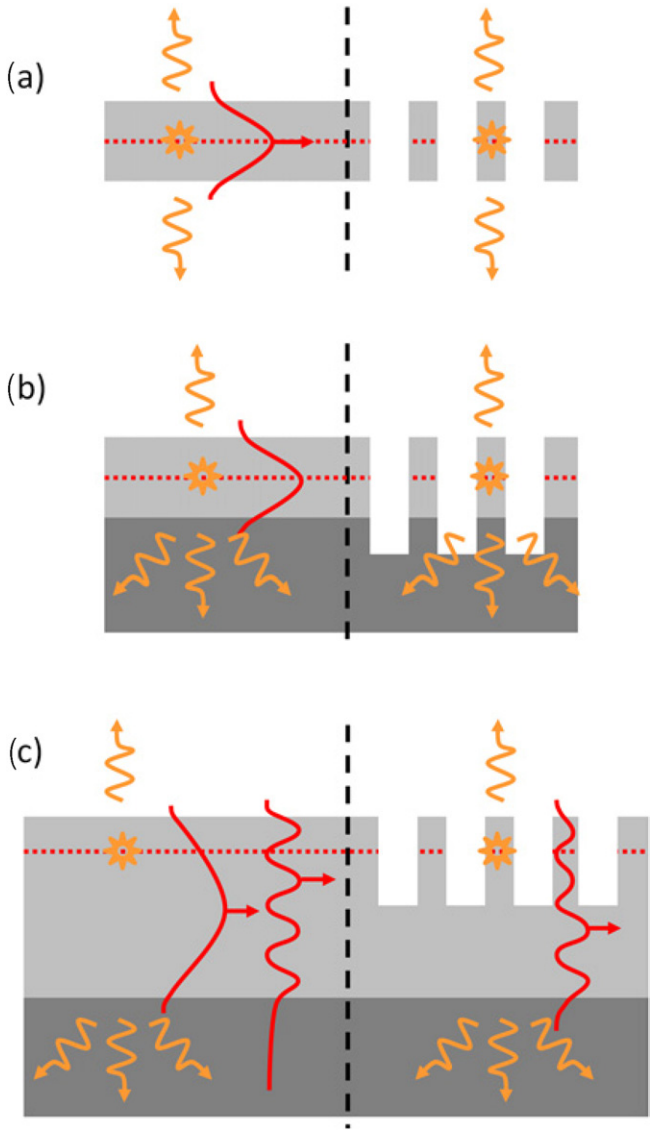

Figure 14. Comparison of device geometries for the band-gap approach. The left and right half of each structure indicate the radiative channels without and with a PhC, respectively. The horizontal dotted line is the emitting medium. (*a*) Membrane geometry; emission into the guided mode can be suppressed, leading to emission in air only. (*b*) Waveguide on a substrate: detrimental radiative channels to the substrate are present, and cannot be suppressed by the PhC. (*c*) Multimode waveguide on a substrate: in addition to emission to the substrate, some of the guided modes are present after the PhC is etched and can still channel light emission (achieving a full band gap for all modes is a difficult task).

the extraction cone ($k_\parallel < n_{\text{ext}} k_0$), but for a harmonic of the Bloch mode. If it is satisfied, this harmonic is propagative in the extraction medium where it can radiate power: light is therefore diffracted out-of-plane. The wavevector of the Bloch mode then acquires an imaginary part:

$$k_\parallel \rightarrow k_\parallel + \mathrm{i}k''. \tag{10}$$

Thus the Bloch mode decays along its propagation with a power dependence:

$$|E|^2 \propto \mathrm{e}^{-2k''x}. \tag{11}$$

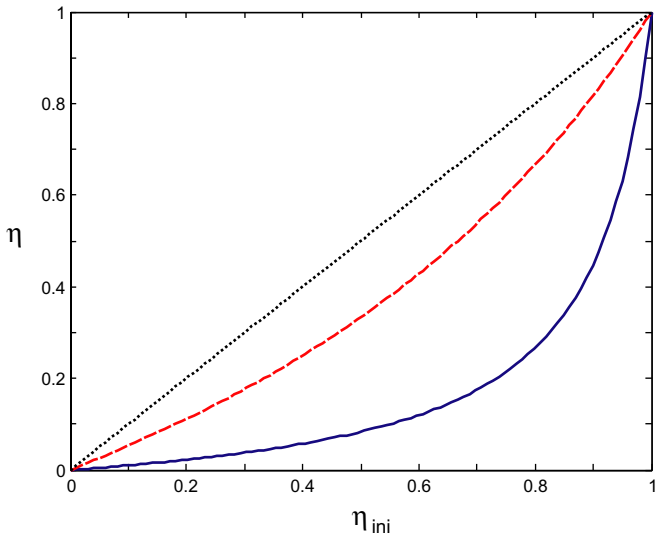

Figure 15. Evolution of internal quantum efficiency η_{IQE} after band-gap opening, which fully suppresses guided mode emission, versus initial internal quantum efficiency η_{ini}. The dotted line corresponds to $\eta_{\text{IQE}} = \eta_{\text{ini}}$, i.e. the situation without inhibition. The full and dashed curves, respectively, assume the following values for $\tau_{\text{air}}/\tau_{\text{guided}}$: 0.1 (realistic case) and 1 (very optimistic case) assuming another effect is used to channel emission into extracted light, on top of using the PhC. In the realistic case, η_{IQE} is significantly reduced even for high values of η_{ini}.

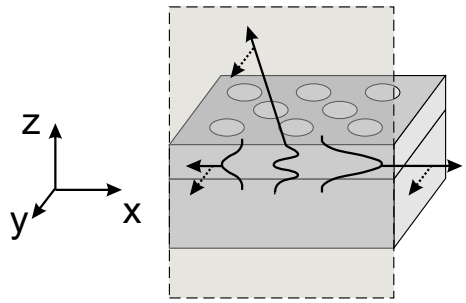

Figure 16. Sketch of a Bloch mode in a PhC-LED. The mode is composed of harmonics—one of which is here propagative in air and causes diffraction loss (also termed outcoupling).

Graphically, the condition of equation (9) can be represented in figure 17. The mode becomes leaky when its dispersion (folded in the reduced Brillouin zone) enters the air cone defined by $k_\parallel < k_0$. The cutoff frequency for this condition depends on the propagation direction of the mode: in the case of a triangular lattice for instance, it occurs first along the ΓM direction and last along the ΓK direction.

In this context, the two main figures of merit for light extraction are thus its angular dependence and its outcoupling efficiency. The angular dependence refers to the fact that for a given frequency and crystal type, only some (azimuthal and polar) angles of propagation can be diffracted out-of-plane. An ideal design yields diffraction for all angles (e.g. all guided modes) and is called omnidirectional. The outcoupling efficiency characterizes the length scale over which the mode is extracted. As seen from equation (11), this decay length is directly related to the imaginary part of the wavevector by $L_{\text{decay}} = 1/2k''$. It is a complex function of the parameters

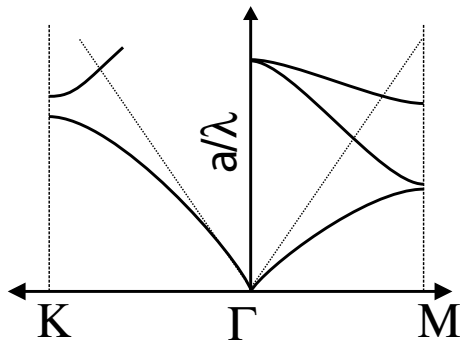

Figure 17. Band structure of a Bloch mode. The periodicity folds the dispersion relation of the guided mode in the reduced Brillouin zone. When the mode crosses the light line (i.e. when a harmonic satisfies equation (9)), diffraction to air is allowed. The corresponding cutoff frequency varies with propagation directions (here, it is different along ΓM and ΓK) so that a proper design is necessary to extract light propagating in all directions, for a given emission energy.

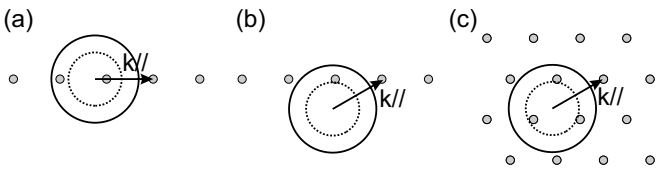

Figure 18. Ewald constructions. The solid circle represents the light cone of the substrate, the dashed circle the light cone of air. The arrow is the mode's wavevector and the points the reciprocal lattice. (*a*) 1D grating, propagation along the grating direction. Diffraction is allowed both to air and to the substrate. (*b*) Same as (*a*) with off-axis propagation: no diffraction to air is allowed. (*c*) 2D triangular lattice: diffraction to air becomes possible again.

of the PhC, as we will discuss in the following section. This optical decay of the guided mode, useful as it leads to light extraction, has to be evaluated against all other loss mechanisms due to various dissipation paths, which will diminish the extracted light fraction.

4.2. Some trends of diffraction efficiency

Reference [18] presents an in-depth discussion of the impact of various parameters on the diffraction efficiency of the PhC. It shows that, to a large extent, the in-plane and vertical (epitaxial) directions can be decoupled to understand the structure. We summarize some of the main conclusions below. In the in-plane directions, choice of the crystal lattice determines which azimuthal angles lend themselves to extraction. The structure in the vertical direction governs scattering efficiency.

4.2.1. In-plane directions. In the in-plane directions, choice of the crystal lattice (crystal type and period) determines which azimuthal angles φ will lend themselves to light extraction. As shown in figure 18, this is not trivial: one needs enough reciprocal lattice points to open diffraction channels for any φ and thus enable omnidirectional extraction. Clearly, a 1D lattice is not enough. The optimal choice of lattice depends on the refractive index n of the LED—a larger n will require

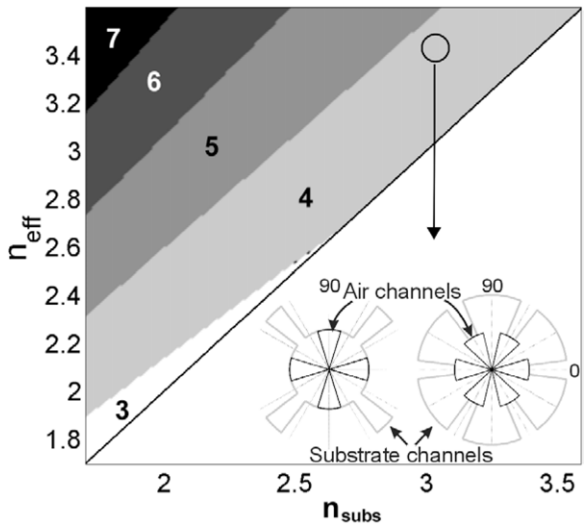

Figure 19. Upper left: optimal number N of nearest-neighbors in the reciprocal space, as a function of the guided mode's effective index and of the substrate/cladding index (extraction toward air). Lower right: illustration in the case of GaAs: diffraction channels toward air (black) and substrate (gray) as a function of azimuthal angle φ. The inner circle corresponds to one diffraction channel, the outer circle to two channels. Left: $N = 4$, right: $N = 6$. Reproduced with permission from [18]. Copyright 2007 IEEE.

more reciprocal lattice points for extraction. However, the picture is largely complicated by possible extraction into the LED's substrate guided modes. Increasing the number of diffraction channels also opens more detrimental diffractions to the substrate, and recovering this light can be difficult.

For this reason, use of a large pitch ($a \gg \lambda$) is usually sub-optimal: although it opens many diffractions to the extraction medium, it opens even more channels to the substrate. A better solution is to operate closer to the second Bragg order ($a \sim \lambda/n$) where the impact of substrate loss is mitigated. The optimal type of the lattice depends on the indices of the waveguide and of the substrate—figure 19 illustrates this. For instance, a simple triangular lattice is a good choice for the case of GaN on sapphire due to the low effective index of guided modes ($n \sim 2.4$).

For better performance, however, especially in the case of high n (such as in AlInGaP), one has to resort to more complex crystal lattices—such as Archimedean tilings. In such lattices, only a few reciprocal lattice vectors carry a strong diffraction efficiency and are concentrated along rings in k-space; they can be used for extraction to air, while detrimental diffractions due to other reciprocal lattice vectors are limited [20, 89].

We note that the optimal lattice is different in cases where substrate loss is not an issue—for instance in flip-chip LEDs where the substrate is removed (which can be carried out both for the InGaN and the AlInGaAsP systems). In such a situation, one usually wants to employ a larger period to increase the number of diffraction channels.

4.2.2. Vertical direction. The design of the PhC along the vertical direction is crucial in determining extraction efficiency. Indeed, diffraction of a guided mode by the PhC is directly dependent on the coupling between the mode and the PhC. In

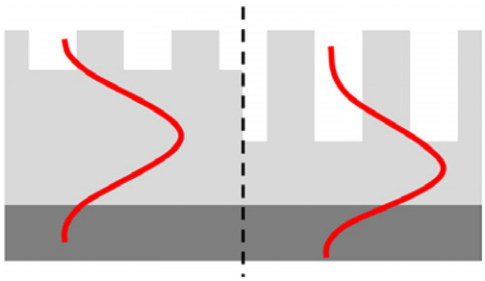

Figure 20. Monomode waveguide: mode profile versus PhC etch depth. If the PhC is shallow (left) the mode is mostly localized in the unetched waveguide and diffraction is limited. The PhC can be etched close to mode cutoff (right), forcing a strong penetration of the mode in the PhC. Also note the increased penetration in the substrate, giving rise to increased losses if this layer is absorptive.

most cases, guided modes have an evanescent profile in the PhC because they have a large effective index (close to that of the semiconductor matrix, i.e. the waveguide core) while the PhC layer has a lower average index. Penetration of the mode's electric field profile in the PhC governs the coupling and the value of k''.

As mentioned, the decay length of the mode due to diffraction is $L_{\text{decay}} = 1/2k''$. In practice, typical PhC pitches are in the range $a \sim 200$–500 nm. Therefore, a value $k'' = 0.1$ (in units of a^{-1}) would yield $L_{\text{decay}} \sim 1$–$2.5\ \mu$m (an extremely fast extraction, over a few periods only). A value $k'' = 0.001$ corresponds to $L_{\text{decay}} \sim 100$–$250\ \mu$m—an acceptable value, still on the same scale as the LED structure (provided there are no competing absorption mechanisms with a much shorter decay length)—and can be seen as an upper bound for desirable values of k''.

As discussed in [18], several PhC depth regimes can be distinguished. Very shallow PhCs (up to a few tens of nm) are in the Rayleigh scattering regime and weakly diffracting. Once a sufficient depth is attained however (a few hundred nm, corresponding to the typical leakage depth of evanescent mode in the PhC layer), diffraction efficiency becomes weakly dependent on the PhC depth, because modes tend to be pushed away from the low-index PhC and in the core of the waveguide.

In a monomode regime, one can etch quite aggressively to ensure quick diffraction of the mode, as sketched in figure 20.

Figure 21 depicts the modeled field profile in such a case. We consider a hypothetical GaN membrane partially perforated by an air grating. For simplicity we consider a 1D grating, so that the Bloch harmonics can be characterized by a single index p. As can be seen, the membrane is thin enough that the mode significantly penetrates the PhC. The fundamental ($p = 0$) harmonic resembles a guided mode. The $p = -1$ harmonic is propagative in air and enables light extraction. The maximum amplitude of the $p = 0$ and $p = -1$ harmonics is similar, suggesting a strong diffraction efficiency—indeed the calculation yields $k'' = 0.03$ for this mode, or an extraction length $L_{\text{decay}} \sim 15a$ (only a few micrometers in absolute units).

In a multimode structure, on the other hand, some of the modes (namely, the lowest-order modes, which are strongly localized in the unetched waveguide core) remain poorly

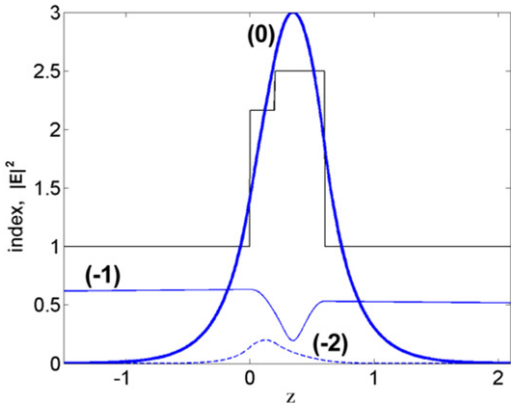

Figure 21. Harmonics of a Bloch mode in a GaN membrane (total thickness $0.6a$, perforated to a depth $0.2a$ by a 1D square air grating of period a and filling factor 0.3, at a reduced frequency $a/\lambda = 0.44$). The (-1) harmonic is propagative in air. The average index profile of the membrane is also indicated. Reproduced with permission from [17]. Copyright 2006 EDP Sciences.

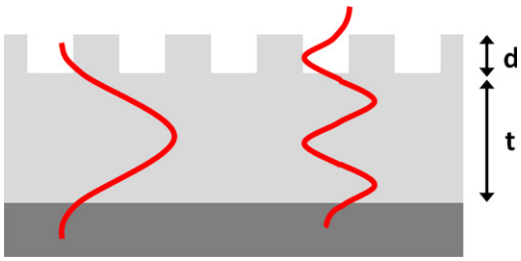

Figure 22. Typical modal profiles of a low- and a high-order mode. The low-order mode (in this case, the fundamental) is evanescent in the PhC region while the high-order mode is propagative. As the photonic coupling is proportional to the integral overlap between the PhC and the mode profile, high-order modes tend to have higher scattering efficiency.

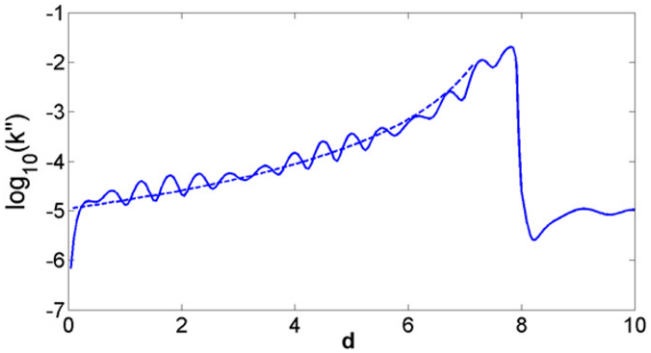

Figure 23. Imaginary part k'' of the wavevector due to light diffraction for the fundamental mode, versus PhC etch depth. The considered structure is a multimode GaN-on-sapphire waveguide of total thickness $8a$, etched with a triangular PhC ($f = 0.35$, ΓM direction, $u = 0.44$, depth d/a). The dashed line indicates the fit $k'' \sim t^3$, valid while the mode is evanescent in the PhC. Reproduced with permission from [18]. Copyright 2007 IEEE.

extracted. Figure 22 depicts schematic modal profiles of low- and high-order modes.

Figure 23 shows the modeled diffraction efficiency versus PhC depth d (in units of a), for the fundamental mode of a multimode GaN structure: it remains weak except for a very

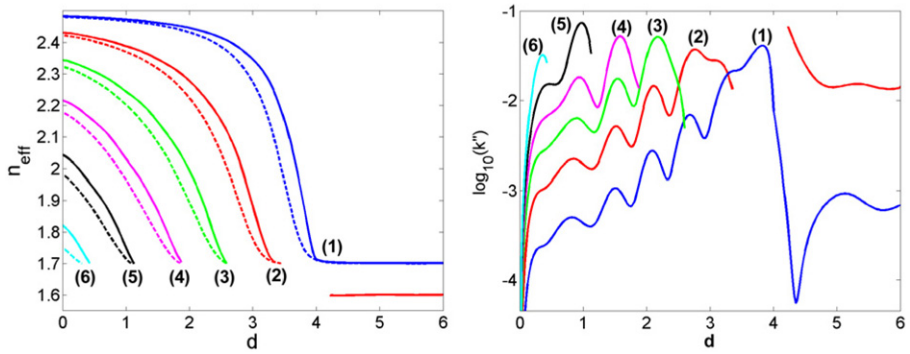

Figure 24. Extraction versus PhC depth in a multimode PhC waveguide. The considered structure is a multimode GaN-on-sapphire waveguide of total thickness $4a$, etched with a triangular PhC ($f = 0.5$, ΓM direction, $u = 0.39$, depth d/a). Left: effective index of the TE (solid) and TM (dashed) modes. Right: corresponding value of k'' for the TE modes. Reproduced with permission from [17]. Copyright 2006 EDP Sciences.

deep etch—as a reminder, a value $k'' = 10^{-3}$ can be seen as a minimum for decent extraction. As shown in [18], in the perturbative regime where the mode is evanescent in the PhC, its extraction efficiency k'' is governed by the unetched waveguide thickness t—namely $k'' \sim t^{-3}$. Here, $t < 2a$ is required for good extraction.

Figure 24 shows the diffraction efficiency for all TE modes in a multimode GaN waveguide. For the unetched waveguide, 6 TE modes are supported. As the PhC is etched deeper, high-order modes get cut off while diffraction improves for low-order modes. Again, we see that good extraction of the fundamental is only possible for an unetched core thickness $t \sim 2a$, where most of the other modes have been cut off. In a realistic structure, this means one needs to leave less than 500 nm of GaN unetched (out of an initial thickness 4–8 μm). This is clearly challenging: fabrication of such a deep-etch structure is not feasible from a practical standpoint, and electrical injection would be very challenging for the same reasons as in the full-band-gap approach (section 3). Experimental proof of this limitation will be discussed in section 4.4.

Finally, one needs to keep in mind that the value of k'' due to diffraction is only relevant when compared with the sources of dissipative loss in the LED—such as absorption in metallic contacts and the active region. Figure 25 illustrates this point in the case of a laser lift-off (LLO) PhC-LED. In these LEDs, which will be described and discussed in section 4.5.2, the p-GaN is covered with a metallic mirror whose absorption directly competes with PhC extraction. Clearly, a high-reflectivity metal is necessary to obtain good extraction.

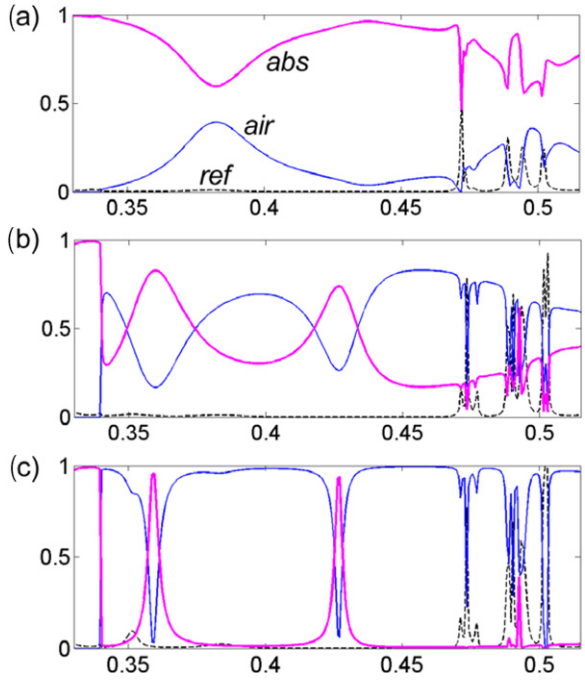

Figure 25. Modeled balance, as a function of normalized frequency $u = a/\lambda$, of absorption (thick magenta line), extraction to air (thin blue line) and reflection (dashed black line) for three implementations of LLO-PhC-LEDs with various p-mirrors. In each case the GaN layer is 600 nm thick, and etched by a triangular PhC (depth 270 nm, filling factor 0.3). (*a*) Au mirror, 20 nm SiO_2 layer optical insulation between mirror and LED. (*b*) Au mirror, 200 nm SiO_2 layer optical insulation between mirror and LED. (*c*) Ag mirror, 200 nm SiO_2 layer optical insulation between mirror and LED. Reproduced with permission from [21]. Copyright 2006 American Institute of Physics.

4.3. Experimental realizations in conventional III–V compounds

4.3.1. Early work, AlGaAs. When the disruptive possibilities of PhCs for LEDs appeared, the natural optoelectronic semiconductor to attempt implementation was GaAs. However there was no true need to improve GaAs LEDs, as their efficiency was not a limiting factor in mass applications such as remote control, unlike the case of solid-state lighting. Thus, GaAs, and also to some extent InP, were used more as vehicles for the first demonstrations [32]. GaAs has the advantage of a relatively large index contrast with AlAs or AlOx, allowing guided modes in relatively thin layers on a substrate. Such factors were key to the record extraction of 28–29% by a planar GaAs micro-cavity structure for instance [90].

4.3.2. More recent compounds: AlInGaAs, AlInGaP. However, these advantages tend to vanish when it comes to the parent compound AlInGaAs or AlInGaP [51]. In these

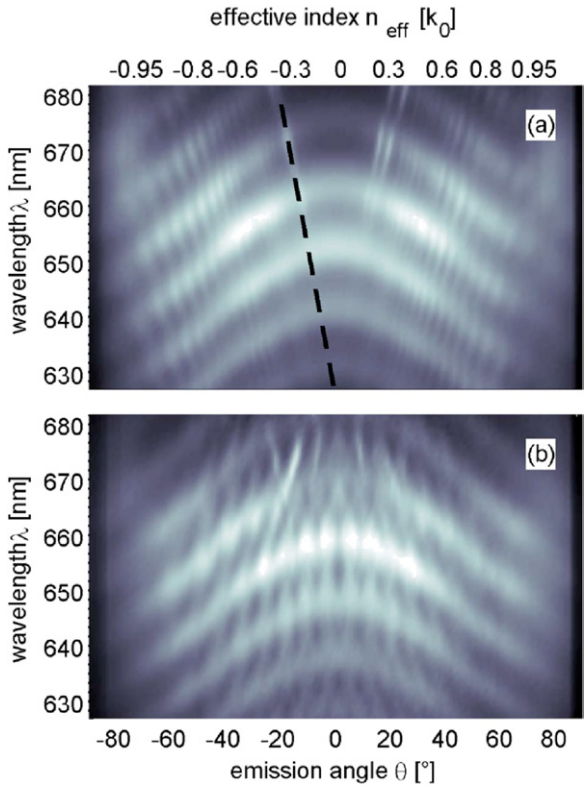

Figure 26. Far-field patterns of AlInGaP LEDs (resolved in wavelength and angle), illustrating the impact of the reciprocal lattice vector G. (a) $G = 3.4k_0$ (small lattice constant) (b) $G = 1.7k_0$ (larger lattice constant). Depending on the value of G, different types of guided modes are extracted—corresponding to different sets of diffraction lines in the air cone. Reproduced with permission from [8]. Copyright 2008 American Institute of Physics.

materials, well suited for emission in the red to orange range, the vertical index contrast is weaker, and structures are thicker.

Therefore, the first impression was that a top grating would not act as strongly as it would on a single guided mode. Nevertheless the interest of OSRAM-OS, most notably, triggered in-depth studies of the issue. A first promising report in [55] gave improvements of over a factor of two but starting from devices with modest efficiency due to their GaAs substrate. Triggered by the advent of thin-film LED with back-mirrors, integration of PhC extractors to this class of structures with a fairly good initial EQE was addressed in a recent string of papers [8–10, 112].

The lattice constant was then used as the central parameter, and although it is an in-plane parameter, it can be considered as a handle to indirectly probe the role of the vertical structure: the various modes visit the vertical structure in different ways according to their propagation angle, which is directly related to their in-plane propagation constant. This work uses the concept of effective index, directly related to the propagation constant, which we will develop further in section 4.4. Targeting modes of a given effective index thanks to a given in-plane periodicity is then a relevant strategy: the lattice constant of the extracting PhC appears as a way to select modes whose effective index indicates that they can be extracted due to their vertical profile. Figure 26 illustrates

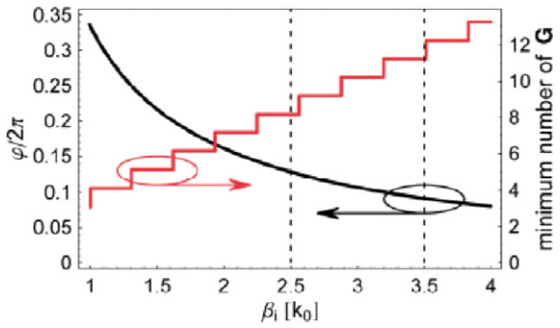

Figure 27. Left scale: fraction of the in-plane directions diffracted to air by a vector of the reciprocal lattice, as a function of the in-plane k-vector. Right scale: minimum number of reciprocal lattice vectors with length G necessary for extracting all in-plane directions to air. Reproduced with permission from [112]. Copyright 2009 Wiley.

how the choice of the lattice constant selects which modes are extracted.

However, the integrated behavior of extraction versus lattice constants involves several averaging steps and is a rather smooth function, limiting the returns of this strategy if it is not complemented by other spectral or angular effects. In the case of GaAs and AlInGaP, the largest guided mode wavevector is typically $k = 3k_0$, and its extraction is optimal for reciprocal wavevector of nearly the same magnitude, $G = 3.0k_0$–$3.4k_0$. In such a case, even a hexagonal lattice only extracts 56% of the guided light to air through its six first-order channels. The corresponding approach of optimal lattice with 'adjustable angular symmetry' calls for more reciprocal vectors than shown in figure 19, although the trend of figure 27 is similar to that we described above.

The most notable result for a red device was reported in [8], with an LED emitting at $\lambda = 650$ nm reaching an EQE of 15.5% in air and 26% with encapsulation, and an EQE enhancement of 2.6. The extraction of comparable record non-patterned devices is 5.9%: these are resonant-cavity LEDs which use transparent conductive oxide and gold contacts to achieve a planar micro-cavity (thus circumventing the weak reflectivities of semiconductor DBR stacks in this AlInGaP composition range). This extraction is rather low because such cavities have relatively weak micro-cavity enhancements, due to metal absorption.

As a consequence of this analysis and of the fact that proper extraction was achieved only for some of the modes, a more successful result is obtained only for a combination with a thinning strategy for the device which in turn allows sticking to the choice of a shallow PhC, since the fractional overlap with the grating remains large enough to grant a sufficiently quick extraction. The relatively surprising result in this work is the better extraction for the shorter G values, $G = 1.5k_0$, i.e. for the largest period of the PhC (∼500 nm). The extraction of guided modes of low effective index (see section 4.4 for details of this quantity), which is important in this thin structure, is determined as a key factor for the observed behavior in the detailed analysis. Care should be taken, however, to assess the possible role of etching quality for shorter pitches.

Another important trend in this situation, notably for display application rather than lighting, is the sizable gain

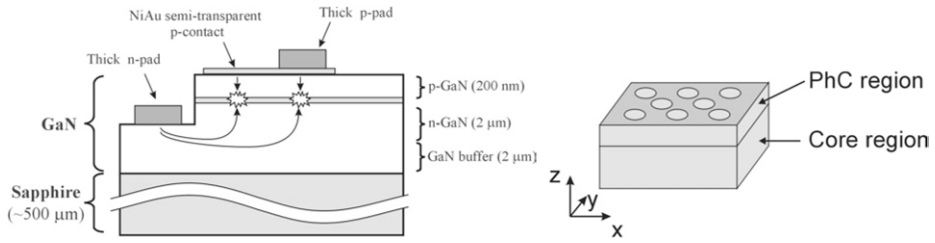

Figure 28. Left: typical cross-section of a GaN-based LED. Right: geometry of a surface PhC in a GaN LED. The PhC is only etched in part of the GaN waveguide.

in directionality (or brightness). In other words, if we consider extraction in a limited angular range in air, then the enhancement can be significant: the emitter is actually non-Lambertian, concentrating 31% of light in a 30° aperture, against 25% for a Lambertian case.

Finally, the study compares favorably the temperature dependence of a PhC-LED with that of the same underlying micro-cavity LED (MCLED): the PhC extraction mechanisms have more room in k-space to occur, and therefore prove more stable against temperature. A subsequent theoretical account confirmed the main trends but acknowledged that quantitative fitting was delicate [111].

The trends found above can be confronted with those found for a similar GaN configuration, although we will study GaN in more detail later. In a subsequent work [9], the same team found that extraction was enhanced by a factor 1.8 and directionality by a factor 4.3. The argument used was, however, of some generality, involving that with a somewhat larger air fraction than commonly used, the diffraction efficiency at the second-order diffraction vectors could result in substantial extraction gain because the losses of the modes able to undergo this latter diffraction channel are comparatively smaller with respect to quantum well reabsorption notably. In principle, testing whether this strategy has a more general impact would be a nice idea, but the range of effective indices spanned by useful guided modes is usually more restricted than in AlInGaP, making the test delicate.

At the present stage, PhCs can successfully provide extraction gains in AlGaInP devices, but the requirement for thinner devices in the sub-micrometer range seems very demanding in the near future. Quicker progress is expected from a variety of other approaches relevant to AlInGaP.

It should be noted that various other light-extraction schemes are employed by the industry in these materials and show excellent performance. Some are based on geometric optics: a GaAs thin layer can be transferred on a transparent GaP substrate, which is then shaped for enhanced extraction beyond 60% [60]. Thin-film substrateless solutions, based on a similar implementation in GaN, are also efficient: [102] demonstrated a red LED based on thin-film technology with a wall-plug efficiency of 61%. Today, various industrial actors have adopted this approach for high-efficiency, high-brightness red chips. The existence of these various efficient approaches obviously raises the required performance for adoption of a PhC-based approach.

4.4. Experimental realizations in InGaN: first attempts, surface PhCs

After the appearance of III-nitride LEDs in the 1990s, the prospect of their widespread lighting application at the turn of the millennium reignited the research on PhC-assisted light extraction, because the different geometry and constraints of this semiconductor family led to different paths for optimization. The first nitride PhC-LEDs were demonstrated in 2002 [78, 79], and numerous designs have been proposed since then—an amount and variety unique to this system. We first discuss the early attempts using a surface PhC geometry, and then focus on more sophisticated schemes.

Figure 28 shows the typical cross-section of an InGaN LED layer grown on a sapphire substrate. Due to materials quality issues, growth has to start with a GaN buffer layer that is 3 to 6 μm thick to reduce defects before the active region is grown, and the pn junction is located close (100–200 nm) to the surface and capped by p-doped GaN. The easiest way to form a PhC in such a structure is therefore to etch the surface of the epitaxial layers. One can retain a shallow etch (∼100 nm) which does not pierce through the active region, or etch a deeper PhC if a stronger photonic coupling is sought.

Early implementations opted for a shallow etch in part for practical reasons—GaN is a hard material and shallow PhCs are more readily obtained. A shallow etch is also more tempting because it leaves the active region intact. The first measurements of PhC on GaN were reported in 2003–2004 by Kansas State University [79], where the PhC were studied in near-field optical microscopy. The same group later demonstrated current-injected devices [78]. The final light-extraction enhancement of these first devices was quite modest: ×1.7–2, compared to a design with low extraction. Moreover, the formation of the PhC negatively impacted the electrical characteristics of the LED. Other groups aimed for a slightly deeper etch, but never more than a few hundred nm.

Wierer *et al* also proposed an alternative design in [109]: to circumvent the damage to the p-GaN, a tunnel junction is created so that the top layer of the LED is n-doped and can resist the etch damage. This structure is shown in figure 29: recombinations happen away from the metallic contact and below the PhC region. Again, the extraction enhancement was only ×1.5. The authors also demonstrated a first example of directionality control by tuning the pitch of the PhC.

As we can see, however, none of these early implementations yielded very high performance. Absolute performance (e.g. calibrated extraction efficiency) was never

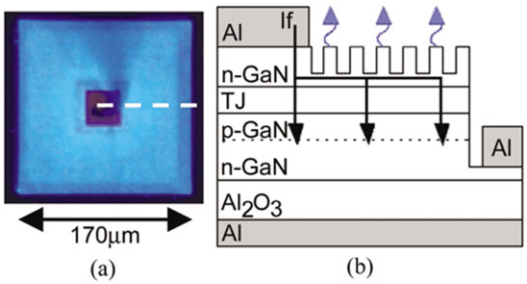

Figure 29. Tunnel-junction PhC-LED. (*a*) Top view of the LED. The emitting region is patterned with a PhC. (*b*) Cross-section of the device showing current spreading in the tunnel junction. Reproduced with permission from [109]. Copyright 2004 American Institute of Physics.

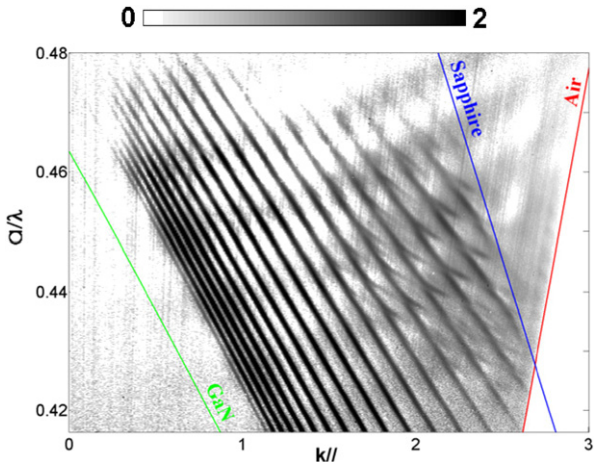

Figure 30. Experimental photonic band structure of a GaN PhC-LED with a shallow etch. The gray scale is in $\log_{10}$ scale. Various dispersion lines are shown. The air line ($n = 1$) corresponds to the light cone. All the modes are enclosed between the sapphire line ($n = 1.7$) and the GaN line ($n \sim 2.4$), as sketched in figure 31. However, a number of modes very close to the GaN line are not observed experimentally: these are the low-order modes, which are not well extracted by the PhC. Reproduced with permission from [25]. Copyright 2005 American Institute of Physics.

reported, but the enhancements were typically less than a factor of 2, the reference being a standard GaN-on-sapphire LED whose extraction efficiency can be expected to be ∼10–20% at best.

In [25], a team comprising the present authors investigated the optical properties of such shallow PhC structures with angle-resolved photoluminescence experiments. The measurement enabled them to derive the experimental photonic band structure of the extracted modes, as shown in figure 30. This measurement reveals the existence of a large number of photonic modes, stemming from the multimode nature of the GaN waveguide (figure 31). The key conclusion of [25] is that only some of the guided modes supported in the GaN layer (the high-order modes) are prone to efficient interaction with a shallow PhC: the low-order modes are strongly confined in the GaN layer and barely overlap with the PhC, thus yielding very weak diffraction efficiency. This experimental result is in line with the theoretical discussion in section 4.2.2.

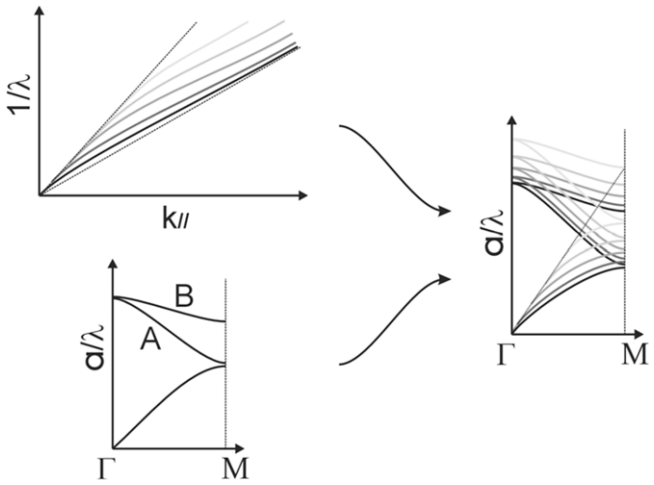

Figure 31. Construction of the photonic band structure in a GaN PhC-LED: the thick GaN waveguide supports tens of guided modes, each characterized by a dispersion relation. The bands are folded in the reduced Brillouin zone due to the periodicity brought by the 2D PhC. Those photonic bands which cross the air line are diffracted to air, and collected in the experiment of figure 30.

This explains the modest extraction improvements observed in all early implementations of surface PhC-LEDs. The general physical message was later confirmed by the AlInGaP studies reported above: surface gratings do not extract all modes, unless a specific structure is used to address this issue.

To quantify the importance of this limitation, we introduce the effective index of a guided mode:

$$n_{\text{eff}} = k_{\parallel}/k_0, \tag{12}$$

where $k_{\parallel}$ is the in-plane wavevector of the mode and $k_0 = 2\pi/\lambda_0$ the wavevector in free space. This notion is in principle ill-defined for a Bloch mode since $k_{\parallel}$ is only defined modulo the reciprocal lattice vectors $\boldsymbol{G}$. However, for a shallow PhC, one harmonic of the Bloch mode carries the majority of the power (see the typical modal profile of such a Bloch mode in figure 21) and the concept of effective index remains relevant.

Let us call n_{PhC} the average value of the refractive index in the PhC layer. We now define a mode as a high-order mode if $n_{\text{eff}} < n_{\text{PhC}}$ and a low-order mode otherwise. For low-order modes the main harmonic of the mode is evanescent in the PhC and the overlap is small, whereas for high-order modes the harmonic is propagative and overlaps well with the PhC. Therefore, one can set a rough cutoff $n_{\text{eff}} = n_{\text{PhC}}$ for well-extracted modes.

Typically, the implementations described above used a PhC with filling factor $f \sim 0.3$–0.35, yielding $n_{\text{PhC}} = \sqrt{f + (1-f)n_{\text{GaN}}} \sim 2$–$2.1$. This means that modes are poorly extracted when $n_{\text{eff}} > 2.1$, corresponding to a propagation angle $\theta \sim 60°$ from vertical. Taking into account the angle-dependent emission pattern from quantum wells, this means that ∼30% of the total emitted light does not interact well with the PhC! Reducing the filling factor f of the PhC somewhat mitigates this effect, but is not desirable because a small $f < 0.2$ lowers the overall diffraction efficiency of the PhC.

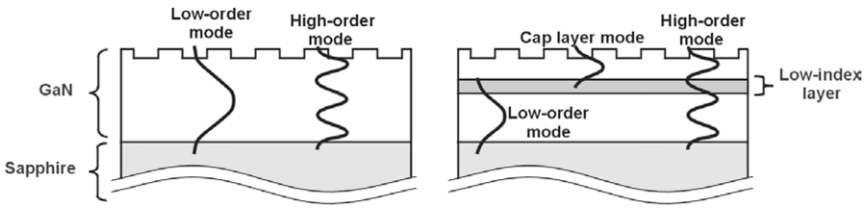

Figure 32. Distribution of guided modes (left) in a standard GaN structure and (right) in a structure with an AlGaN layer for modal confinement. The AlGaN cladding creates a cap-layer mode confined close to the surface of the LED for improved interaction with the PhC. Reproduced with permission from [22]. Copyright 2006 American Institute of Physics.

We note that even after nearly a decade of research on the subject, the surface PhC approach remains the focus of much work. Several groups have tried to circumvent the damage to the *p*-GaN by depositing a transparent contact (typically ITO) and forming the PhC in the ITO rather than in the p-GaN directly. In this case, the electrical performance of the device is essentially unaffected. The optical performance, however, is degraded for two reasons. First, the index contrast between ITO ($n \sim 1.8$) and air is modest, leading to a weak photonic strength. Second, the average index of the patterned ITO layer is low ($\sim$1.3) so that very few of the guided modes of the structure interact with it. This illustrates an important and often-neglected trade-off in designing an efficient PhC light extractor: index contrast should be maximized for good photonic strength, but a layer with a low average index tends to repel guided modes.

In conclusion, this analysis suggests that the PhC design along the vertical direction is crucial in GaN-based LEDs. Simply forming a surface PhC is not sufficient for good extraction, and the PhC geometry and the guided modes distribution must be adapted to one another to improve their interaction. In the following section, we review such attempts.

4.5. Experimental realizations in InGaN: advanced structures

In the past few years, several implementations were suggested to increase the PhC interaction with the guided mode of the structure.

4.5.1. Tailored guided mode distribution. A first approach consists in retaining a surface PhC but varying the refractive index profile in the structure, so as to tailor the distribution of guided modes. Figure 32 shows how the introduction of an AlGaN cladding below the p–n junction affects the profile of guided modes. AlGaN with $x_{\mathrm{Al}} \sim 15$–20% has a low index $n_{\mathrm{AlGaN}} \sim 2.3$ (the amount of Al in the film being limited by strain). Modes whose effective index is lower than n_{AlGaN} are essentially unaffected by the presence of this layer. However, modes of higher effective index are confined on either side of the cladding. Modes confined below the cladding—which are also those modes poorly extracted by a surface PhC—do not overlap with the active region, and therefore do not receive SpE. Meanwhile, the layer above the cladding acts as a thin waveguide, which can support a few modes—so-called *cap-layer modes* (CLM). If the cap layer is thin enough, it contains only one mode that overlaps well both with the active region (thus receiving a substantial fraction of SpE) and with the surface PhC (thus being efficiently diffracted). Therefore, the modes which receive SpE are either high-order modes or the cap-layer mode, all of which are well extracted.

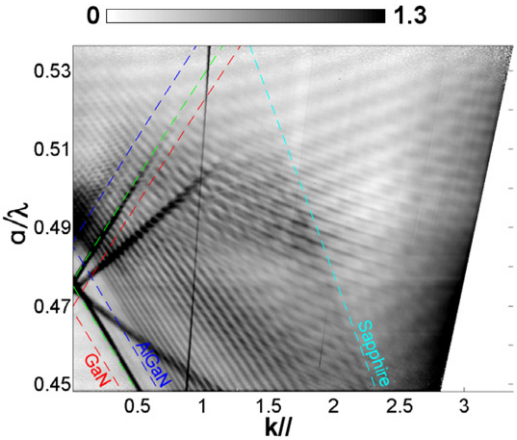

Figure 33. Experimental photonic band structure of a GaN PhC-LED with an AlGaN layer for modal confinement. The gray scale is in $\log_{10}$ scale. In contrast to figure 30, an intense line is seen between the GaN and AlGaN dispersion lines: it corresponds to diffraction of the cap-layer mode (CLM). Reproduced with permission from [22]. Copyright 2006 American Institute of Physics.

This concept was introduced and demonstrated in [22]. The effect of the AlGaN layer is confirmed by measuring the angle-resolved pattern of the LED, as was shown above for a regular structure. In this case the CLM appears as an intense additional mode in the band structure (figure 33), with an effective index $n_{\mathrm{eff}} \sim 2.4$. The strong intensity of the CLM compared with other modes (note that the figure is in log scale) confirms that it channels a large fraction of the total emission.

In spite of this proof of concept, the performance of the resulting LED remains limited: the enhancement over a reference LED is estimated to $\times$1.7–2, corresponding to an extraction efficiency in air $\sim$20–24%. This can partly be attributed to the lack of optimization of the structure. Moreover, one drawback of this approach is that it still requires a surface PhC etched in the p-GaN. This makes the contacting scheme difficult: one has to resort to a semi-transparent metallic p-contact (which is in practice quite lossy) or deposit a transparent conducting oxide layer such as ITO, which lowers the index contrast and also causes some absorption. In any case, the interaction of the various modes with the PhC still remains limited, yielding rather large extraction lengths of one to a few hundred micrometers.

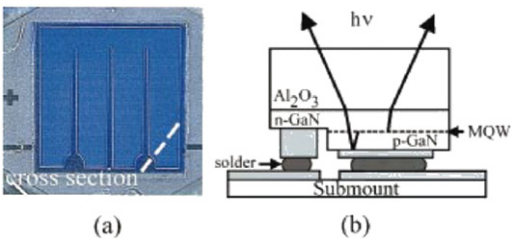

Figure 34. Flip-chip GaN LED: the LED is flipped on a carrier and uses a large-area reflective p-contact. Part of the epilayer is etched down to the n-GaN to provide the n-contact. Reproduced with permission from [110]. Copyright 2001 American Institute of Physics.

4.5.2. Flip-chip, thin film PhC-LEDs. While the previous approach mostly focused on top-emitting LEDs, the preferred approach in the LED industry—especially for high-power chips—is the so-called flip-chip geometry (figure 34) introduced in [110]. In this case, the p-layer of the LED is fully covered by a high-reflectivity mirror such as silver, which also serves as the p-electrode. The LED then emits light through the sapphire substrate. The geometry enables good thermal dissipation and is therefore adapted to high drive currents. A subsequent improvement for light extraction is to remove the sapphire substrate (using the laser lift-off (LLO) technique) and to alter the surface of the LED. Through photo-electro-chemical etching, one obtains a random texturing of the n-side of the LED (see figure 41 in section 5). This approach is very efficient and is widely used in the industry, yielding extraction efficiencies of ∼65% in air and ∼80% in epoxy [60, 92].

Instead of using a random surface texture, one can opt for a PhC patterning and try to make the light extraction efficiency better than in the random case.

Moreover, the n-side of the LED can be thinned down—for instance by mechanical polishing or by dry etching—in order to enter the micro-cavity regime: when the LED thickness is of the same order as the wavelength, the radiation pattern of the LED is affected and its extraction efficiency can be improved. Indeed, instead of supporting many modes inside and outside the extraction cone (in which case the extraction efficiency varies with the ratio of solid angles), the LED supports only one mode in the extraction cone and a few guided modes, enabling departure from the statistical ratio of solid angles. Such LEDs are called MCLEDs [6] and have been demonstrated in III-nitrides in [36, 83]. While the micro-cavity approach itself can only boost extraction efficiency to ∼45% because it never prevents the existence of guided modes [6, 28, 105], it can be combined with a PhC structure to also extract guided modes.

In this case the structure design is complex, as was already known for GaAs-based systems [27]. One has to design the micro-cavity for resonant extraction, but also make sure that the remaining guided modes are prone to efficient interaction with the PhC. A first demonstration of such a structure was reported in [21]. The combination of the micro-cavity effect and the diffractive effect of the PhC was confirmed by band structure measurements. However, these structures suffered from an unoptimized optical design (namely, lossy mirrors) and performed poorly. As already discussed above (figure 25), choice of a high-reflectivity p-mirror is essential in the case of an LLO-PhC-LED.

More recently, a very efficient structure following this approach was reported in [108] (figure 35). In that work, a wide variety of experimental designs was spanned: the pitch, depth and type of the PhC lattice were varied systematically on-wafer in order to determine an optimal design. Moreover, the GaN layer was thinned down to 500 nm–1 μm in order to harness the micro-cavity effect in conjunction with PhC extraction. Finally, a low-loss Ag-based p-mirror was employed to reduce dissipation in the LED. In order to determine C_{ex}, η_{IQE} was measured by various means. The best structures display an extraction efficiency ∼73%. The corresponding PhC is an Archimedean A13 lattice [3, 88] with a lattice constant $a = 455$ nm, a filling factor $f \sim 0.3$ and a depth $d = 250$ nm. It is noteworthy that the optimal pitch in that work is rather large: the PhC no longer operates near the second Bragg order. As discussed in section 4.2.1, in the presence of a reflective p-mirror diffraction to the substrate is no longer an issue, which enables the use of such a large pitch.

It was the first time that a PhC-based GaN LED demonstrated performance superior to the commonly employed random surface texturing. To date, this work constitutes a record for reported extraction efficiency to air. Moreover, the structure employed a realistic device geometry. Despite this demonstration of high performance, the adoption of the technology by the industrial world is also dictated by other factors (such as cost of manufacturing and the necessity to modify a well-established process) and remains uncertain at this point.

Finally, recent work also studied the added benefit of directionality in a LLO-PhC structure [87] and concluded that directionality can be strongly affected by all the parameters of the LED. Figure 36 shows how varying the depth of the PhC layer modifies the far-field pattern. This can be understood by remembering that the guided mode dispersion is mainly determined by the thickness of the unetched core of the LED, which is implicitly varied in this experiment. The studies by Bergenek and by Wiesmann with a first account of these trends should also be mentioned [9, 112].

Rangel *et al* also studied the relative performance of the PhC approach and the surface roughness approach in a thin-film structure (figure 37): in their implementation, the PhC-LED is slightly brighter than the roughened LED. The absolute EQE performance reported in this work is not large compared with state-of-the-art industry results. This can be attributed both to the lower quality of the epitaxy, and to the unoptimized metal contacts used, which yield larger optical losses. However, the comparison of PhCs and surface roughness on the same wafer provides a fair benchmark for a given level of optical dissipation mechanisms. We will further explore the comparison of the PhC approach and the surface roughness approach in section 5.

4.5.3. Embedded PhC. As seen above, the key difficulty lies in ensuring a strong interaction between the guided modes and the diffracting PhC. To this effect, several groups have

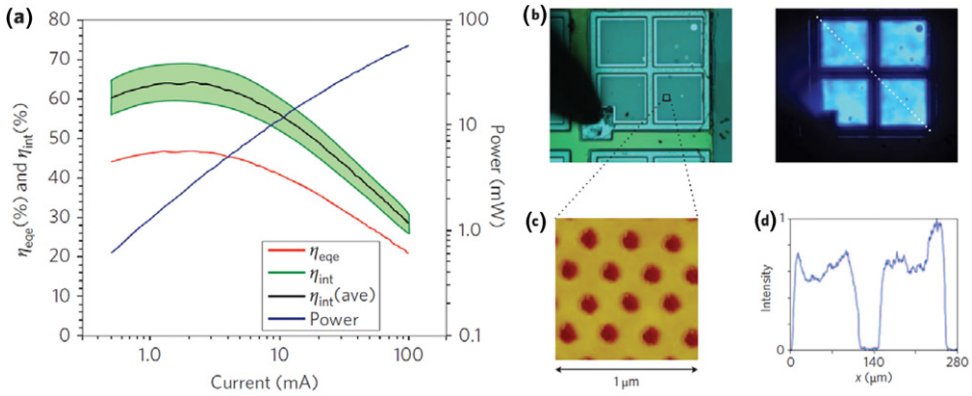

Figure 35. LLO-PhC-LED with high-extraction efficiency. (*a*) External quantum efficiency (red), total light output power (blue), estimated bounds for η_{IQE} (green area) and average η_{IQE} (black) versus current. (*b*) Top view of unbiased (left) and biased (right) PhC-LEDs. The LED sides are $\sim$200 μm in length. (*c*) Top-view atomic force microscope image of the triangular lattice PhC. (*d*) Cross-section of the light intensity profile corresponding to the oblique white dotted line of the biased case in (*b*). Reproduced with permission from [108]. Copyright 2009 Nature Publishing Group.

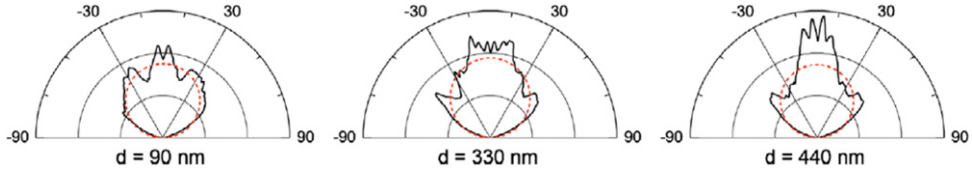

Figure 36. Experimental far-field pattern of thin-film PhC-LEDs with varying PhC depths of $d = 90$ nm, 330 nm, 440 nm. The dashed line shows a Lambertian reference. Reproduced with permission from [87]. Copyright 2011 American Institute of Physics.

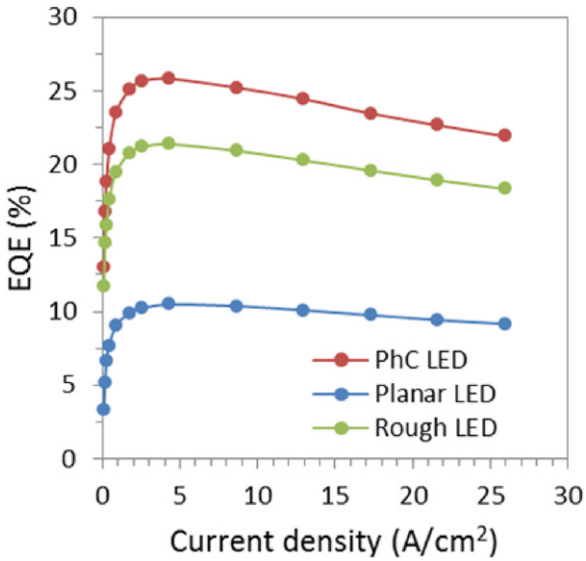

Figure 37. Comparison of external quantum efficiency for smooth (blue), rough (green) and PhC (red) LEDs. In this case the PhC-LEDs are slightly brighter than the roughened LEDs [85].

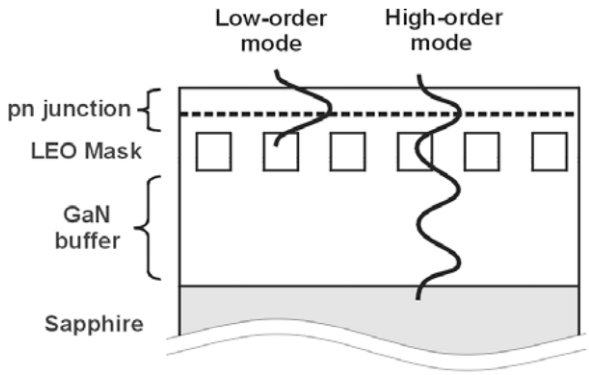

Figure 38. Cross-section of a LEO PhC-LED. The embedded dielectric layer serves as a mask for regrowth and as a PhC for light diffraction. Reproduced with permission from [26]. Copyright 2008 American Institute of Physics.

suggested inserting the PhC *within* the epitaxial layers. In practice, this can be achieved using the method of lateral epitaxial overgrowth (LEO) where a hard mask (typically SiN or SiO_2) is deposited on a GaN template, patterned and covered by GaN in a subsequent epitaxial step. Figure 38 displays a typical cross-section of such a LEO structure.

This approach offers several key advantages. First, the properties of the PhC can be optimized to ensure a very efficient diffraction of all modes. Because the PhC is placed inside the epilayer, even low-order modes have a relatively large overlap with it. Second, the resulting epitaxial structure is planar and fully compatible with standard LED fabrication techniques. The difficulty of forming contacts around the PhC is avoided, and no specific post-processing is necessary. Notably, a simple flip-chip geometry can be used, which makes this approach amenable to high-power LEDs.

However, fabrication of such a structure is not trivial. While the technique of LEO has been extensively studied in the past decade [40], it is usually applied to laser diodes, where the SiO_2 stripes being overgrown are large (several μm to tens of μm) and 1D. In the present context, the dimensions are much smaller (fractions of a μm) and high-extraction efficiency can

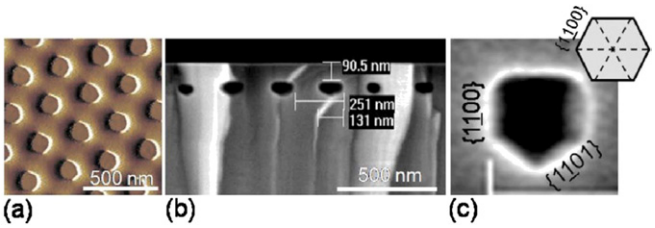

Figure 39. Air-gap embedded PhC structure. (*a*) AFM of the etched GaN sample before regrowth. (*b*) SEM cross-section after regrowth. (*c*) SEM vertical cross-section of an air gap showing crystallographic facets. Reproduced with permission from [72]. Copyright 2009 American Institute of Physics.

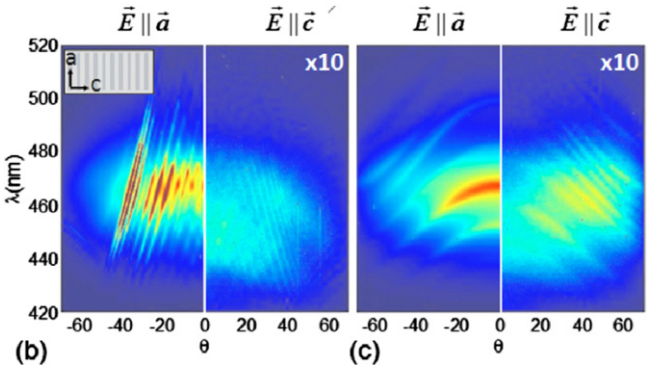

Figure 40. Angle-resolved emission diagram versus propagation direction in an *m*-plane GaN LED with (*b*) and without (*c*) an air-gap embedded PhC. Due to the polarized emission from *m*-plane GaN and to the polarization-conserving properties of the 1D PhC, the external emission diagram remains polarized along the *a*-axis. Reproduced with permission from [71]. Copyright 2011 American Institute of Physics.

only be achieved using a 2D PhC. Thus the growth process must be adapted to this new geometry and optimized to minimize defects—the coalescence front of the regrown layer being prone to the formation of threading dislocations.

An early demonstration points out that the extraction efficiency can be increased by maintaining the overgrown region thin enough [26]. However, the corresponding implementation only employed a 1D grating, limiting the performance. Several other demonstrations were subsequently produced by various groups, but they usually insisted on the growth technique more than on the optical design of the PhC.

An essential design parameter is the thickness of the overgrown layer containing the active layer. It must be thin enough to ensure good interaction of the guided modes with the PhC, ensuring that the guided modes are extracted before being dissipated along its propagation (by free carrier absorption, quantum well reabsorption, metal losses, etc). As the guided mode least interacting with the PhC is the fundamental ($j = 1$) mode, it is a good probe to assess diffraction efficiency. Matioli *et al* modeled the extraction length of that mode as a function of overgrown layer thickness and buried PhC depth, a typical extraction length being on the order of 100 μm [73].

Recently, a new design employing air-gap PhCs (rather than typical inclusions of a dielectric material such as SiO_2) was introduced in [72] as shown in figure 39. Using this approach, a 2D demonstration with an optimized design producing a very high-extraction efficiency of 94% (extraction to epoxy) was reported in [73]. Although the error bar is large, the reported performance is superior to that of surface-roughened structures. However, the structure employed is impractical; superior performance in a realistic LED geometry still remains to be demonstrated.

4.5.4. Embedded PhC in m-plane GaN LEDs. More recently, embedded PhCs were applied to a new class of GaN-based LEDs. Until recently, the majority of GaN structures were grown along the *c*-plane on a foreign substrate (usually sapphire, SiC and more recently Si). However, in the last few years, high-quality native GaN substrates have become available and have prompted growth of devices along other crystal planes, such as the *m*-plane, the *a*-plane and semipolar orientations. These orientations open exciting new possibilities for optoelectronic applications, as they enable the reduction of the polarization fields (caused by the crystal's wurtzite symmetry) that govern the device physics (carrier transport and recombination rates) of *c*-plane GaN LEDs. In particular, *m*-plane GaN LEDs and laser diodes have demonstrated spectacular recent progress, in part attributed to the absence of polarization fields.

Another intriguing property of *m*-plane GaN LEDs is the polarization properties of the emitted light. Due to the symmetry of the valence bands, the top facet emission is strongly polarized along the *a*-axis. Interestingly, the guided light is directional (it propagates along the *c*-axis) and is polarized along the *a*-axis (at least when the quantum wells are strained, which is the case for useful visible wavelengths around $\lambda = 450$ nm and beyond). Thus, a polarization-conserving light-extraction scheme is highly desirable, as it would enable high-efficiency fully polarized LEDs, which are desirable in display applications. Typical approaches to light extraction, such as surface roughening, unfortunately scramble polarization. Properly designed PhCs, on the other hand, can conserve polarization—especially in this simple case, where all the guided light possesses a well-defined polarization. In [71], such an implementation was demonstrated. The authors grew *m*-plane LEDs with an embedded 1D PhC grating (this is enough for proper extraction here, due to the unusual directionality of the guided light). The grating conserved the polarization of the guided light, yielding an LED with a highly polarized emission spectrum. Figure 40 illustrates the polarized angle-resolved emission of such a structure along the two nonequivalent in-plane axes.

5. Comparison of diffracting PhCs and random surface roughening

The approach described in section 4.1—using the PhC as a diffracting element to outcouple guided modes—is generally seen as the most promising one to obtain high-efficiency PhC-based LEDs. This is because it is compatible with planar fabrication, and because it has led to the best experimental results to date. However, a key question for real-world application is whether PhC-based LEDs can compete with the solutions currently used in the industry.

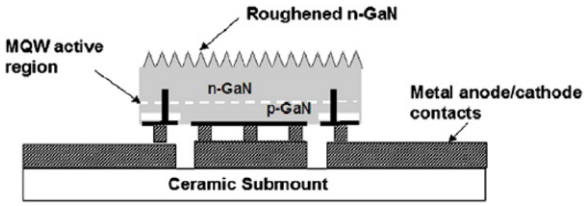

Figure 41. Surface-roughened LEDs are a mainstream approach to light extraction in the industry. Here, the thin film flip-chip structure introduced by Philips Lumileds. Reproduced with permission from [92]. Copyright 2006 American Institute of Physics.

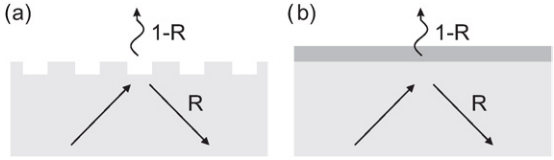

Figure 42. Plane wave impinging on a surface with reflectivity $R < 1$. (*a*) Patterned structure, part of the power is diffracted (*b*) Metallic mirror, part of the power is absorbed.

Nowadays, random surface roughening of a thin-film GaN LED is commonly used in the industry and yields very high-extraction efficiency (∼65% in air and ∼80% in epoxy, according to [60]) (figure 41). This roughening is obtained by removing the substrate (SiC or sapphire), and etching the n-side of the GaN layer with a photo-electro-chemical process [36]. For PhC approaches to be competitive, they must therefore display higher performance and/or lower production cost than surface-roughened LEDs (SR-LEDs).

In the following, we discuss light extraction from SR-LEDs and argue that some of the key limitations for light extraction described previously are equally valid for SR-LEDs. For comparison, we focus on LLO-PhC-LEDs such as those of section 4.5.2: they are the closest PhC-based system to SR-LEDs, and therefore offer a fair comparison. For simplicity, we will present PhC calculations in TE polarization only and in the ΓM direction (unless otherwise stated), but the results have much more general validity.

5.1. Another look at diffraction of guided modes

In section 4.1, we considered the PhC as a periodic perturbation to a waveguide, which induced loss in the guided modes. In the following, we will build a lossy mode 'from the bottom up', starting from plane waves. Let us first consider a single interface between two media (figure 42), with a specular reflectivity R lower than unity—this may be due to absorption (e.g. if one of the materials is a lossy metal) or to scattering (e.g. in the case of a corrugated interface, such as a PhC). If a plane wave impinges on the interface, its intensity is decreased by a factor R. Let us now consider a closed structure (figure 43) with another, perfectly reflective interface at the bottom (this could be a perfect metallic mirror, or a dielectric interface beyond the critical angle). We call h the thickness of the waveguide. The plane wave bounces off both interfaces, eventually forming a mode (with in-plane wavevector $k_{\|} = k' + \mathrm{i}k''$) if a vertical resonance condition is met. In order to relate the modal loss coefficient k'' to the 'ray-tracing' one-bounce loss, we equate the losses after a round-trip in the vertical cavity:

$$I = R.I_0 = I_0 \exp -2k'' x_{\text{bounce}} \tag{13}$$

where $x_{\text{bounce}} = 2h \tan(\theta)$. This yields

$$k'' = -\frac{\ln(R)}{4h \tan(\theta)}. \tag{14}$$

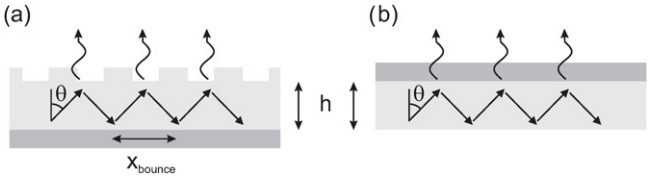

Figure 43. Same as figure 42 but in a closed structure: the plane wave forms a guided mode. (*a*) PhC structure with a perfect (lossless) bottom mirror. (*b*) Waveguide with a lossy mirror and total internal refraction at the bottom.

This relationship was introduced in [19] in a similar context. We will illustrate and discuss this result in two cases.

First, let us consider the simple case of a dielectric GaN waveguide between air and a lossy metal (figure 43(*b*)). We vary the thickness h of the waveguide, so that the number and propagation angle of guided modes varies. We compute the dispersion of these modes with a 1D scattering-matrix method. Figure 44(*a*) shows the effective index of the modes as a function of h. For the thinnest case ($h = 100$ nm) only one mode is supported. As h increases, more modes are supported and their effective index n_{eff} increases, manifesting a stronger localization in the GaN layer. All modes have an effective index n_{eff} between 1 and $n_{\text{GaN}} = 2.4$. Figure 44(*b*) shows the corresponding modal loss k'', together with the prediction from equation (14): as can be seen, both results are close provided that the modes are well localized in the waveguide.[6] Figure 44(*c*) presents the same result in a different fashion: here the loss is plotted versus the modes' propagation angle θ (as the thickness h is implicitly varied). We reach the same conclusion: away from their cutoff, all modes converge to the prediction of equation (14). In particular, this is always the case at large angles, where k'' converges to zero. In a thick waveguide where many modes are supported, most modes are far from cutoff and follow this trend—especially, all the low-order modes do.

Next, let us consider a GaN waveguide with a PhC and a lossless mirror (figure 43(*a*)). Here, loss is due to scattering by the PhC: the value of R describes the one-bounce scattering efficiency. Again, we vary the thickness h of the waveguide so that the modes span various propagation angles. For simplicity here, we only consider the fundamental Bloch mode of the structure and compute its dispersion with a 3D S-matrix method—as mentioned, the behavior of other low-order modes

[6] The discrepancy for modes close to the cutoff comes from the Goos–Hänchen effect, i.e. the additional lateral propagation of the mode in evanescent media [42, 75]. The expression for x_{bounce} could be modified to account for this, but this is beyond the scope of the present discussion.

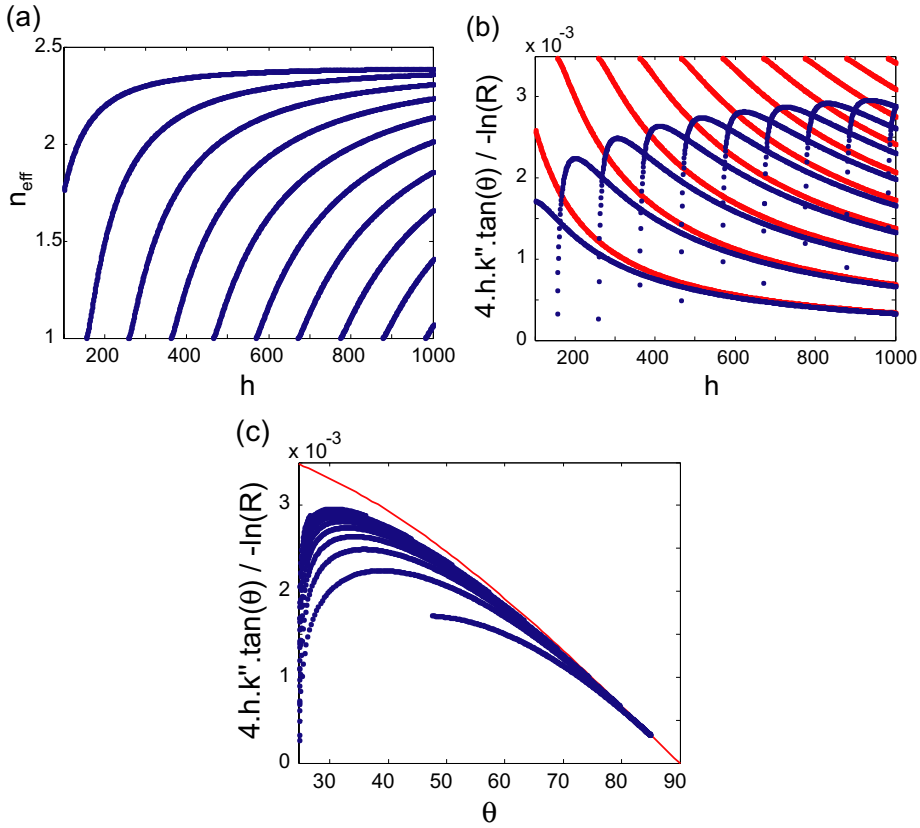

Figure 44. (*a*) Dispersion of guided modes in a metal/GaN/air waveguide: depending on the waveguide thickness h, a number of modes are supported. (*b*) Corresponding modal loss parameter $4hk''\tan(\theta)$ (dashed blue line), compared with $-\ln R$ (full red line): the two quantities converge away from the mode cutoff, following equation (14). (*c*) Same quantities as (*b*) but represented versus mode propagation angle θ rather than waveguide thickness: at large θ, losses vanish following R.

will be similar to that of the fundamental. Figure 45(*a*) shows the effective index of the mode as h varies: the result is very close to that of figure 44. Figure 45(*b*) compares the modal loss of the mode with the prediction of equation (14), as a function of propagation angle. The modal loss is modulated by Fabry–Pérot fringes (corresponding to vertical resonances of the radiated harmonic, which can quench diffraction or increase it by a factor of 2), but its envelope follows the prediction of equation (14). Figure 45(*c*) clarifies the behavior at large angles. In conclusion, we see that the Bloch modes merely 'dress' the one-bounce loss $R(\theta)$ (in other words, they comb this loss at the propagation angles corresponding to coherent interference).

5.2. Competition between PhC diffraction and metal losses in LLO-PhC-LEDs

By relating single-bounce loss to modal loss in equation (14), we see that k'' vanishes at large angles for two reasons. The first is the geometric contribution $\tan(\theta)$, which merely accounts for the larger lateral propagation when the incidence angle increases. The second contribution is $\ln(R)$ and represents the loss/scattering efficiency of the interface. The important result is that this contribution also vanishes at large angles. This fact is trivial for the case of metallic losses, where R is the Fresnel coefficient that is known to go to unity for $\theta = 90°$. Figure 46 exemplifies this fact in a few external cases.

However (and unfortunately), it can also be shown that R goes to unity for large θ in the case of a periodic scattering surface. We illustrate this in figure 47, where $R(\theta)$ (obtained from an S-matrix calculation) is shown for two structures. This is the key result of this section. The reason for this behavior is that, at large θ, light barely penetrates the scattering layer so that scattering vanishes (in other words, the radiating dipole induced in the PhC layer vanishes). We see here that this effect is not related to the existence of guided modes, but rather a fundamental property of a thin-film scattering surface.

The generality of this trend is related, in our opinion, to the small available transverse momentum, once a large longitudinal momentum is chosen along the interface (glancing angle). Everyday-life manifestations of 'good' behavior from rough or wavy interfaces at grazing angles are reflections of point light sources (city lights, car lights) on water or hardly wet asphalt, which take the form of a line, suffering almost no transverse scattering. We also note that similar results have been obtained with a different approach by the computer graphics imaging community: it is generally known that large-angle scattering by a rough reflector is dominated by a specular peak or a specular lobe [44, 76, 99].

In the above, we have focused on the *specular* reflection coefficient R. Our result therefore means that glancing-angle light undergoes specular reflections both at metal and PhC interfaces, and retains its propagation angle θ (e.g. the light

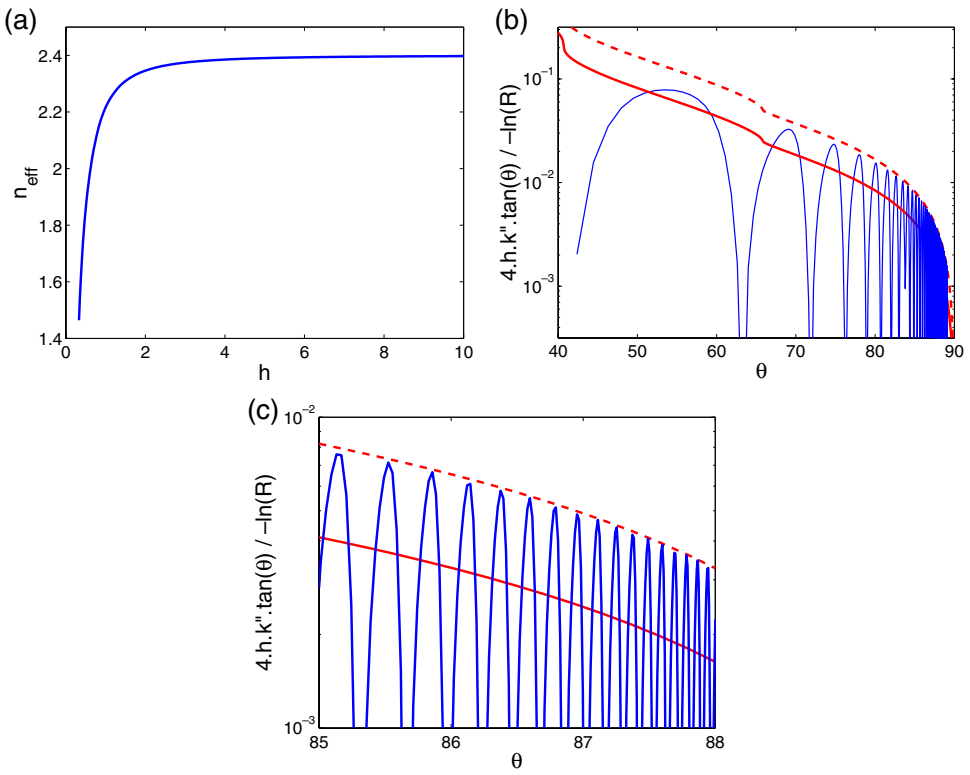

Figure 45. (a) n_{eff} of the fundamental Bloch mode as a function of h. (b) Corresponding modal loss parameter $4hk''\tan(\theta)$ (blue), compared with $-\ln R$ (red) and $-2\ln R$ (dashed). Losses oscillate due to interferences, but follow the envelope of $\ln R$. The interferences can either quench losses or increase them by 2: the peak value of the modal loss follows the dashed curve. (c) Zoom detailing the large-angle behavior of (b).

is neither extracted, nor redirected to other angles within the LED that may subsequently be extracted). Since this large-angle trend is similar for the (useful) PhC scattering and the (detrimental) metal loss, one can wonder how these two loss mechanisms balance out (this question is relevant, for instance, in the important case of a LLO-PhC-LED previously described in section 4.5.2).

Obviously, the result depends on the metal and on the PhC structure considered. First, we consider a PhC structure with weak photonic strength ($f = 0.3$, $t = 0.5$, $u = 0.45$). These parameters are typical of perturbative surface PhCs for GaN-on-sapphire LEDs, where one wants to remain at the second Bragg order to avoid diffractions in sapphire (as also considered in [9, 112]).

Figure 48(a) shows the ratio $\ln(R_{\text{PhC}})/\ln(R_{\text{metal}})$ for various metals. This quantity represents the competition between PhC scattering and metal absorption. As can be seen, this ratio converges to a constant value at large angles, because the overlaps with the metal and PhC vary in a similar fashion. Even for an Ag mirror with optimistic index values, the competition is not favorable at large angles: about half of the light is absorbed rather than scattered. Worse reflectors yield worse results. An indirect experimental verification of this effect was reported in [86], where the authors observed nearly identical performance for LLO-PhC-LEDs with thicknesses of 3.5 μm and 800 nm: the independence of cavity thickness is due to the constant ratio of metal and PhC losses.

Figure 48(b) shows the same result for a PhC design with stronger photonic coupling ($f = 0.5$, $t = 1$, $u = 0.8$).

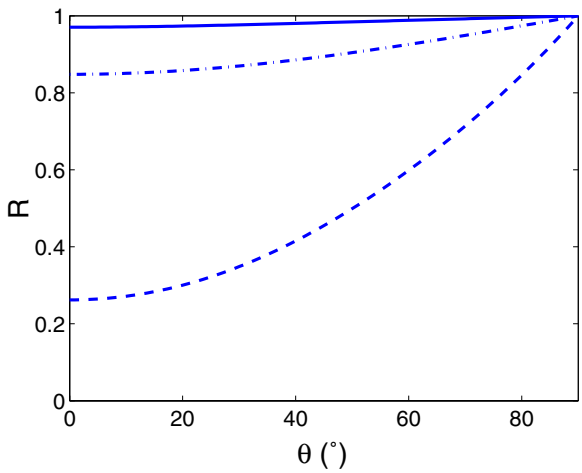

Figure 46. Fresnel reflectivity versus angle of incidence at a GaN/metal interface, at a wavelength $\lambda = 450$ nm. Full: Ag, index after [50]. Dashed–dotted: Au, index after [50]. Dashed: Al, index after [81]. In all cases the reflectivity goes to unity at large angles.

This design is similar to the optimal design reported in [108] (notably, a large pitch can be used since the sapphire substrate is replaced by a reflector). Here, the PhC scattering dominates the metal loss even at large angles. We note that this figure considers the *total* scattering and not the scattering to air, so it merely shows that light will be redirected to other angles before it is absorbed by the metal—however, such behavior naturally leads to efficient extraction to air after a few bounces (the

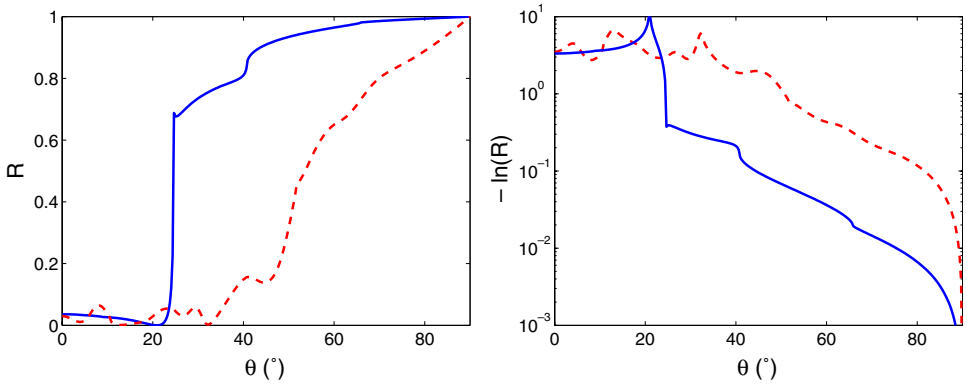

Figure 47. Specular reflectivity versus angle for two PhC designs. Full line: weak scattering ($f = 0.3$, $h = 0.5$, $u = 0.45$), dashed line: strong scattering ($f = 0.5$, $h = 1$, $u = 0.8$), left: R in linear scale. For the weak PhC, R is still reminiscent of the Fresnel reflection coefficient, with a cutoff at the critical angle. Right: loss parameter $-\ln(R)$ for comparison with figure 45.

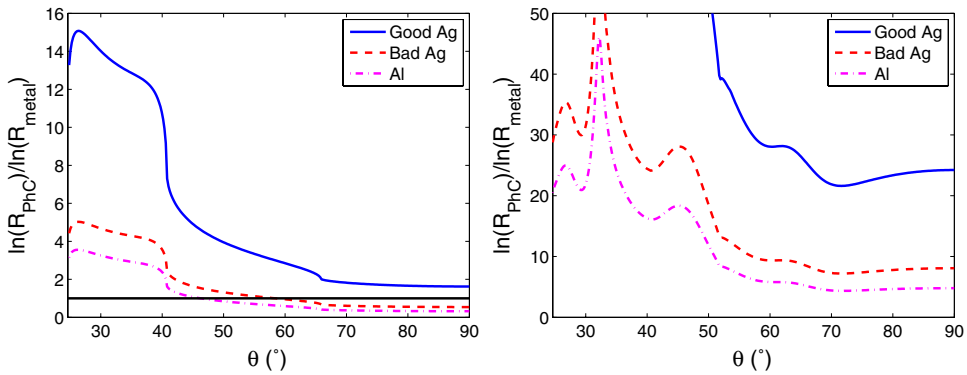

Figure 48. Ratio $\ln(R_{\mathrm{PhC}})/\ln(R_{\mathrm{metal}})$ representing the competition between PhC diffraction and metal losses for various metals: full: Ag with high reflectivity (index from [50]), dashed: Ag with poor reflectivity (index from [81]), dashed–dotted: Al. The PhC structure is of the form GaN/PhC/air, where the PhC has a triangular lattice made of GaN rods in an air matrix (filling fraction f, thickness t, reduced frequency u, calculations along ΓM). Left: plotted ratio for a PhC with weak scattering ($f = 0.3$, $t = 0.5$, $u = 0.45$), right: plotted ratio for a PhC with strong scattering ($f = 0.5$, $t = 1$, $u = 0.8$).

essential point is to avoid 'closed-loop' propagation directions which are not randomized at all). Therefore, the competition between scattering and metal losses can be favorable with a good PhC design and an excellent reflector.

However, there remains a problematic point: the diffraction length of the PhC still diverges at glancing angles. Figure 49 indicates the diffraction length $L_{\mathrm{decay}} = 1/2k''$ following equation (14) for various PhC designs. As expected, this length becomes prohibitive at large angles even for a strongly diffracting PhC: it quickly exceeds 100 μm, which means that extraction of light would only happen if it propagates at such a large glancing angle over more than this distance. In a realistic LED, however, discrete elements (such as the n-contacts, sidewalls and other features) are present every few hundred μm and they will absorb this light. Again, this result is in part due to the geometric contribution $\tan(\theta)$ and in part to the detrimental evanescence of the fields in the low-index PhC. To illustrate this, we also consider a hypothetical high-index PhC (same design as before, but replacing the air with a matrix of index $n = 3.8$, thus retaining the same index step): here, diffraction is efficient up to much larger angles; it is limited by the geometric contribution $\tan(\theta)$ but not by R going to unity. Unfortunately, such transparent, manufacturable, high-index materials are not available.

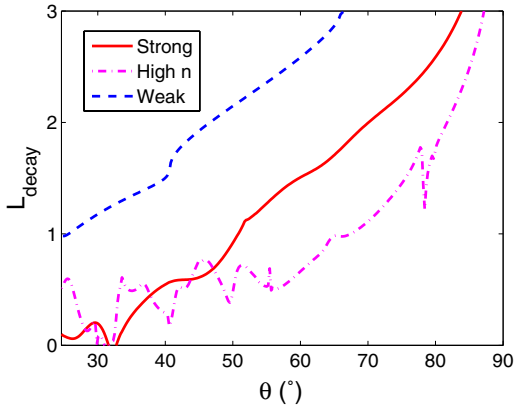

Figure 49. Decay length L_{decay} due to scattering by the PhC (log scale, in μm), as given by equation (14). Dashed: PhC with weak photonic strength, same design as in figure 48(a), full: PhC with strong photonic strength, same design as in figure 48(b), dashed–dotted: same as previous, but with high-index PhC: GaN rods ($n = 2.4$) in a matrix of index $n = 3.8$. Vertical axis in $\log_{10}$ scale.

In conclusion, we have shown how the difficulty of diffracting glancing-angle light is intrinsic to periodically textured surfaces. In the following section we will argue that this result also applies to SR-LEDs.

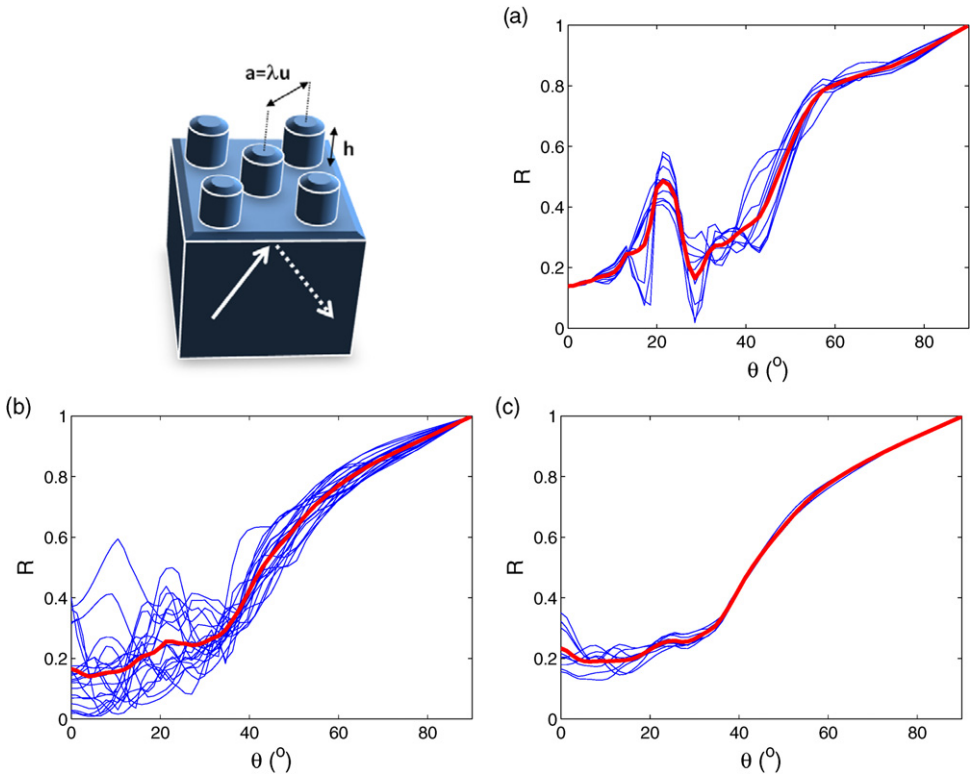

Figure 50. Considered geometry and successive statistical averaging steps of specular reflectivity versus angle for various PhC designs. We consider GaN/PhC/interfaces with GaN rods in an air matrix (filling fraction $f = 0.3$) and TE polarization. (*a*) Thin lines: individual configurations ($\varphi = 0$–2π, $u = 1$, $h = 1$), thick line: averaging over φ. (*b*) Thin lines: averages over φ ($u = 0.8$–1.2, $h = 1$), thick line: subsequent averaging over u. (*c*) Thin lines: averages over u ($h = 0.6$–1.4), thick line: final averaging over h.

5.3. Diffraction efficiency for surface-roughened LEDs

We now consider a similar approach for the description of scattering by a random roughened surface. Again, we begin by considering a periodic corrugated interface, whose surface features are on the order of those found in a SR-LED—namely, 500 nm–1 μm height fluctuation. From an S-matrix calculation, we obtain the scattering efficiencies in various diffraction orders. In order to describe the properties of a random surface, we can now average the obtained scattering over multiple configurations, as shown in figure 50. This neglects possible impact of height correlations on the scattering cross-sections, but we believe such effects to be unimportant for this general discussion. First, we average over the azimuthal angle φ, which smooths out the grating anomalies. Then, to account for variations in the in-plane distance between surface features, we perform the calculation for a distribution of reduced frequencies u and average over those. Finally, we vary the PhC depth d to account for feature size variation.

Of course, the final result will depend on the details of the statistical distribution we choose—clearly, the small-angle behavior is rather dependent on the configuration (essentially due to Fabry–Pérot-like resonances close to normal incidence). However, it is obvious from figure 50 that some features are common to all configurations and will be conserved in the average result, independent of the distribution. This is especially the case for the large-angle decrease of the scattering efficiency. This trend is directly related to the difficulty of extracting glancing-angle light, as argued above.

One may wonder if the details of the shape of the scattering feature modifies this result: PhC-LEDs usually employ cylinder-like corrugations (either holes or rods), whereas SR-LEDs display pyramid-like features. Figure 51 compares the scattering efficiency of the two types of surfaces (averaged as above, and for a similar choice of feature sizes). As can be seen, the large-angle behavior is nearly identical for both—this is not surprising since it is governed by evanescent mode leakage in the scattering layer, which mostly depends on the average index of the scattering layer and not on the details of its geometry.

Interestingly, we note that the typical feature size observed in GaN SR-LEDs happens to be quite close to that which yields the best experimental results in PhC-LEDs: according to [108], optimal PhC-LDE performance is obtained for pitches $a \sim 500$ nm, which is comparable to the characteristic length of a GaN SR-LED as revealed by SEM [37]. In this sense, it is a fortunate coincidence that the procedures used for producing SR (PEC etching or hot ionic etching) yield such close-to-optimal dimensions. This also implies that the angular behavior of scattering efficiency will be similar in SR-LEDs and in good PhC-LEDs.

5.4. PhC- and SR-LEDs: common limitations

The above discussion illustrates a key result in comparing PhC- and SR-LEDs: the decrease in diffraction efficiency at large angles, which dominates the performance of PhC-LEDs, is also observed in SR-LEDs. Indeed, this effect

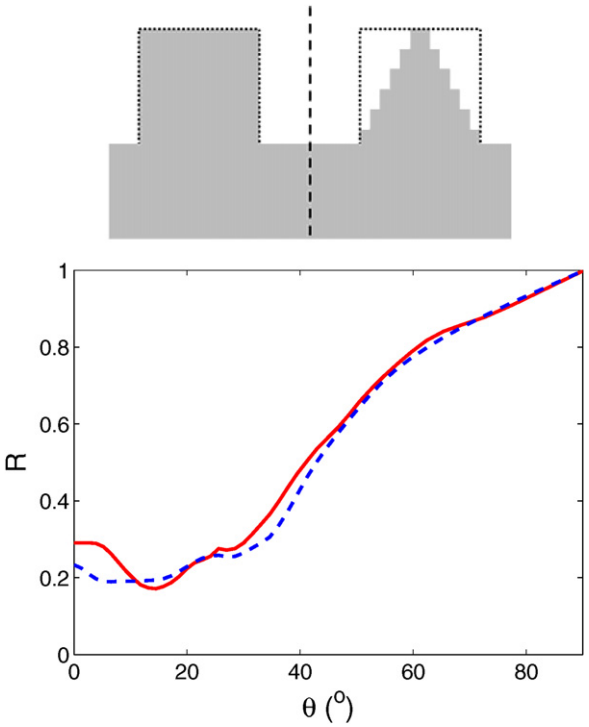

Figure 51. Comparison of two PhC corrugations: cylindrical rods versus pyramids. Top: sketch of the structures. The base footprint is identical. The pyramid's slanted sidewall profile is approximated by six slices of decreasing filling fraction. Bottom: comparison of specular reflectivities (full line: pyramids, dashed line: cylindrical rods). Both calculations are averaged over $\varphi = 0$–2π, and over $u = 0.8$–1.2. The PhC has a filling fraction $f = 0.3$ and is further averaged over $h = 0.6$–1.4. The pyramids have a base filling fraction $f = 0.3$ and a height $h = 1$.

is intrinsic to planar corrugated interfaces: as long as the momentum of light is vanishing in the direction normal to a rough or periodic interface, little scattering occurs because the important dimension is then the inverse of the vertical wavevector, and only corrugations of this 'superwavelength' size will substantially diffract such beams.

Designing the random scattering surface in an SR-LED is usually not possible—most roughening processes yield similar geometries. On the other hand, in some implementations of PhC-LEDs, more freedom of design is available to increase light extraction. For instance, the record results obtained in [108] in PhC-MCLEDs rely on the synergetic use of cavity effects and PhC diffraction. The embedded structures discussed in section 4.5.3 are also attractive, because they decouple the index of the extraction medium from the index contrast of the PhC—this enables extraction to an encapsulant while maintaining the large index contrast of a GaN/air PhC. In addition, all modes can have a strong overlap with the PhC, even at high incidence angle, as the modes fully overlap the PhC due to the similar high index on both sides of the PhC. Similarly, a non-planar design, for instance comprising wedged layers to progressively 'strip' grazing angles, can also accomplish light extraction beyond several of the limitations of planar structures—see [63] for an inspiring use of such wedged waveguides. Therefore, we conclude that some implementations of PhC-LEDs, while they are currently non-conventional, can surpass the performance of SR-LEDs if care is taken to address the underlying limiting mechanisms we described.

5.5. Effect of encapsulation on light extraction

In practice, LEDs are nearly always encapsulated in a high-index medium (such as a silicone or epoxy), to increase both robustness and light extraction. The impact of encapsulation on light extraction is an important one and is seldom studied for PhC-LEDs. Qualitatively, one can expect two counter-acting effects. On the one hand, it is easier to extract directly to a medium of higher index n: the solid angle of the extraction cone increases $\sim n^2$, which increases the number of leaky harmonics. On the other hand, the index contrast of the diffracting interface (be it a PhC or a roughened surface) decreases, and therefore so does the diffraction efficiency of the corrugated interface. Based on the above arguments, we can expect that encapsulation will have a similar effect for PhCs and random textures (at least for multimode structures), because they rely on the same basic scattering mechanisms.

These two effects are illustrated in figure 52, where we compare the diffuse reflectivities R_{diff} for a PhC extracting into air and into an encapsulant of index $n = 1.5$. R_{diff} represents the total power sent back in the structure (and hence not extracted) after one bounce.

In the weak scattering case (figure 52(a)), R_{diff} is still close to the Fresnel reflectivity for a planar interface, although the PhC allows some extraction beyond the critical angle. The first effect of the encapsulant is obviously to widen the extraction cone for direct extraction. Furthermore, diffraction beyond the critical angle also becomes easier: in the case of diffraction to air, there exists a range of angles that are not extracted (no harmonic falls in the light cone, $R_{\text{diff}} = 1$) while all angles are diffracted in the encapsulated case. In this configuration, performance is clearly dominated by the availability of diffracting channels, so that encapsulating is beneficial at all angles.

In the strong scattering case (figure 52(b)), the shape of R_{diff} is more complex, due to the contribution of multiple scattering harmonics. Here, diffraction channels to air are available at all angles because the structure operates at a higher frequency. However, the trends are qualitatively the same as in figure 52(a), and once again encapsulation improves extraction at all angles because the availability of more diffracting channels overcomes the weaker index contrast.

From the experimental standpoint as well, the net effect of encapsulation is known to always be beneficial. This is demonstrated by results from the industry in SR-LEDs, where encapsulation gains are known to increase extraction efficiency by 20–40% [60]. It is noteworthy that low-loss structures tend to display lower encapsulation gains. Indeed light has to 'bounce' more times for extraction into air than into an encapsulant, and is therefore more sensitive to losses; thus an increase in optical loss will penalize extraction to air more than to an encapsulant, raising the encapsulation gain.

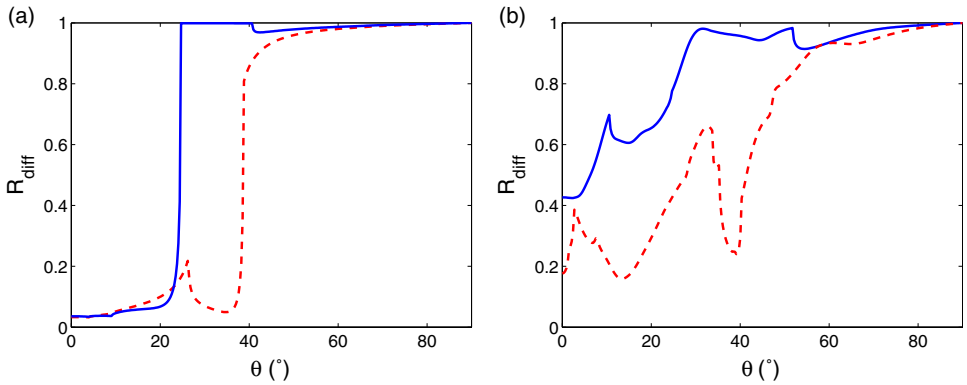

Figure 52. Impact of encapsulation on the diffuse reflectivity R_{diff} for a PhC surface. Full line: extraction to air. Dashed line: extraction to an encapsulant (index $n = 1.5$). The structures are the same as in figure 48. (*a*) Weak scattering. (*b*) Strong scattering.

6. Hybrid approaches

So far, we have considered the use of PhCs to produce either a band gap or out-of-plane diffraction. We now discuss approaches which mix the two effects—the general idea being to use a partial band gap to alter the emission pattern of the LED, and to complement it with a diffraction grating for light extraction.

6.1. Doubly periodic PhC-LED

This idea was first introduced by Fehrembach *et al* [34]. Figure 53 sketches the functioning principle of such a structure. Here, the PhC is made of two superimposed lattices. The first lattice operates at the first Bragg order and opens a nearly omnidirectional band gap so that guided light propagation is only allowed in a limited set of narrow angular ranges around the K direction of the reciprocal lattice (e.g. just below the cutoff frequency where the full band gap would open)—a form of in-plane collimation. The second lattice has a doubled periodicity, therefore operating at the second Bragg order, and providing out-of-plane diffraction of the guided mode.

A relevant question is that of the fraction of the total light emitted into guided modes in the case of a partial band gap—in other words, is there a detrimental Purcell effect ($F_{\text{p}} < 1$) such as that discussed in section 3.3.2? It turns out that the radiative lifetime is roughly constant as long as the band gap is not full: the same amount of guided light is emitted, but channeled toward azimuthal angles where light propagation is allowed—thus it has more 'internal luminance'. This is shown in figure 54, where it can be seen that the photonic DOS, rather than vanishing, remains finite below the cutoff frequency corresponding to the full band gap. Therefore, the amount of guided light is roughly unaffected. This circumvents an essential drawback of the full-band-gap approach (mentioned in section 3): when guided emission is totally quenched, the radiative lifetimes get much longer and the effect of non-radiative recombinations becomes critical, as the associated decrease in internal quantum efficiency overcomes the increase in extraction efficiency. We note that figure 54 pertains to a GaN membrane whereas [34] considers a GaAs LED on a substrate, but the same considerations regarding radiative channels apply in both cases.

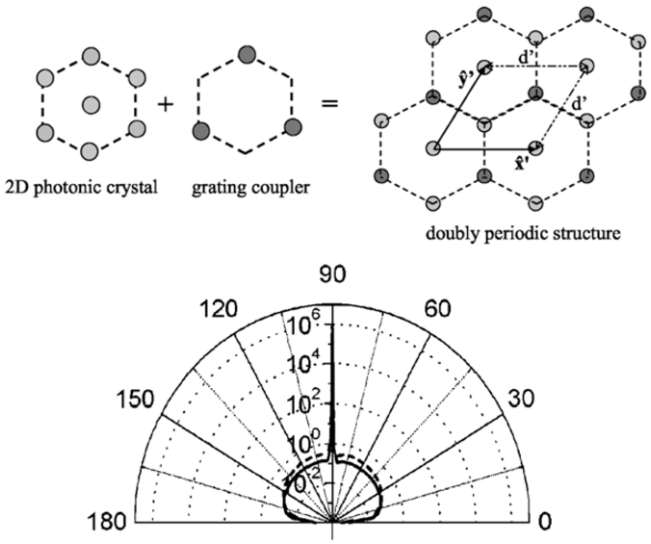

Figure 53. (*a*) Principle of the doubly periodic PhC-LED. A first grating operates at the first Bragg order and opens a band gap in nearly all azimuthal directions, restricting and collimating guided emission to a limited set of narrow angular ranges. A second grating operates near the second Bragg order and diffracts the collimated guided light near normal incidence. (*b*) Calculated far-field pattern: the monochromatic emission is highly directional. Reproduced with permission from [34]. Copyright 2001 American Institute of Physics.

Just like the diffraction grating approach (section 4), the doubly periodic PhC approach requires that diffraction of the guided mode be very efficient for high light extraction. In principle, the task is made easier here because the propagating guided modes are collimated in a set of narrow angular ranges around the ΓK direction: the PhC design can be optimized for this direction, and the requirement that all azimuthal angles be diffracted is lifted. As an additional benefit, the extraction of the guided mode is highly directional, again because guided light only propagates along specific azimuthal angles. In the implementation of [34], the authors predict a very high extraction efficiency and directionality with near-perfect performance under a monochromatic assumption: SpE must occur exactly below the full-band-gap cutoff frequency. However, inhomogeneous broadening of emission implies that some light will actually not be emitted at the optimal design frequency.

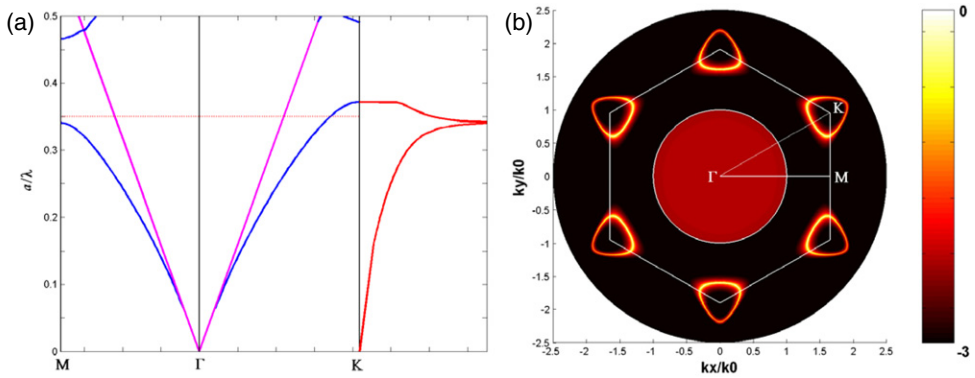

Figure 54. (*a*) Typical band structure of a PhC membrane (left of (*a*)) and corresponding DOS ρ (right of (*a*)): ρ is maximal at the band edge at the M point (Van Hove singularity) but then retains a finite value until the band edge at the K point. It then falls abruptly to zero (complete band gap). Just below this cutoff frequency, the emission rate into guided modes is constant but guided modes are only allowed along the 6 ΓK directions. (*b*) Corresponding angle-resolved emission diagram (e.g. emission versus in-plane wavevector K), at a frequency $u = 0.35$ (dashed line in (*a*)) in log scale. The only radiative channels are the extraction cone in air (points with $|k| < 1$) and the guided modes localized close to the six K points. Reproduced with permission from [19]. Copyright 2007 Optical Society of America.

Even so, practical implementation of this approach is challenging, mostly because of its high demands on fabrication accuracy. Moreover, to obtain a nearly full band gap, large photonic strength is required. In practice this requires etching air holes through the cores of the waveguide—here again the tolerance is low (a shallow etch will fail to open a band gap, and a deep etch will push the mode away from the waveguide). A few studies targeting realistic vertical structures suggest that the implementation is still difficult [3].

6.2. GaN PhC-LEDs with patterned active region

A somewhat similar concept was investigated theoretically in a GaN-based structure by the present authors in [19]. The structure considered in this case is slightly more complicated due to the growth constraints of GaN: as already discussed, many modes are carried by the micrometer-thick GaN layer so that in general obtaining a band gap for all modes is challenging. However, we can consider a structure with a partial etch as in figure 55. The PhC is here pierced through the active region—as shown in [53], the surface defects caused by the etching process can be efficiently removed by a proper annealing step. Figure 55 shows the radiative channels one would intuitively expect in this structure: radiative modes, low-order guided modes localized in the GaN core and high-order guided modes propagating in the GaN core and in the patterned region.

As shown in [19], another radiative channel actually exists: the PhC layer supports quasi-guided Bloch modes—a surprising result since its average index is lower than that of the underlying GaN layer. One may think of the similar situation of guiding in air of a PhC fiber thanks to a higher index silica cladding, behavior possible for modest lengths because, again, R tends to unity at grazing angles. The number of such modes increases with the thickness of the PhC layer, just as it would in a regular waveguide—the low-order modes being less prone to leakage. A large fraction of the emission is channeled into these modes: indeed, low-order modes localized in the GaN buffer are evanescent in the PhC layer and do not couple to the active region (figure 55), whereas the quasi-guided Bloch modes are strongly localized around the active region.

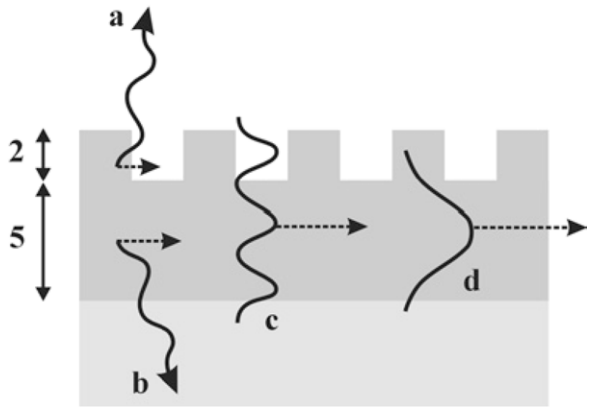

Figure 55. GaN epitaxial layer with a partial PhC etch going through the active region. The conventional radiative channels are indicated: (a) and (b) propagative modes in air and the substrate, (c) high-order guided mode and (d) low-order guided mode localized in the unetched GaN core.

Figure 56 exemplifies this in a case where the PhC layer is thin enough to support only one quasi-guided mode. The emission diagram is clearly reminiscent of figure 54: it is composed of a continuum of emission for $|k| < 1.8$ (emission into air and the sapphire substrate), and of six resonances corresponding to the quasi-guided Bloch mode. Here, as in figure 54, the lattice opens a partial band gap so that the quasi-guided Bloch mode is localized around the K points.

Here again, the Purcell factor retains reasonable values: it is slightly diminished with respect to an unetched structure (mostly due to the lowering of the average index in the PhC layer, which decreases the photonic DOS), but thanks to the quasi-guided modes, the photonic DOS is not significantly depleted, in contrast to a full-band-gap approach.

This approach has so far not been implemented in full devices; photoluminescence experiments have been presented in structures similar to that of figure 55 [53] but these were not especially designed to operate close to a partial band gap.

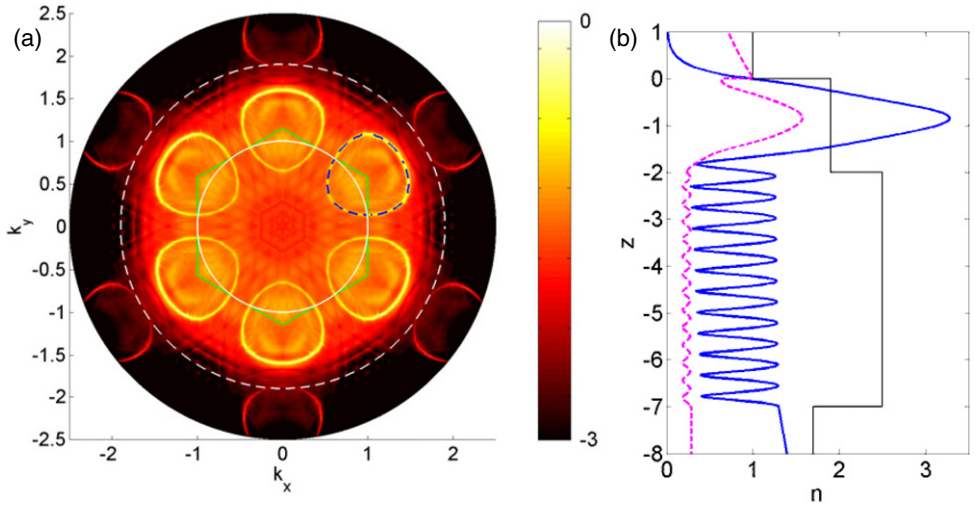

Figure 56. (*a*) Emission diagram of a quantum well embedded in a partially etched GaN structure, as a function of in-plane wavevectors kx, ky. The full circle corresponds to the air cone, and the dashed circle to the GaN cone (e.g. to an effective index $n_{\text{eff}} = n_{\text{GaN}}$). Emission inside the GaN cone is constituted of a uniform continuum and six sharp emission isolines, corresponding to enhanced emission in the quasi-guided mode supported by the PhC layer. (*b*) Field profile of the quasi-guided Bloch mode (full line: fundamental, dashed line: $n = -1$ radiative harmonic). Surprisingly, the mode is strongly confined in the PhC layer despite its low average index. Reproduced with permission from [19]. Copyright 2007 Optical Society of America.

One difficulty is that the implementation of [53] used dry etching to form the PhC, which is expected to damage the p-doping. It should be noted, however, that the direct growth of such structures (sometimes called GaN nano-wires or nano-columns) is an active subject of research, with the intent to obtain electrically injected devices [1].

7. Radiative lifetime enhancement—the Purcell effect

As already mentioned, optimizing the internal quantum efficiency η_{IQE} plays a major role in the efficiency of real-world devices. At room temperature, $\eta_{\text{IQE}} \sim 90\%$ for high quality AlInGaP compounds in the red, which leaves little room for improvement. On the other hand, η_{IQE} in this system decreases at shorter wavelength (for amber LEDs for instance) due to poor carrier confinement. Likewise, improving material quality remains a challenge in GaN-based LEDs, especially at high current density where η_{IQE} decreases (the so-called 'efficiency droop' [23, 24, 56, 93]). Moreover, high-temperature operation is in general detrimental to η_{IQE}.

Therefore, it is tempting to employ photonic effects to improve η_{IQE}. Namely, the Purcell effect described in section 2.1 enables a shortening of the radiative lifetime when the Purcell factor F_{p} is larger than unity. If the non-radiative lifetime remains constant, η_{IQE} is improved—the converse effect to that shown in figure 15 when $F_{\text{p}} < 1$.

In the following, we discuss different ways to harness the Purcell effect to enhance SpE and improve η_{IQE}. Regarding applications, we mostly focus on the case of GaN-based LEDs, where the demands for improvement are especially important.

7.1. 1D Fabry–Pérot cavities

The easiest way to modify the distribution of guided modes in a device is to resort to planar mirrors (either metallic or dielectric) in order to create a cavity [6]. Due to the interference condition between the mirrors, such a structure supports resonant photonic modes called Fabry–Pérot modes.

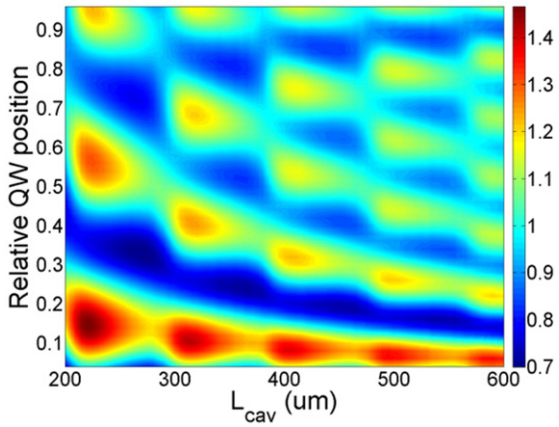

Figure 57. Purcell factor F_{p} for a MCLED (GaN layer sandwiched between an Ag mirror and air), as a function of cavity thickness and relative position of the emitting quantum well in the cavity (0 corresponding to the Ag mirror and 1 to the air interface). F_{p} is modulated as the quantum well sweeps nodes and antinodes of the cavity's resonant modes.

This principle is employed in MCLEDs, which we already evoked in section 4.5.2. However, prospects are limited as regards the Purcell effect in a micro-cavity: even in a thin cavity with efficient mirrors, the modulation F_{p} is typically limited to a few tens of per cent. Figure 57 displays the Purcell factor for a realistic GaN structure (obtained from a 1D S-matrix calculation): F_{p} increases by ~40% at best. Reference [47] shows that even in the case of ideal lossless mirrors and a perfect monochromatic emitter, F_{p} is limited to 3. Intuitively, this can be justified by the lack of confinement in such a structure: the field is still free to propagate in two of the three

spatial dimensions, and it is not possible to significantly alter the photonic environment with respect to a bulk situation.

7.2. 1D band-edge enhancement

In addition to the use of a 1D PhC as a mirror to form a cavity, the PhC can also be considered directly as an emitting medium. In this case, another mechanism can enhance SpE: the presence of a photonic band edge. Indeed near the band edge the photonic DOS increases and the photonic group velocity decreases (leading to an increased localization of the electric field)—both effects can lead to an enhancement of SpE rate according to Fermi's golden rule.

The exploitation of this strategy seems appealing because the enhancement is not related to a specific emitter position in space (unlike cavity-based approaches, which will be discussed below). In the initial push for PBG application, this idea was, however, treated with some confusion concerning directionality [98]. The band-edge frequencies depend on the emission direction, be it for 1D or higher dimensional periodicity. But in spite of a full understanding of 3D-periodic structures, clarification of the topic of band-edge enhancement *per se* in 1D came through some comparatively scarce and recent studies.

Another surprising element is that a 1D periodic system had been heavily modeled in the 1980s: the distributed feedback (DFB) laser. A workhorse for DFB and DBR laser studies was the coupled mode theory (CMT). Splendid studies such as those by Henry in [45] provided all the tools needed from the physics point of view to link laser and SpE properties. However, the laser community was not inspired by PBG concepts or by accounts of band edge at cutoff in ideal (perfect-metal-coated) wires [57].

In spite of the relative ease of the exercise, SpE and CMT were not thoroughly knitted together in that period, with attempts to go back to explicit multilayer formulations [30, 69]. Reference [5] recently gave an account of the use of CMT and SpE in a multimode situation, using source terms much as in [4, 104]. This work was helpful in interpreting strong spectrally periodic modulations of SpE in the case of 'stripes of minigaps' appearing in broad periodic waveguides.

Coming back to the multilayer case, the above-mentioned study [98], together with [2, 29], gave insightful approaches to analytical 1D treatments of DOS and local DOS. Their clever link of the transmission phase to the wavevector and then to the group velocity and the DOS was widely adopted because it provided SpE-related properties from a simple transmission calculation. However, the typical resulting spectra, with peaks at band edges and a depletion in the gap, were essentially already known in the DFB laser community.

Eventually, in 2010, [62] presented an experimental report on crystal vacancy emission in a multilayer structure (figure 58). Thanks to the very low absorption at excitation and emission wavelengths in this system, it was possible to observe the full sequence of angle-dependent band-edge emission enhancement, with a signal from the 'bulk' of a periodic structure. Indeed, the main enemy of band-edge enhancement in a large volume in practice is absorption. We

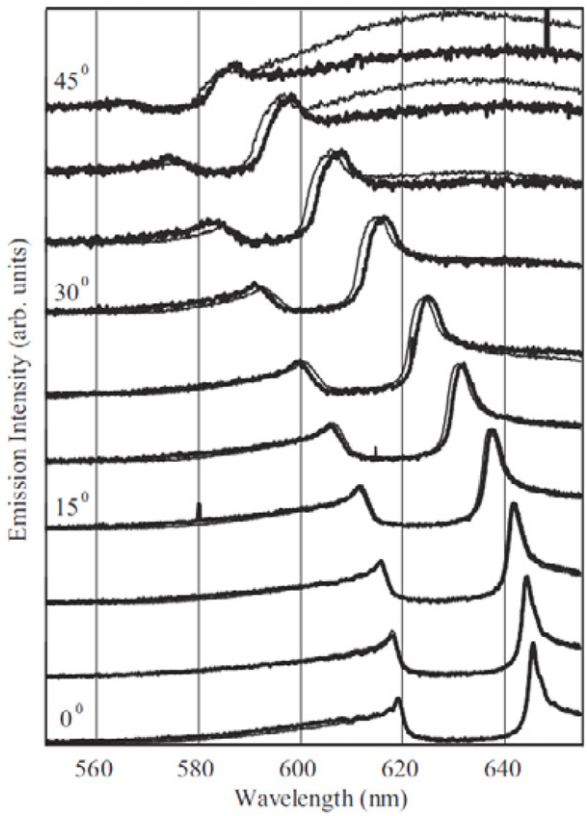

Figure 58. Emission spectra around the band-edge from a multilayer Ta_2O_5/SiO_2 structure, as a function of wavelength and emission angle. One can observe a sharp SpE enhancement near the band edge, whose wavelength drifts with angle. Reproduced with permission from [62]. Copyright 2010 Optical Society of America.

can argue that this impediment has delayed the appearance of such conclusive studies, but that at the same time, it means that concentrated emitters with substantial luminous intensity cannot exploit this scheme due to their inherent absorption in the SpE regime. More quantitative studies on this compromise would be interesting.

A last difficulty is the general challenge to combine electrical injection with a strongly modulated periodic pattern. One can therefore wonder how much of the enhancement effect is conserved when locating the emitter just aside a PBG structure. According to [58, 59] the inhibition effects vanish quite rapidly in such a strategy, but the band-edge peak is reasonably resistant to a shift of 100–200 nm. Therefore, one viable option to use band-edged enhancement would be a sandwich structure, where an emitting layer with proper injection is confined between photonically engineered media.

7.3. Plasmon-enhanced emission

Plasmon-assisted LEDs have spurred intense activity recently, especially for light extraction from GaN-based LEDs.

7.3.1. Principle of operation. The Purcell effect is never strong in a regular Fabry–Pérot cavity, as discussed above. However, in a cavity with a metallic mirror, a different kind of photonic mode is supported: surface plasmon polaritons

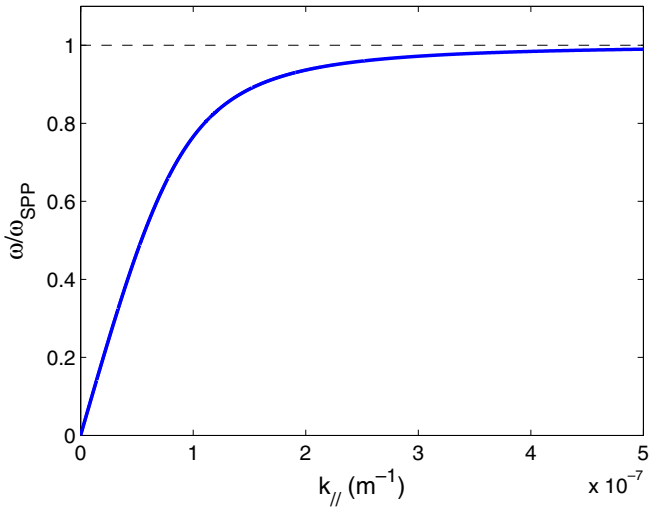

Figure 59. Dispersion relation of a surface plasmon at a metal/air interface. The metal follows a Drude model.

(SPPs). These modes correspond to an electronic excitation that is localized at the metal/semiconductor interface and strongly evanescent in both media. The most common model to describe the dielectric function of a metal near a plasmon resonance is the Drude model $\epsilon_m = 1 - \omega_m^2/\omega^2$, where ω is the light frequency and ω_m the bulk plasmon resonance. At an interface with a dielectric of index n, the SPP resonance frequency is then $\omega_{\mathrm{SPP}} = \omega_m/\sqrt{(1+n^2)}$. Figure 59 displays the dispersion relation of a SPP at a metal/air interface in this case.

The photonic DOS associated with SPPs becomes very large close to ω_{SPP}, mostly due to the small group velocity of the SPP. In accordance with Fermi's golden rule (equation (3)) this enables a very large Purcell factor F_{p}—much like the enhancement near a photonic band edge just evoked. In a Drude model for instance, the SPP's dispersion diverges at ω_{SPP} and so does F_{p}. However, coupling of electron–hole pairs to the SPP is only possible if the emitting quantum well overlaps with the SPP's field. SPPs are strongly localized at the metal/dielectric interface and display decay lengths of a few tens of nm only. Such thicknesses are very challenging from a device standpoint: most materials require a thicker layer for good doping. For instance, in the case of GaN, typical p-layers are more than 100 nm thick.

The understanding of the modification of various optical phenomena (luminescence, Raman scattering) in connection with plasmonics is the topic of thousands of papers. Many subtleties arise between scattering properties and emission properties, for instance. However, the basic trends already mentioned in the 1984 review by Ford and Weber in [35] are essentially correct: the favorable Purcell effect due to SPP comes at the expense of some added losses. The best results can be obtained at typically 10–20 nm above a metal surface—even though the local DOS of the SPP would still increase as one further approaches the metal, so does the probability to directly excite the continuum of electron–hole pairs in the metal, an irreversible loss with a very high DOS. Notably, the huge enhancements of SERS (surface enhanced Raman scattering) related to 'hot spots' of plasmons between metallic particles do not apply for ordinary SpE enhancements.

Reference [41] first documented experimental evidence of coupling of luminescence from a GaN sample to surface plasmons. The authors perform photoluminescence experiments on a GaN sample where the quantum wells are covered by a 12 nm GaN cap. As seen in figure 60, when the sample is coated with a thin Ag layer, PL is suppressed close to the SPP resonance at 3.2 eV because electron–hole pairs emit into plasmons rather than into free photon modes. It is clear from the *suppression* of signal in this experiment that, although coupling to plasmons can readily be obtained with the proper geometry, extraction of the light emitted in the SPP mode is a key issue. Indeed, SPPs are by nature guided near the metal layer, and are not emitted to air. Therefore, plasmon-assisted extraction can be a viable option only if the light emitted in the SPP mode can subsequently be efficiently redirected to air. We will discuss the corresponding challenge below.

7.3.2. Light extraction of surface plasmons—the importance of metal loss. To extract the light emitted in SPPs, one has to break the in-plane invariance of the structure which ensures the existence of the SPP, thus enabling the SPP to be diffracted to air. This can be carried out in two ways: by randomly disordering the metallic surface or by forming a PhC (similarly to the PhCs of section 4, which acted as a diffraction grating for guided modes). Accurate calculations of plasmon extraction are complex and depend on the details of the geometry. Rather than going into such details, we consider the general question: given the typical behavior of extraction and metal properties at optical frequencies, can we expect efficient extraction?

Most discussions found in the literature consider an ideal Drude-like lossless metal. In practice, however, losses are always present and can critically modify the properties of the SPP. Figure 61 displays the actual dispersion of a SPP at a GaN/Ag interface. In contrast to figure 59, the dispersion no longer diverges close to the plasmon resonance. Rather, it reaches a maximum slope before folding back in the so-called 'anomalous dispersion' region. Thus, the Purcell effect is limited to a finite value.

This effect was discussed in detail in [49]: the authors study radiation close to a metallic interface both in a classical and a quantum framework, and find that dissipative losses broaden the resonance and thus limit the value of F_{p}. As shown in figure 62 for the case of a Au/InP interface, F_{p} close to the plasmon resonance is overestimated by a factor of 2 if metal absorption is ignored. In the same paper, the authors also discuss how the presence of patterning affects the radiation process. Because the PhC scattering introduces additional loss for the plasmonic mode, its dispersion relation is further broadened and F_{p} is reduced even more.

Another critical point is the metal absorption, which manifests itself as an imaginary part in the wavevector of the SPP. Figure 61 also indicates the decay length of a plasmon at a planar Ag/GaN interface induced by absorption. As can be seen, loss is actually very strong in this (important) example, especially when one approaches the plasmon resonance: L_{decay}

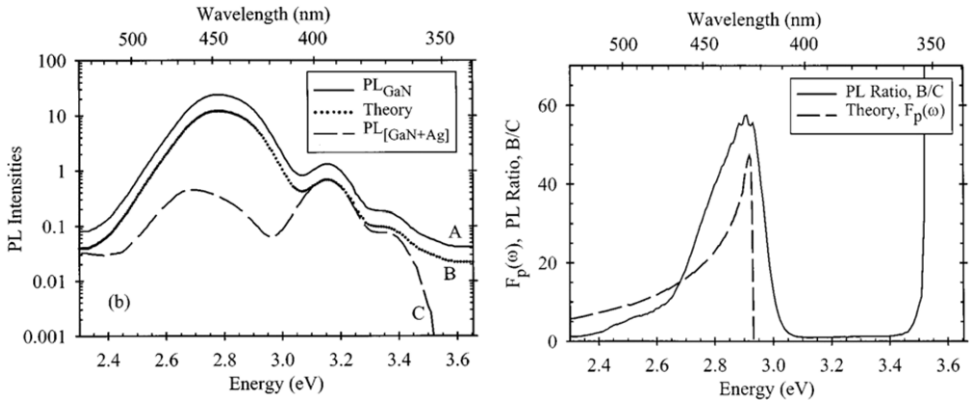

Figure 60. Left: photoluminescence spectra for a bare GaN sample and the same sample covered with a thin Ag layer. The dotted line shows the bare spectrum with attenuation. The GaN/Ag spectrum shows a strong deviation due to coupling to SPP. Right: the ratio of PL spectra shows a spectral dependence similar to the theoretical Purcell effect F_p. Reproduced with permission from [41]. Copyright 1999 American Physical Society.

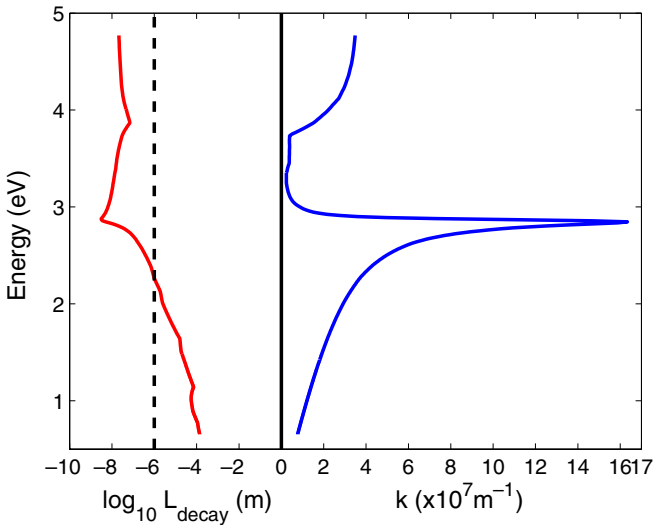

Figure 61. Dispersion of the surface plasmon at a GaN/Ag interface, using realistic index values. The vertical axis is the photon energy in eV. Right: real part k of the wavevector. Due to dissipation close to and above the plasmon resonance, the dispersion (and therefore the density of state) remains finite. Left: decay length $L_{\text{decay}} = 1/2k''$ (in log scale). For photon energies close to the plasmon resonance L_{decay} becomes shorter than 1 μm (dashed line).

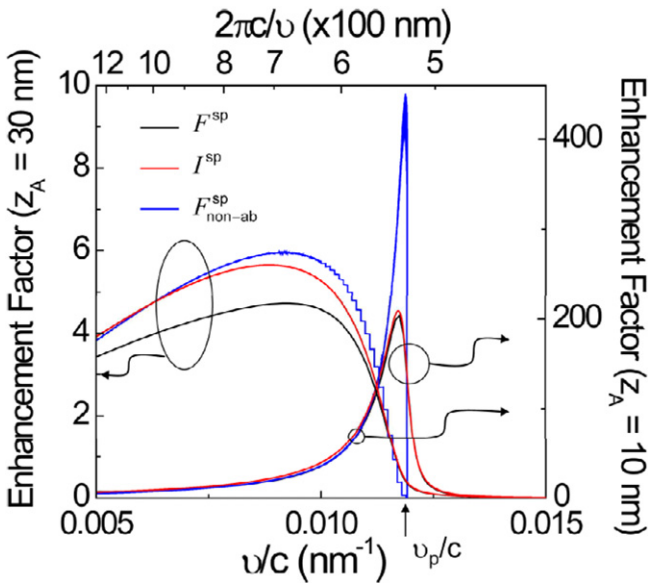

Figure 62. Enhancement factor (i.e. F_p) as a function of light frequency for a Au/InP interface, with a dipole located at a distance 30 nm (left scale) and 10 nm (right scale) from the interface. The lossless calculation (blue) yields a larger F_p than the quantum (black) and classical (red) calculations including losses, especially close to the interface. Reproduced with permission from [49]. Copyright 2010 American Institute of Physics.

is shorter than 1 μm in a broad band around the resonance, and less than 10 nm at the resonance! In this case, light extraction of the SPP by a PhC becomes practically impossible—even with a very efficient PhC grating, several periods would be necessary to extract the plasmon. Of course, this loss calculation pertains to a simple planar interface; the presence of the PhC would modify metal absorption, but likely not enough to bring it to a reasonable value.

In other words, the practical use of the SPP scheme faces a trade-off: while η_{IQE} can be increased thanks to the Purcell effect, losses in the metal can also significantly decrease the extraction efficiency, so that the LED's external quantum efficiency is not necessarily improved. Obviously, the SPP approach is more promising if η_{IQE} is low to begin with, leaving large room for improvement.

This trade-off was studied through a simple analytical model by Khurgin *et al* in [54]. The authors consider a dielectric/metal interface corrugated by a 1D or 2D PhC and estimate the diffraction rate from CMT. By comparing this extraction channel to the metal losses and integrating over all directions, they obtain the approximate extraction efficiency of the system. The conclusion is very pessimistic: in the case of GaN, the trade-off is such that use of the SPP approach would only pay off for an initial efficiency $\eta_{\text{IQE}} < 0.1\%$. Of course, in state-of-the-art material used in commercial LEDs, η_{IQE} is much higher (several tens of per cent under operating conditions). Therefore, the SPP approach is by far not compelling in this system, and could only find applications in materials with very poor η_{IQE}. Figure 63 illustrates this result.

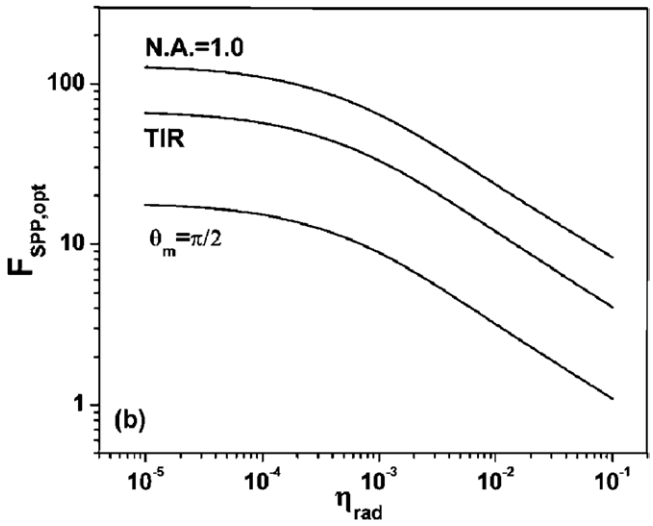

Figure 63. Enhancement of external quantum efficiency F_{SPP} (e.g. ratio of external efficiency after SPP enhancement to initial external efficiency) as a function of internal quantum efficiency η_{rad}. The various lines correspond to numerical apertures for collection. $NA = 1$ is for a structure with a planar interface to air and no additional extraction features. The case $\theta_m = \pi/2$ corresponds to possible extraction at all angles of propagation, and is the closest to a realistic LED with surface roughness. The enhancement decreases for higher η_{IQE}. Reproduced with permission from [54]. Copyright 2007 Optical Society of America.

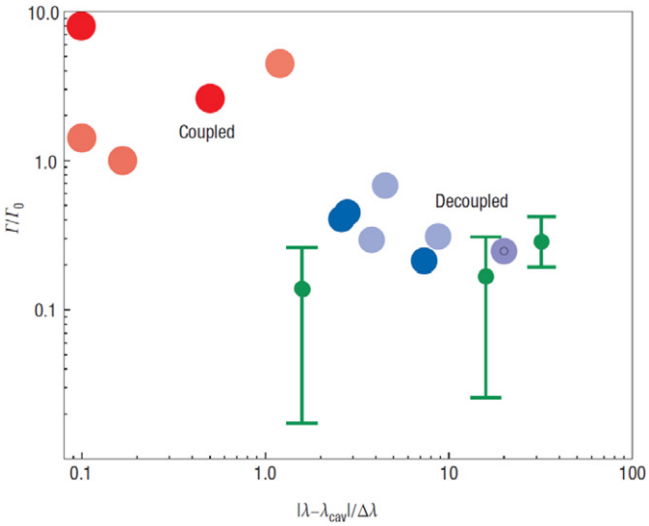

Figure 64. Quantum dots in high-Q PhC nanocavities. Experimental (circles) and calculated (bars) relative emission rates (Γ) for various detunings between exciton wavelength λ and the PhC cavity mode wavelength Λ_{cav}, normalized by the linewidth of the cavity mode spectrum $\Delta\lambda$. Γ_0 is the emission rate without a PhC. Reproduced with permission from [77]. Copyright 2007 Nature Publishing Group.

7.3.3. Conclusion on the plasmonic approach. In practice, light extraction assisted by surface plasmons is thus limited to very specific situations:

- the initial internal quantum efficiency should be low enough for the associated Purcell factor to be interesting,
- the active region must be placed very close to the metallic mirror (10 to 20 nm), which presents a challenge to forming a pn junction.
- the SPP should display low loss, so that it can be extracted to air before it is absorbed in the metal.

These conditions make this approach an unlikely candidate for GaN-based LEDs. This pessimistic condition is at odds with the flourishing experimental activity on the field in recent years. This effort was spurred by promising initial results in photoluminescence experiments in [80], which displayed a tenfold enhancement of the PL signal in the presence of an Ag mirror located 10 nm from the quantum wells. However, it appears likely that this impressive result was due to an improper normalization of the excitation efficiency—namely absorption of the incoming laser can be significantly increased in the presence of a metal, especially in the usual case of resonant pumping where the direct laser absorption in an uncorrugated structure is on the order of 1%.

Indeed, despite several years of effort, significant enhancements have only been observed in PL. Implementations in electrically injected devices, where absorption artifacts are absent, usually display much more modest enhancements (on the order of $\times 2$), which can easily be explained by the conventional effect of a metallic mirror in the near-field.

Somewhat related to the SPP approach, the nano-antenna concept could still open some more favorable opportunities. It stands somewhere between SPPs and the physics of localized plasmons, while also employing antenna physics in that the resonator is tuned in size to optimize the emitter–field coupling [43].

7.4. 2D PhC cavities and the Purcell effect

As appears from the above discussion, it is difficult to obtain a significant Purcell effect in a 1D structure (in addition to the plasmon approach) because the field is weakly confined and a significant modification of the DOS is impossible. Use of 2D PhCs (together with a vertical confinement by a waveguide or membrane) lifts this limitation and enables more significant manifestations of the Purcell effect.

To obtain a high F_{p} requires an optical cavity which supports one or several strongly resonant modes to which the light emitter is coupled. This is challenging for a variety of reasons. First, the source size is limited to the size of the cavity, which seriously limits the output power of such a source (one could consider using several cavities, but the loss of epitaxial real estate to the PhC areas is still an issue). Moreover, good tuning to the cavity mode (both in terms of position and emission wavelength) is required for a large F_{p} enhancement. Finally, electrical injection of such a device is very difficult—as we have already discussed, it is challenging to form electrodes on a membrane structure.

Numerous teams have reported on the observation of significant Purcell factors in PhC defect cavities under optical injection—see for instance [31].

Figure 64 shows experimental measurements of the Purcell effect for several quantum dots coupled to high-Q PhC cavities [77]. The value of F_{p} is derived from photoluminescence lifetime measurements. Large

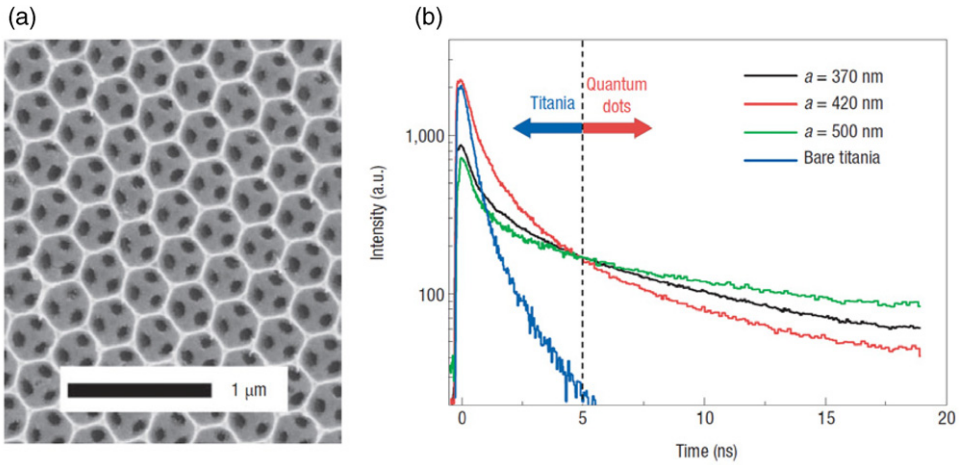

Figure 65. Modification of SpE lifetime of CdSe quantum dots embedded in a TiO_2 inverse opal 3D PhC. (*a*) SEM image of the (1 1 1) face of the structure. (*b*) Measured photoluminescence decay curves with three different lattice constants a. Sample $a = 370$ nm (black curve) is a reference without PC behavior. Reproduced with permission from [77]. Copyright 2007 Nature Publishing Group.

enhancements ($F_p \sim 10$) can be obtained, but only for perfect spectral tuning to the cavity mode.

An alternative to using a PhC cavity is an engineered waveguide suited to enhance the Purcell factor, and also the beta factor (i.e. the fraction of SpE emitted in the mode of interest). Intuitively, a wire intrinsically channels a lot of light in a single mode. Experimental results are less compelling than one could expect, as recently demonstrated on well-characterized pillars with no periodicity and only a mirror to emit photons on a single side [12]. The best Purcell factor is then only 1.5 in GaAs, although the beta factor on-axis can exceed 0.95 on a really broad band. This makes this object attractive for single-photon sources.

Can a waveguide be engineered with periodicity to enhance its Purcell effect on a broad band? This is an advanced variation of the idea of the band-edge enhancement discussed in section 7.2. This has been proposed in PhC waveguides and so-called photon guns [64, 70, 117]. But here again, experimental results have been relatively far from expectations. This is probably on account of complex quantum-dot dynamics in a high Purcell factor regime, with the increased DOS interacting with the continuum of electronic excitation accompanying the dot's quantized state—a more complex situation than in the similar atomic system.

7.5. 3D structures and Purcell effect

Finally, one can also consider employing a 3D PhC where strong field confinements are possible. The theoretical gains in F_p can be large in this case, if the emitter is properly placed in the PhC and tuned spectrally [15]. However, as discussed in section 3, fabrication of 3D PhCs is very challenging, and imperfections in the structure can quickly spoil the resonances that give rise to a large F_p. References [52, 77] present some implementations of 3D PhCs, and measurements of lifetime modifications in such structures (figure 65). Of course, this approach can also lead to the converse effect of inhibited SpE [65].

Due to its difficult implementation and the inherent limitations on output power, it currently appears that the use of 3D PhC cavities will at best be limited to low-threshold/low-power lasers, while application to LEDs is unlikely.

We also note that, in addition to the use of periodic structures to harness the Purcell effect, one can also consider the use of disordered photonic media. In this case, one does not rely on the formation of a band gap or of an engineered cavity mode *per se*. Rather, random fluctuations of the optical field can lead to significant enhancements to the local photonic DOS. Emitters located at the corresponding position can then benefit from a significant Purcell effect. Reference [91] reports on experimental observation of this effect in ZnO powder, and demonstrates values of F_p as high as 8.

8. Conclusion

We have reviewed various possible uses of PhCs to modify the spontaneous emission in LEDs.

One of the most well known is the full-band-gap approach, where the PhC is used to prevent the existence of guided modes, so that all emitted light propagates in air. Despite its conceptual simplicity, such a system is very difficult to implement in real devices—in part because it requires an impractical geometry, and also because the increase of spontaneous-emission lifetime strongly worsens the impact of any non-radiative channel. Despite some proofs of principle in low-temperature experiments, practical application remains elusive.

The diffraction grating approach, less drastic, allows for propagation of guided modes but uses the PhC as a diffracting element to extract these. This concept has been heavily studied theoretically and experimentally, in conventional III–V materials and especially in GaN-based LEDs. The design of the PhC extractor is of utmost importance. Most importantly, one must consider all the guided modes in the structure and ensure proper extraction of each. This is most challenging for modes propagating at large off-normal angles, which has

spurred a variety of advanced designs for improved light–PhC coupling. This approach has yielded some of the most promising results in real-world devices, and also opens intriguing possibilities for exotic emitters such as non-polar GaN LEDs. We have seen that optimization of the extractor was heavily dependent on the semiconductor system, which imposes limitations in terms of physical properties as well as material properties.

After proposing a model for light scattering from a roughened surface, we have compared the properties of light extraction in a PhC-LED and in a surface-roughened LED. We have argued that one of the key challenges (extraction of glancing-angle light) was common to both approaches, which explains the similar performance of good PhC extractors and surface-roughened LEDs. However, we note that, in principle, PhC-LEDs offer more freedom of design to beat these limitations.

More advanced designs, which make use of band-gap effects and diffractive effects at the same time, offer very promising theoretical performance. However, they are more complex and less robust to implement, and a convincing experimental demonstration is still lacking.

Finally, we have considered systems that aim at modifying the spontaneous-emission lifetime via the Purcell effect. Again, this effect is difficult to harness in practical devices. Plasmon-based approaches are usually hampered by prohibitive losses at optical frequencies. The use of two-dimensional PhC cavities can yield large F_{p} values but is not straightforwardly compatible with devices with a useful output power, while the fabrication difficulties of 3D PhC structures make them impractical in the short term.

In view of the excellent performance obtained nowadays in commercial devices (either by chip shaping or surface roughening), it is clear that only a fully optimized PhC system could prove compelling enough to find a practical application. Advanced applications of the diffraction grating concept are the most likely candidate for this task, as they are compatible with real-world requirements and offer a wide design space for optimization.

Acknowledgments

The activity of CW at UCSB has been supported as part of the 'Center for Energy Efficient Materials' at the University of California, Santa Barbara, an Energy Frontier Research Center funded by the US Department of Energy (DOE), Office of Science, Office of Basic Energy Sciences under Award No DE-SC0001009.

References

[1] Bavencove A L *et al* 2010 GaN-based nanowires: from nanometric-scale characterization to light emitting diodes *Phys. Status Solidi* a **207** 1425–7

[2] Bendickson J M, Dowling J P and Scalora M 1996 Analytic expressions for the electromagnetic mode density in finite, one-dimensional, photonic band-gap structures *Phys. Rev.* E **53** 4107–21

[3] Benisty H, Danglot J, Talneau A, Enoch S, Pottage J M and David A 2008 Investigation of extracting photonic crystal lattices for guided modes of GaAs-based heterostructures *IEEE J. Quantum Electron.* **44** 777–89

[4] Benisty H, De Neve H and Weisbuch C 1998 Impact of planar microcavity effects on light extraction: I. Basic concepts and analytical trends *IEEE J. Quantum Electron.* **34** 1612–31

[5] Benisty H and Khayam O 2011 Spontaneous emission and coupled-mode theory in multimode 1-D systems with contradirectional coupling *IEEE J. Quantum Electron.* **47** 204–12

[6] Benisty H, Stanley R and Mayer M 1998 Method of source terms for dipole emission modification in modes of arbitrary planar structures *J. Opt. Soc. Am.* A **15** 1192–201

[7] Benisty H and Weisbuch C 2006 Photonic crystals *Progress in Optics* vol 49 ed E Wolf (Amsterdam: Elsevier) pp 177–313

[8] Bergenek K, Wiesmann C, Wirth R, O'Faolain L, Linder N, Streubel K and Krauss T F 2008 Enhanced light extraction efficiency from AlGaInP thin-film light-emitting diodes with photonic crystals *Appl. Phys. Lett.* **93** 041105

[9] Bergenek K, Wiesmann C, Zull H, Rumbolz C, Wirth R, Linder N, Streubel K and Krauss T F 2009 Strong high order diffraction of guided modes in micro-cavity light-emitting diodes with hexagonal photonic crystals *IEEE J. Quantum Electron.* **45** 1517–23

[10] Bergenek K, Wiesmann C, Zull H, Wirth R, Sundgren P, Linder N, Streubel K and Krauss T F 2008 Directional light extraction from thin-film resonant cavity light-emitting diodes with a photonic crystal *Appl. Phys. Lett.* **93** 231109

[11] Blanco A *et al* 2000 Large-scale synthesis of a silicon photonic crystal with a complete three-dimensional bandgap near 1.5 micrometres *Nature* **405** 437–40

[12] Bleuse J, Claudon J, Creasey M, Malik N S, Gerard J-M, Maksymov I, Hugonin J-P and Lalanne P 2011 Inhibition, enhancement, and control of spontaneous emission in photonic nanowires *Phys. Rev. Lett.* **106** 103601

[13] Boroditsky M, Gontijo I, Jackson M, Vrijen R, Yablonovitch E, Krauss T, Cheng C C, Scherer A, Bhat R and Krames M 2000 Surface recombination measurements on III–V candidate materials for nanostructure light-emitting diodes *J. Appl. Phys.* **87** 3497–504

[14] Boroditsky M, Krauss T F, Coccioli R, Vrijen R, Bhat R and Yablonovitch E 1999 Light extraction from optically pumped light-emitting diode by thin-slab photonic crystals *Appl. Phys. Lett.* **75** 1036–8

[15] Chen J-F, Hong R-T and Yang J-Y 2010 Modified spontaneous emission rate in three-dimensional layer-by-layer photonic crystals with planar defects *J. Appl. Phys.* **107** 023110

[16] Coldren L and Corzine S W 1995 *Diode Lasers and Photonic Integrated Circuits* (New York: Wiley) chapter 4 pp 139–44

[17] David A 2006 High efficiency GaN-based LEDs: light extraction by photonic crystals *Ann. Phys. Fr.* **31** (6) 1–235

[18] David A, Benisty H and Weisbuch C 2007 Optimization of light-diffracting photonic-crystals for high extraction efficiency LEDs *J. Disp. Technol.* **3** 133

[19] David A, Benisty H and Weisbuch C 2007 Spontaneous emission in GaN/InGaN photonic crystal nanopillars *Opt. Express* **15** 17991–8004

[20] David A, Fujii T, Matioli E, Sharma R, Nakamura S, DenBaars S P, Weisbuch C and Benisty H 2006 GaN light-emitting diodes with Archimedean lattice photonic crystals *Appl. Phys. Lett.* **88** 073510

[21] David A, Fujii T, Moran B, Nakamura S, DenBaars S P, Weisbuch C and Benisty H 2006 Photonic crystal laser

lift-off GaN light-emitting diodes *Appl. Phys. Lett.* **88** 133514

[22] David A, Fujii T, Sharma R, McGroddy K, Nakamura S, DenBaars S P, Hu E L, Weisbuch C and Benisty H 2006 Photonic-crystal GaN light-emitting diodes with tailored guided modes distribution *Appl. Phys. Lett.* **88** 061124

[23] David A and Gardner N F 2010 Droop in III-nitrides: comparison of bulk and injection contributions *Appl. Phys. Lett.* **97** 193508

[24] David A and Grundmann M J 2010 Droop in InGaN light-emitting diodes: a differential carrier lifetime analysis *Appl. Phys. Lett.* **96** 103504

[25] David A, Meier C, Sharma R, Diana F S, DenBaars S P, Hu E, Nakamura S, Weisbuch C and Benisty H 2005 Photonic bands in two-dimensionally patterned multimode GaN waveguides for light extraction *Appl. Phys. Lett.* **87** 101107

[26] David A, Moran B, McGroddy K, Matioli E, Hu E L, DenBaars S P, Nakamura S and Weisbuch C 2008 GaN/InGaN light emitting diodes with embedded photonic crystal obtained by lateral epitaxial overgrowth *Appl. Phys. Lett.* **92** 113514

[27] Delbeke D, Bienstman P, Bockstaele R and Baets R 2002 Rigorous electromagnetic analysis of dipole emission in periodically corrugated layers: the grating-assisted resonant-cavity light-emitting diode *J. Opt. Soc. Am.* A **19** 871–80

[28] Delbeke D, Bockstaele R, Bienstman P, Baets R and Benisty H 2002 High-efficiency semiconductor resonant-cavity light-emitting diodes: a review *IEEE J. Sel. Top. Quantum Electron.* **8** 189–206

[29] Dowling J P 1999 Dipole emission in finite photonic bandgap structures: an exactly solvable one-dimensional model *J. Light. Technol.* **17** 2142–51

[30] Duan G H, Gallion P and Debarge G 1990 Analysis of the phase-amplitude coupling factor and spectral linewidth of distributed feedback and composite-cavity semiconductor-lasers *IEEE J. Quantum Electron.* **26** 32–44

[31] Englund D, Fattal D, Waks E, Solomon G, Zhang B, Nakaoka T, Arakawa Y, Yamamoto Y and Vuckovic J 2005 Controlling the spontaneous emission rate of single quantum dots in a two-dimensional photonic crystal *Phys. Rev. Lett.* **95** 013904

[32] Erchak A A, Ripin D J, Fan S, Rakich P, Joannopoulos J D, Ippen E P, Petrich G S and Kolodziejski L A 2001 Enhanced coupling to vertical radiation using a two-dimensional photonic crystal in a semiconductor light-emitting diode *Appl. Phys. Lett.* **78** 563–5

[33] Fan S H, Villeneuve P R, Joannopoulos J D and Schubert E F 1997 High extraction efficiency of spontaneous emission from slabs of photonic crystals *Phys. Rev. Lett.* **78** 3294–7

[34] Fehrembach A L, Enoch S and Sentenac A 2001 Highly directive light sources using two-dimensional photonic crystal slabs *Appl. Phys. Lett.* **79** 4280–2

[35] Ford G W and Weber W H 1984 Electromagnetic-interactions of molecules with metal-surfaces *Phys. Rep.—Rev. Sect. Phys. Lett.* **113** 195–287

[36] Fujii T, David A, Schwach C, Pattison P M, Sharma R, Fujito K, Margalith T, Denbaars S P, Weisbuch C and Nakamura S 2004 Micro cavity effect in GaN-based light-emitting diodes formed by laser lift-off and etch-back technique *Japan. J. Appl. Phys.* **43** L411–3

[37] Fujii T, Gao Y, Sharma R, Hu E L, DenBaars S P and Nakamura S 2004 Increase in the extraction efficiency of GaN-based light-emitting diodes via surface roughening *Appl. Phys. Lett.* **84** 855–7

[38] Fujita M, Takahashi S, Tanaka Y, Asano T and Noda S 2005 Simultaneous inhibition and redistribution of spontaneous light emission in photonic crystals *Science* **308** 1296–8

[39] Gérard J M, Cabrol O and Sermage B 1996 InAs quantum boxes: Highly efficient radiative traps for light emitting devices on Si *Appl. Phys. Lett.* **68** 3123

[40] Gibart P 2004 Metal organic vapour phase epitaxy of GaN and lateral overgrowth. *Rep. Prog. Phys.* **67** 667–715

[41] Gontijo I, Boroditsky M, Yablonovitch E, Keller S, Mishra U K and DenBaars S P 1999 Coupling of InGaN quantum-well photoluminescence to silver surface plasmons *Phys. Rev.* B **60** 11564–7

[42] Goos F and Hänchen H 1947 Ein neuer und fundamentaler Versuch zur Totalreflexion *Ann. Phys.* **436** 333–46

[43] Greffet J-J, Laroche M and Marquier F 2010 Impedance of a nanoantenna and a single quantum emitter *Phys. Rev. Lett.* **105** 117701

[44] He X D, Torrance K E, Sillion F X and Greenberg D P 1991 A comprehensive physical model for light reflection *Comput. Graph.* **25** 175–186

[45] Henry C H 1986 Theory of spontaneous emission noise in open resonators and its application to lasers and optical amplifiers *J. Light. Technol.* **4** 288–97

[46] Ho K M, Chan C T and Soukoulis C M 1990 Existence of a photonic gap in periodic dielectric structures *Phys. Rev. Lett.* **65** 3152–5

[47] Ho S T, Wang L and Park S 1999 Spontaneous emission control and microcavity light emitters *Confined Photon Systems* ed H Benisty *et al* (Berlin: Springer) pp 243–97

[48] Ishizaki K, Okano M and Noda S 2009 Numerical investigation of emission in finite-sized, three-dimensional photonic crystals with structural fluctuations *J. Opt. Soc. Am.* B **26** 1157–61

[49] Iwase H, Englund D and Vuckovic J 2010 Analysis of the Purcell effect in photonic and plasmonic crystals with losses *Opt. Express* **18** 16546–60

[50] Johnson P B and Christy R W 1972 Optical-constants of noble-metals *Phys. Rev.* B **6** 4370–9

[51] Joray R, Ilegems M, Stanley R P, Schmid W, Butendeich R, Wirth R, Jaeger A and Streubel K 2006 Far-field radiation pattern of red emitting thin-film resonant cavity LEDs *IEEE Photon. Technol. Lett.* **18** 1052–4

[52] Jorgensen M R, Galusha J W and Bartl M H 2011 Strongly modified spontaneous emission rates in diamond-structured photonic crystals *Phys. Rev. Lett.* **107** 143902

[53] Keller S *et al* 2006 Optical and structural properties of GaN nanopillar and nanostripe arrays with embedded InGaN/GaN multi-quantum wells *J. Appl. Phys.* **100** 054314

[54] Khurgin J B, Sun G and Soref R A 2007 Enhancement of luminescence efficiency using surface plasmon polaritons: figures of merit *J. Opt. Soc. Am.* B **24** 1968–80

[55] Kim T, Leisher P O, Danner A J, Wirth R, Streubel K and Choquette K D 2006 Photonic crystal structure effect on the enhancement in the external quantum efficiency of a red LED *IEEE Photon. Technol. Lett.* **18** 1876–8

[56] Kioupakis E, Rinke P, Delaney K T and Van de Walle C G 2011 Indirect Auger recombination as a cause of efficiency droop in nitride light-emitting diodes *Appl. Phys. Lett.* **98** 161107

[57] Kleppner D 1981 Inhibited spontaneous emission *Phys. Rev. Lett.* **47** 233–6

[58] Koenderink A F, Kafesaki M, Soukoulis C M and Sandoghdar V 2005 Spontaneous emission in the near field of two-dimensional photonic crystals *Opt. Lett.* **30** 3210–2

[59] Koenderink A F, Kafesaki M, Soukoulis C M and Sandoghdar V 2006 Spontaneous emission rates of dipoles in photonic crystal membranes *J. Opt. Soc. Am.* B **23** 1196–206

[60] Krames M R, Shchekin O B, Mueller-Mach R, Mueller G O, Zhou L, Harbers G and Craford M G 2007 Status and

future of high-power light-emitting diodes for solid-state lighting *J. Disp. Technol.* **3** 160–75
[61] Kuhn A and Ljunggren D 2010 Cavity-based single-photon sources *Contemp. Phys.* **51** 289–313
[62] Kuroda K, Sawada T, Kuroda T, Watanabe K and Sakoda K 2010 Enhanced spontaneous emission observed at one-dimensional photonic band edges *J. Opt. Soc. Am.* B **27** 45–50
[63] Large M J, Large T and Travis A R L 2010 Parallel optics in waveguide displays: a flat panel autostereoscopic display *J. Disp. Technol.* **6** 431–7
[64] Lecamp G, Lalanne P and Hugonin J P 2007 Very large spontaneous-emission beta factors in photonic-crystal waveguides *Phys. Rev. Lett.* **99** 023902
[65] Leistikow M D, Mosk A P, Yeganegi E, Huisman S R, Lagendijk A and Vos W L 2011 Inhibited spontaneous emission of quantum dots observed in a 3D photonic band gap *Phys. Rev. Lett.* **107** 193903
[66] Li Z Y and Zhang Z Q 2000 Fragility of photonic band gaps in inverse-opal photonic crystals *Phys. Rev.* B **62** 1516–9
[67] Lodahl P, van Driel A F, Nikolaev I S, Irman A, Overgaag K, Vanmaekelbergh D and Vos W L 2004 Controlling the dynamics of spontaneous emission from quantum dots by photonic crystals *Nature* **430** 654–7
[68] Lourtioz J-M, Benisty H, Berger V, Gerard J-M, Maystre D and Tchelnokov A 2009 *Photonic Crystals: Towards Nanoscale Photonic Devices* ed Lourtioz (Berlin: Springer)
[69] Makino T 1991 Transfer-matrix formulation of spontaneous emission noise of DFB semiconductor-lasers *J. Light. Technol.* **9** 84–92
[70] Manga Rao V S C and Hughes S 2007 Single quantum-dot Purcell factor and beta factor in a photonic crystal waveguide *Phys. Rev.* B **75** 205437
[71] Matioli E, Brinkley S, Kelchner K M, Nakamura S, DenBaars S, Speck J and Weisbuch C 2011 Polarized light extraction in *m*-plane GaN light-emitting diodes by embedded photonic-crystals *Appl. Phys. Lett.* **98** 251112
[72] Matioli E, Keller S, Wu F, Choi Y-S, Hu E, Speck J and Weisbuch C 2009 Growth of embedded photonic crystals for GaN-based optoelectronic devices *J. Appl. Phys.* **106** 024309
[73] Matioli E, Rangel E, Iza M, Fleury B, Pfaff N, Speck J, Hu E and Weisbuch C 2010 High extraction efficiency light-emitting diodes based on embedded air-gap photonic-crystals *Appl. Phys. Lett.* **96** 031108
[74] McKinsey 2011 Lighting the way: perspectives on the global lighting market (*Market Report*) http://img.ledsmagazine.com/pdf/lightingtheway.pdf
[75] Merano M, Aiello A, 't Hooft G W, van Exter M P, Eliel E R and Woerdman J P 2007 Observation of Goos–Hanchen shifts in metallic reflection *Opt. Express* **15** 15928–34
[76] Nayar S K, Ikeuchi K and Kanade T 1991 Surface reflection—physical and geometrical perspectives *IEEE Trans. Pattern Anal. Mach. Intell.* **13** 611–34
[77] Noda S, Fujita M and Asano T 2007 Spontaneous-emission control by photonic crystals and nanocavities *Nature Photon.* **1** 449–58
[78] Oder T N, Kim K H, Lin J Y and Jiang H X 2004 III-nitride blue and ultraviolet photonic crystal light emitting diodes *Appl. Phys. Lett.* **84** 466–8
[79] Oder T N, Shakya J, Lin J Y and Jiang H X 2003 III-nitride photonic crystals *Appl. Phys. Lett.* **83** 1231–3
[80] Okamoto K, Niki I, Shvartser A, Narukawa Y, Mukai T and Scherer A 2004 Surface-plasmon-enhanced light emitters based on InGaN quantum wells *Nature Mater.* **3** 601–5
[81] Palik E D 1991 *Handbook of Optical Constants of Solids II*. (San Diego: Academic)
[82] Park H G, Kim S H, Kwon S H, Ju Y G, Yang J K, Baek J H, Kim S B and Lee Y H 2004 Electrically driven single-cell photonic crystal laser *Science* **305** 1444–7
[83] Pattison P M, Sharma R, David A, Waki I, Weisbuch C and Nakamura S 2006 Gallium nitride based micro-cavity light emitting diodes emitting at 498 nm *Phys. Status Solidi* a **203** 1783–6
[84] Piprek J (ed) 2007 *Nitride Semiconductor Devices: Principles and Simulation* (New York: Wiley)
[85] Rangel E 2011 *PhD Thesis* University of California at Santa Barbara
[86] Rangel E, Matioli E, Chen H-T, Choi Y-S, Weisbuch C, Speck J S and Hu E L 2010 Interplay of cavity thickness and metal absorption in thin-film InGaN photonic crystal light-emitting diodes *Appl. Phys. Lett.* **97** 061118
[87] Rangel E, Matioli E, Choi Y-S, Weisbuch C, Speck J S and Hu E L 2011 Directionality control through selective excitation of low-order guided modes in thin-film InGaN photonic crystal light-emitting diodes *Appl. Phys. Lett.* **98** 081104
[88] Rangel E, Matioli E, Speck J S, Weisbuch C and Hu E L 2011 Impact of the vertical layer structure on the emission directionality of thin-film InGaN photonic crystal LEDs *CLEO: 2011–Laser Applications to Photonic Applications (OSA Technical Digest)* CMA3 (CD)
[89] Rattier M, Benisty H, Schwoob E, Weisbuch C, Krauss T F, Smith C J M, Houdre R and Oesterle U 2003 Omnidirectional and compact guided light extraction from Archimedean photonic lattices *Appl. Phys. Lett.* **83** 1283–5
[90] Rattier M, Benisty H, Stanley R P, Carlin J F, Houdre R, Oesterle U, Smith C J M, Weisbuch C and Krauss T F 2002 Toward ultrahigh-efficiency aluminum oxide microcavity light-emitting diodes: guided mode extraction by photonic crystals *IEEE J. Sel. Top. Quantum Electron.* **8** 238–47
[91] Sapienza R, Bondareff P, Pierrat R, Habert B, Carminati R and van Hulst N F 2011 Long-tail statistics of the Purcell factor in disordered media driven by near-field interactions *Phys. Rev. Lett.* **106** 163902
[92] Shchekin O B, Epler J E, Trottier T A, Margalith T, Steigerwald D A, Holcomb M O, Martin P S and Krames M R 2006 High performance thin-film flip-chip InGaN-GaN light-emitting diodes *Appl. Phys. Lett.* **89** 071109
[93] Shen Y C, Mueller G O, Watanabe S, Gardner N F, Munkholm A and Krames M R 2007 Auger recombination in InGaN measured by photoluminescence *Appl. Phys. Lett.* **91** 141101
[94] Sozuer H S and Dowling J P 1994 Photonic band calculations for woodpile structures *J. Mod. Opt.* **41** 231–9
[95] Sprik R, VanTiggelen B A and Lagendijk A 1996 Optical emission in periodic dielectrics. *Europhys. Lett.* **35** 265–270
[96] Stringfellow G B 1997 Materials issues in high-brightness light-emitting diodes *High Brightness Light Emitting Diodes* ed G B Stringfellow and G Crawford (San Diego, CA: Academic) pp 1–45
[97] Tikhodeev S G, Yablonskii A L, Muljarov E A, Gippius N A and Ishihara T 2002 Quasiguided modes and optical properties of photonic crystal slabs *Phys. Rev.* B **66** 045102
[98] Tocci M D, Scalora M, Bloemer M J, Dowling J P and Bowden C M 1996 Measurement of spontaneous-emission enhancement near the one-dimensional photonic band edge of semiconductor heterostructures *Phys. Rev.* A **53** 2799–803
[99] Torrance K E and Sparrow E M 1967 Theory for off-specular reflection from roughened surfaces *J. Opt. Soc. Am.* **57** 1105

[100] Tsao J Y, Saunders H D, Creighton J R, Coltrin M E and Simmons J A 2010 Solid-state lighting: an energy-economics perspective *J. Phys. D: Appl. Phys.* **43** 354001
[101] Villeneuve P R and Piche M 1994 Photonic bandgaps in periodic dielectric structures *Prog. Quantum Electron.* **18** 153–200
[102] von Malm N, Wirth R, Illek S and Steegmuller U 2010 Concepts for future solid state lighting solutions *Proc. SPIE* **7784** 778411
[103] Wang Q, Stobbe S and Lodahl P 2011 Mapping the local density of optical states of a photonic crystal with single quantum dots *Phys. Rev. Lett.* **107** 167404
[104] Weber J P and Wang S 1991 A new method for the calculation of the emission-spectrum of DFB and DBR lasers *IEEE J. Quantum Electron.* **27** 2256–66
[105] Weisbuch C *et al* 2004 Recent results and latest views on microcavity LEDs *Proc. SPIE* **5366** 551
[106] Weisbuch C and Vinter B 1991 *Quantum Semiconductor Structures, Fundamentals and Applications* (Boston, MA: Academic)
[107] Whittaker D M and Culshaw I S 1999 Scattering-matrix treatment of patterned multilayer photonic structures *Phys. Rev.* B **60** 2610–8
[108] Wierer J J, David A and Megens M M 2009 III-nitride photonic-crystal light-emitting diodes with high extraction efficiency *Nature Photon.* **3** 163–9
[109] Wierer J J, Krames M R, Epler J E, Gardner N F, Craford M G, Wendt J R, Simmons J A and Sigalas M M 2004 InGaN/GaN quantum-well heterostructure light-emitting diodes employing photonic crystal structures *Appl. Phys. Lett.* **84** 3885–7
[110] Wierer J J *et al* 2001 High-power AlGaInN flip-chip light-emitting diodes *Appl. Phys. Lett.* **78** 3379–81
[111] Wiesmann C, Bergenek K, Houdre R, Stanley R P, Linder N and Schwarz U T 2009 Theoretical investigation of the radiation pattern from LEDs incorporating shallow photonic crystals *IEEE J. Quantum Electron.* **45** 1273–83
[112] Wiesmann C, Bergenek K, Linder N and Schwarz U T 2009 Photonic crystal LEDs—designing light extraction *Laser Photon. Rev.* **3** 262–86
[113] Woldering L A, Mosk A P, Tjerkstra R W and Vos W L 2009 The influence of fabrication deviations on the photonic band gap of three-dimensional inverse woodpile nanostructures *J. Appl. Phys.* **105** 093108
[114] Yablonovitch E 1987 Inhibited spontaneous emission in solid-state physics and electronics *Phys. Rev. Lett.* **58** 2059–62
[115] Yablonovitch E 1994 Photonic crystals *J. Mod. Opt.* **41** 173–94
[116] Yablonovitch E, Gmitter T J and Leung K M 1991 Photonic band-structure—the face-centered-cubic case employing nonspherical atoms *Phys. Rev. Lett.* **67** 2295–8
[117] Yao P, Manga Rao V S C and Hughes S 2010 On-chip single photon sources using planar photonic crystals and single quantum dots *Laser Photon. Rev.* **4** 499–516